Titre: Title:	Electro Deposition of Cuprous Oxide for Thin Films Solar Cell Applications
Auteur: Author:	Seyed Mohammad Shahrestani
Date:	2013
Type:	Mémoire ou thèse / Dissertation or Thesis
Référence: Citation:	Shahrestani, S. M. (2013). Electro Deposition of Cuprous Oxide for Thin Films Solar Cell Applications [Mémoire de maîtrise, École Polytechnique de Montréal]. PolyPublie. https://publications.polymtl.ca/1285/

URL de PolyPublie: PolyPublie URL:	https://publications.polymtl.ca/1285/
Directeurs de recherche: Advisors:	Oumarou Savadogo
Programme: Program:	Génie métallurgique

UNIVERSITÉ DE MONTRÉAL

ELECTRO DEPOSITION OF CUPROUS OXIDE FOR THIN FILM SOLAR CELL APPLICATIONS

SEYED MOHAMMAD SHAHRESTANI

DÉPARTEMENT DE GÉNIE CHIMIQUE

ÉCOLE POLYTECHNIQUE DE MONTRÉAL

MÉMOIRE PRÉSENTÉ EN VUE DE L'OBTENTION

DU DIPLÔME DE MAÎTRISE ÈS SCIENCES APPLIQUÉES

(GÉNIE MÉTALLURGIQUE)

DÉCEMBRE 2013

UNIVERSITÉ DE MONTRÉAL

ÉCOLE POLYTECHNIQUE DE MONTRÉAL

Ce mémoire intitulé:

ELECTRO DEPOSITION OF CUPROUS OXIDE FOR THIN FILM SOLAR CELL APPLICATIONS

présenté par: SHAHRESTANI Seyed Mohammad

en vue de l'obtention du diplôme de : Maîtrise ès Sciences Appliquées

a été dûment accepté par le jury d'examen constitué de :

Mme KLEMBERG-SAPIEHA Jolanta-Ewa, Doct., présidente

M. SAVADOGO Oumarou, D. d'état., membre et directeur de recherche

Mme TAVARES Ana, Ph.D., membre

DEDICATION

This thesis is dedicated to my parents,

to my dear wife and children,

to my brothers and sisters.

ACKNOWLEDGEMENT

I wish to express my sincere gratitude to those who helped me in the completion of this thesis.

First and foremost, I have to thank my parents for their love and support throughout my life. Thank you both for giving me life and strength.

I am thankful to my supervisor, Professor Oumarou Savadogo for given me the opportunity to work under his guidance in Laboratory of New Materials for Energy and Electrochemistry systems (LaNoMat).

I thank to my colleagues in Polytechnique Montreal: Carole Massicotte, Ali Seifitokaldani, Majid Talebiesfandarani for their help and creating such a pleasant accompany during my studies.

I also wish to express my gratitude to the members of the staff, my friends and colleagues.

RÉSUMÉ

Des couches semi-conductrices d'oxyde de cuivre de type *p* et de type *n* pour des applications photovoltaïques ont été fabriquées par voie électrochimique avec des approches nouvelles. Les couches minces ont été électro-déposées par polarisation cathodique sur une feuille de cuivre et des substrats d'oxyde d'indium-étain (ou oxyde d'indium dopé à l'étain (ITO)). Les conditions optimales de dépôt (composition, pH et température de l'électrolyte, domaine de potentiel à appliquer) des couches sous forme de films minces ont été identifiée, En particulier les conditions qui permettent d'avoir des couches de type *n* ont été bien identifiée pour la première fois. La configuration d'une pile photo-électrochimique a été utilisée pour caractériser la réponse spectrale des couches. Il a été montré que les couches *p* délivre un photo-courant dans le domaine cathodique et les couches n dans le domaine de potentiel anodique. Les mesures des résistivités électriques des couches électro chimiquement déposées de Cu_2O, de type *p* et *n*, ont montré que la résistivité du Cu_2O de type *p* varie de 3.2×10^5 à 2.0×10^8 Ω.cm selon les conditions de dépôt telles le pH de la solution, le potentiel de dépôt et la température.

L'influence de plusieurs paramètres d'électrodéposition de couches de Cu_2O de type, tels que le potentiel appliqué, le pH et la température du bain, sur la composition chimique, le degré de cristallinité, la taille des grains et l'orientation a été systématiquement étudiée en utilisant la diffraction des rayons X et la microscopie électronique à balayage. Selon le potentiel d'électrodéposition, deux morphologies différentes de surface avec des orientations cristallines préférentielles variées ont été obtenues pour des températures de l'électrolyte de dépôt de 30 °C et un pH de 9.Pour la même température, les couches de Cu_2O de type *p*, hautement cristallines, se trouvent sont obtenues à pH de 12, ce qui indique que la cristallinité dépend du pH du bain.

Aussi, il a été montré que la morphologie des couches de Cu_2O était modifiable en variant le potentiel et la durée de déposition, ainsi que la température de la solution.

Les conditions d'électrodéposition de Cu_2O de type *n* ont été identifies de manière systématique la première fois. L'électrolyte de déposition est à base de 0,01 M d'acétate de cuivre et 0,1 M d'acétate de sodium: a un pH compris entre 4 et 6.3, un potentiel compris entre -0,25 V vs Ag/AgCl et une température de 60^oC. La température optimum de recuit des couches n est de 120-150^oC pour des durées de 30 à 120 minutes. La résistivité des films de type *n* varie entre $5x10^3$ et pH 4 à $5x10^4$ à pH 6.4. Nous avons montré pour la première fois que le barbotage de l'azote dans la cellule d'électrodéposition des couches de type *n* améliore manière significative leur réponse spectrale.

Un procédé d'électrodéposition en deux étapes à été mis en œuvre pour fabriquer la l'homo jonction *p-n* de l'oxyde oxyde cuivreux sur le substrat l'oxyde d'indium-étain (ITO) qui a été utilisé comme un oxyde conducteur transparent. La performance photovoltaïque d'une cellule solaire à homo-jonction *p-n* de Cu_2O a été déterminée. Le courant en court-circuit et la tension de circuit ouvert ont été respectivement déterminés à 235 $\mu A/cm^2$ et 0,35 Volt. Le facteur de remplissage (*FF*) et le rendement de conversion de la lumière en électricité des cellules ont été respectivement évalués à 0,305 et 0,082%.

ABSTRACT

p and *n* type copper oxide semiconductor layers were fabricated by electrochemistry using new approaches for photovoltaic applications. Thin films were electroplated by cathodic polarization on a copper foil or indium tin oxide (ITO) substrates. The optimum deposition conditions (composition, pH and temperature of the electrolyte and applied potential) of the layers as thin films have been identified; in particular the conditions that allow getting the *n*-type layers have been well identified for the first time. The configuration of a photo - electrochemical cell was used to characterize the spectral response of the layers. It was shown that the *p* type layers exhibit a photocurrent in the cathode potential region and *n* layers exhibit photo current in the anode potential region. Measurements of electrical resistivity of electro chemically deposited layers of *p* and *n* type Cu_2O, showed that the resistivity of *p*-type Cu_2O varies from 3.2×10^5 to 2.0×10^8 Ωcm. These values depend the electrodepositing conditions such as the pH of the solution, the deposition potential and temperature.

The influence of several plating parameters of the *p*-type layers of Cu_2O, such as applied potential, pH and temperature of the bath on the chemical composition, degree of crystallinity, grain size and orientation parameters of the sample was systematically studied using X-ray diffraction and scanning electron microscopy. Depending of the electro-deposition potential, two different surface morphologies with various preferential crystal orientations were obtained for the temperatures of the electro-deposition of 30 ° C and pH 9. For the same temperature, the layers of *p*-type Cu_2O of highly crystalline *p*-type are obtained at pH 12, indicating that the crystallinity depends on the pH of the bath.

Also, it has been shown that the morphology of Cu_2O layers was changed by varying the potential and the duration of deposition, as well as the temperature of the solution. The conditions for the electro-deposition of Cu_2O *n*-type were identified consistently for the first time. The electro-deposition electrolyte is based 0.01M acetate copper and 0.1 M sodium acetate: it has a pH between 6.3 and 4, a potential of from 0 to -0.25 V vs. Ag / AgCl and a temperature of 60^oC. The optimum annealing temperature of the *n*-type Cu_2O layers is between 120-150^oC for the annealing time of 30 to 120 minutes. Resistivity of the *n*-type films varies between $5x10^3$ and $5x10^4$ at pH 4 to pH 6.4. We have shown for the first time that bubbling nitrogen gas in the electroplating cell improves significantly the spectral response of the electro-deposited *n*-type thin film.

A two steps electro-deposition process was implemented to make the *p*-*n* homojunction cuprous oxide. Indium tin oxide (ITO) was used as a transparent conductive oxide substrate. A *p*-Cu_2O was electrodeposited on ITO. After heat treatment a thin film layer of *n*-Cu_2O was electrodeposited on top of previous layer. The performance of a *p*-*n* homojunction photovoltaic solar cell of Cu_2O was determined. The short-circuit current and the open circuit voltage were respectively determined to be as 0.35 volts and 235 $\mu A/cm^2$. The fill factor (*FF*) and conversion efficiency of light into electricity were respectively measured to be 0.305 and 0.082%.

CONDENSÉ EN FRANÇAIS

La performance limitée de conversion et le coût élevé des cellules solaires à base de silicium sont les limites essentielles qui empêchent à ce que les piles solaires photovoltaïques deviennent une alternative à l'utilisation de combustibles fossiles qui sont les principales sources d'énergie présentement disponibles même pour l'électrification. Par conséquent, le développement de nouveaux matériaux photovoltaïques à rendements de conversion élevé, à coûts peu onéreux et non toxiques utilisant des procédés économes en énergie est essentiel. Les oxydes de métaux de transition ont un grand potentiel pour répondre à ces exigences. Parmi eux, l'oxyde cuivreux (Cu_2O) est une alternative potentielle au silicium en raison de sa non-toxicité, de la simplicité de et du faible coût de son processus de fabrication à partir de matériaux disponibles en abondance.

Le Cu_2O a une énergie de bande interdite directe de 2,0 eV et un coefficient d'absorption relativement élevé (4×10^5at λ=450nm) dans la région du visible. Son rendement de conversion de la puissance électrique théorique calculée est d'environ 20%. Cependant la compréhension limitée du type de conductivité du semi-conducteur Cu_2O selon les conditions d'élaboration ainsi que la difficulté de son dopage et les difficultés d'élaboration du Cu_2O de type *n* limitent la production efficace de cellules photovoltaïques à base de Cu_2O. L'oxyde cuivreux est un semi-conducteur non stœchiométrique naturellement de type *p* en raison de défauts ponctuels tels que les lacunes de cuivre.

L'objectif de la présente étude était de préparer soigneusement des couches minces de Cu_2O de type *p* et de type *n* en ajustant les paramètres d'électrodéposition et d'obtenir des paramètres de préparation optimale pour la fabrication de cellule solaire à haut rendement à base d'homojunction *p*-*n* de Cu_2O.

Deux substrats différents ont été utilisés comme électrodes de travail pour l'électrodéposition de Cu_2O. L'un était l'oxyde conducteur transparent - ITO (oxyde d'indium-étain) sur un substrat de verre avec une résistance de couche de 18Ω/cm. L'autre était une feuille de cuivre d'une épaisseur de 18 µm.

Deux solutions électrolytiques différentes ont été utilisées pour le dépôt électrochimique Cu_2O. Pour le dépôt de type p Cu_2O, les solutions d'électrolyte est une solution aqueuse contenant 0,4 M de sulfate de cuivre et 3 M de lactate de sodium (NaC_3H_5O3, solution aqueuse à 60% p / p). Pour le type *n* Cu_2O, les solutions d'électrolyte est une solution aqueuse contenant 0,01 M d'acétate de cuivre et de 0,1 M d'acétate de sodium.

Une cellule électrochimique à trois électrodes et à un seul compartiment a été utilisée pour le dépôt de ces films. L'électrodéposition a été réalisée avec un potentiostat Princeton Applied Research 273A. L'électrode de référence commerciale Ag/AgCl (KCl 4M) et une grille de Pt ont été utilisées comme électrode de référence comme contre contre-électrode, respectivement. La température de l'électrolyte est contrôlée entre 30°C et 70°C par sa circulation à travers un bain d'eau thermostaté à l'aide d'un appareil de type Polystat. L'électrodéposition est réalisée en mode potentiostatique à différentes valeurs de potentiel appliquées par rapport à l'électrode de référence. La fenêtre de potentiel appliquée est choisie à partir la courbe de voltampérométrie cyclique (CV). Après dépôt, les films ont été rincés à l'eau déminéralisée et séchés à température ambiante.

La morphologie de surface des films a été étudiée en utilisant un microscope électronique à balayage (MEB). La pureté et orientations cristallines de chacune des couches Cu_2O de type *p* et de type n ont été examinées par diffraction des rayons X (XRD). Les propriétés optiques des

films ont été déterminées par la caractérisation de photocourant réalisée dans une cellule photo-électrochimique à trois électrodes. La conversion des photons de la lumière en énergie électrique a été caractérisée par une jonction solide-liquide appelée cellule photo-électrochimique (PEC). Cette cellule a été utilisée par la mesure des caractéristiques courant-tension (IV) dans l'obscurité et sous éclairement de 80mW/cm^2

Les courbes courant en fonction de la tension (courbes I-V) ont été effectuées afin de déterminer la résistivité des films de Cu_2O de type *p* ou de type *n*. Une électrode Cu circulaire a été placée sur le dessus du film de Cu_2O. Une tension a été balayée entre le substrat et l'électrode supérieure et le courant a été mesuré à température ambiante avec le potentiostat Princeton Applied Research 273A. à l'aide de pente de la courbe I-V de la couche électro déposée et de son épaisseur, la résistivité a été déterminée.

Dans un premier temps, notre étude se démontré que l'augmentation de la température de dépôt élargissait le domaine de potentiel de dépôt de Cu_2O de type vers potentiels cathodiques plus négatifs. Ceci augmentait aussi le courant. Il a été trouvé que la température comprise entre 60-70^oC est une température optimale pour le dépôt de Cu_2O. Ilau aussi été trouvé que le domaine de potentiel utilisé est également l'un des paramètres important pour le dépôt de Cu_2O et que sa valeur doit être maintenue entre -0,2 à -0,6 V vs. Ag/AgCl. Pour des valeurs plus négatives en potentiel, il y a co-déposition de du cuivre (Cu). Afin d'éviter la co-déposition de cuivre, la fenêtre de potentiel utilisé dans cette étude a été maintenue en dessous de -0.5 V vs. Ag/AgCl.

Un autre paramètre jugé important pour optimiser les conditions de dépôt est la valeur du pH de l'électrolyte d'électrodéposition. Les échantillons déposés à partir d'électrolyte dont le pH varie

entre 8 et 13,5 ont montré une réponse photo électrochimique qui est typique de celui d'un semi-conducteur de type *p*.

Tous les échantillons déposés à ce potentiel et avec un électrolyte ayant un pH compris entre 8 et 13,5 donne des couches de Cu_2O pur sans trace de dépôt de Cu ou CuO. Cependant nous avons observé que les couches déposées à pH inférieur à 10 avaient une orientation cristallographique préférentielle selon le plan (100). Cette orientation cristallographique préférentielle était de (111) pour les dépôts effectués à ph supérieur à 11.

La résistivité du film de type *p* déposé diminue légèrement lorsque le pH de la solution augmente. La plus petite valeur ($5x10^5\Omega$.cm) a été obtenue à un pH de 13; ce qui est inférieur de deux ordres de grandeur à celle des films préparés à pH 9,0 ($6x10^7\Omega$.cm). Les résultats montrent aussi que le photo courant augmente avec l'augmentation de pH de la solution. Ainsi le film déposé à un pH de 13 produits deux fois plus de photo courant que le film déposé à un pH de 8,5.

L'effet du pH du bain sur la morphologie et la taille des grains du film de Cu_2O a aussi été étudié. ILa taille des grains augmente avec le pH du bain d'électrodéposition. Le mécanisme qui explique l'effet du pH sur la taille des gains est actuellement inconnu. Nous poursuivons nous études pour comprendre ce phénomène.

Les observations au microscope électronique à balayage montrent que la morphologie de la surface des couches déposées dont les cristaux sont sous forme de pyramides à 4 côtés avec une distribution de taille relativement uniforme pour le plan d'orientation (100). Par contre l'observation de cette morphologie montre de gros cristaux sous forme de pyramides de 3 faces à pour le plan d'orientation (111). La température et le potentiel d'électrodéposition ont aussi un

effet sur la morphologie du dépôt Cu_2O. Ainsi les films préparés à une température élevées (60^oC) a une meilleure cristallinité avec moins de fissures et de défauts dans les cristaux que des dépôts obtenus à 25^oC. Une diminution de la taille des grains a été observée lorsque le potentiel d'électro déposition se déplace vers des valeurs plus négatives dans le domaine compris entre -0,3 à -0,7 V vs Ag/AgCl.

Dans un deuxième temps, des couches de Cu_2O de type *n* ont été déposés dans un bain d'acétate contenant 0,01 M d'acétate de cuivre et de 0,1 M d'acétate de sodium par électrodéposition. La courbe de voltamétrie qui a été réalisée sur une électrode de cuivre et de *p*-Cu_2O a révélé que le potentiel de dépôt doit être plus positif que -0,25 V par rapport à Ag/AgCl pour une température donnée. Les courants correspondants à cette gamme de potentiel sont plus faibles que ceux utilisés pour le dépôt de type *p*-Cu_2O. Cette valeur du courant de dépôt augmente et se déplace vers les potentiels négatifs lorsque le pH augmente. Tous les échantillons préparés dans la gamme de pH de 4,8 à 6,0 fournissent un photo-courant anodique sous illumination dans une pile photo électrochimique ; ce qui confirme leur conductivité de type *n*.

Les résultats montrent que le courant photoélectrique ou la photo-réponse augmente lorsque le potentiel d'électrodéposition des couches se déplace vers des valeurs plus négatives. C'est ainsi que la meilleure photo-réponse été obtenue pour les films de Cu_2O déposé à un potentiel de -0,25 V par rapport à Ag/AgCl.

L'effet du traitement thermique sur les propriétés de photo-réponses et électriques des échantillons de *n*-Cu_2O a été étudié. Après le recuit sous vide pendant 80 min à 150°C, les échantillons ont montré l'amélioration des caractéristiques courant-tension. C'est la première fois que les couches de Cu_2O de type ont pu être préparées dans ces conditions.

Dans un troisième temps un procédé d'électrodéposition en deux étapes à été mis en œuvre pour fabriquer la l'homo jonction *p-n* de l'oxyde oxyde cuivreux sur le substrat l'oxyde d'indium-étain (ITO) qui a été utilisé comme un oxyde conducteur transparent. La performance photovoltaïque d'une cellule solaire à homo-jonction *p-n* de Cu_2O a été déterminée. Le courant en court-circuit et la tension de circuit ouvert ont été respectivement déterminés à 235 $\mu A/cm^2$ et 0,35 Volt. Le facteur de remplissage (*FF*) et le rendement de conversion de la lumière en électricité des cellules ont été respectivement évalués à 0,305 et 0,082%.

TABLE OF CONTENTS

LIST OF FIGURES

LIST OF TABLES

LIST OF ANNEX

Chapter 1 INTRODUCTION

Introduction

As the population of the world continues to grow rapidly and becoming more industrialized, the demand for energy is becoming more critical challenge for the world's population. Therefore competitive, sustainable and secure energy supply is an ever more demanding issue.

Global energy consumption approximately doubled in the last three decades and increased rapidly in 2000-2008 and it is growing about 2.3% per year. According to International Energy Agency (IEA) in 2007, the primary source of energy was fossil fuels with a share of 86.4% (petroleum 36.0%, natural gas 23.0%, and coal 27.4 %,) of total energy sources. In 2009 the global energy consumption of renewable energy sources was 13.1% [1].

The fossil fuels energy sources face a number of challenges including rising prices, security of supply and pollution by carbon dioxide emission. Carbon dioxide is producer of green house effect gases, which increase global temperature by reducing outward radiation and causing anthropogenic climate change. With current rate of fossil fuel consumption it is expected that the concentration of CO_2 reaches the critical level of 750 ppm in 2050 [2]. Since there is no natural decomposition of CO_2 in the atmosphere, it will take 500 to 2000 years to overcome the environmental effect of this level of pollution. As a result, considerable attention has been paid by governments, businesses and consumers to reduce CO_2 emission by supporting the development of alternative energy sources and new technologies for electricity generation. With current technology the only practical solution is to reduce CO_2 emissions to the atmosphere and

minimise the risk of large-scale and long-term changes to our environment. This can be achieved by switching from fossil fuels to alternative energy sources.

Potential alternative energy sources can be solar, geothermal, hydroelectric and wind power. These resources does not deplete as opposed to fossil fuels. Solar energy has huge potential capacity of 120000 TW, which is 7500 times larger than the current annual global energy consumption. Currently the total global energy consumption is estimated to be around 13.5 TW and will increases to 27 TW by 2050 [2]. This means one hour of sun light on earth can provide us with our annual energy use. In other words, at 10% efficiency in solar cells, only 0.1% of the Earth's surface is sufficient to satisfy our present needs of energy. But getting hold to this huge energy reservoir remains an enormous challenge.

Power generation from solar energy is one of the most rapidly growing renewable sources of electricity. Solar power generation has advantages of reducing fossil fuel consumption, production of electricity with less impact on environment, and free power source. Solar energy can be used as solar heating, solar photovoltaic, solar thermal electricity.

In 2011, the IEA said that "the development of affordable, inexhaustible and clean solar energy technologies will have huge longer-term benefits. It will increase countries' energy security through reliance on an indigenous, inexhaustible and mostly import independent resource, enhance sustainability, reduce pollution, lower the costs of mitigating climate change, and keep fossil fuel prices lower than otherwise. These advantages are global. Hence the additional costs of the incentives for early deployment should be considered learning investments; they must be wisely spent and need to be widely shared" [3].

Depending on the method sunlight is captured and converted, solar technologies are divided into passive or active. Active solar techniques use the sun's irradiance, or radiation and electrical or mechanical equipment such as photovoltaic cells, pumps, and fans to convert sunlight into electricity while passive solar techniques rely on the heat of the sun and the thermodynamic properties of the system or materials. In this work active solar technique using solar electricity generated by photovoltaic effect will be studied.

Chapter 2 LITERATURE REVIEW

2.1 Overview

2.1.1 Solar Cell basics

A solar cell is an electronic device which directly converts solar radiation energy into electricity in the process called photovoltaic effect. Light shining on the solar cell create an electrical current or voltage in material which generate electric power. Key factors of this process are the intensity of radiation, the spectral distribution of radiation, light absorption material and design of the external circuit. A variety of materials can potentially satisfy the requirements for photovoltaic energy conversion, however for efficient photovoltaic energy conversion, semiconductor materials in the form of a *p*-*n* junction are essential.

When light strikes material, the incident photons with an energy greater than that of the band gap will excite a negatively charged electron from low energy state (valence band) to a higher energy state (conduction band) leaving behind a passivity charged vacancy (a hole) therefore creating electron-hole pairs. However these generated electron-hole pairs will only exist, for a length of time equal to the minority carrier lifetime before they recombine. If the incident photons have energy lower than that of the band gap the electron energy state will not changed and will immediately relax down and recombine with the hole and the energy will be lost as heat and no current or power can be generated.

The generated electron-hole pairs should be separated and collected before recombination by the action of the electric field. This electric field is created by joining *n*-type and *p*-type semiconductor materials and forming a *p*-*n* junction. A *p*–*n* junction is created by doping, or

growing a layer of crystal doped with one type of dopant on top of a layer of crystal doped with another type of dopant. Since the *n*-type region has a high electron concentration and the *p*-type a high hole concentration, after joining *p*-type and *n*-type semiconductors, electrons near the *p*–*n* interface tend to diffuse from the *n*-type side to the *p*-type side leaving leave holes, positively charged ions, in the *n* region. Similarly, holes flow by diffusion from the *p*-type side to the *n*-type side leaving electrons, negatively charged ions, in the *p* region. Therefore on the *n*-type side, positive ion cores are exposed and on the *p*-type side, negative ion cores are exposed. This will create charged regions and hence internal electrical field nearby the *p*–*n* interfaces. The electrical field will sweeps out the free carries (electrons and holes) and accelerates them in opposite directions causing the depletion of carries, hence, forming the depletion layer or space charge region (Fig. 2-1).

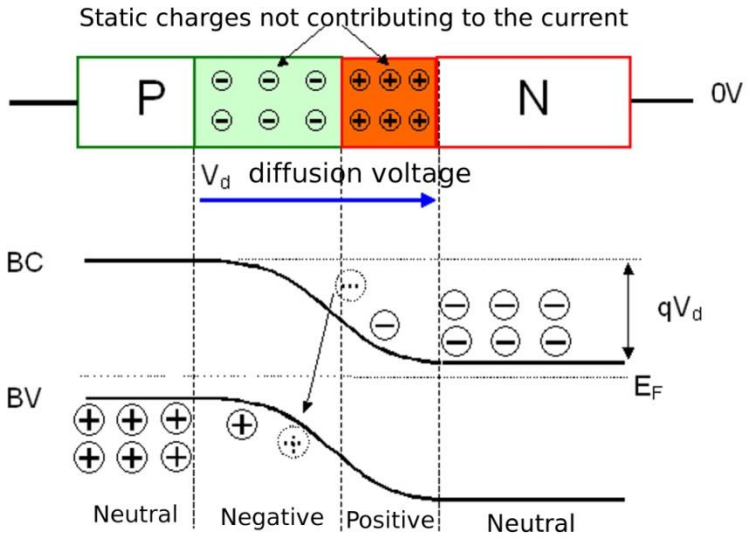

Figure 2-1 A p-n junction in thermal equilibrium with zero bias voltage applied[1].

If the light-generated minority carriers survive long enough to reaches the *p*-*n* junction, it is swept across the junction by the electric field at the junction, where it is now a majority carrier

[1] http://www.optique-ingenieur.org

which is then carried towards the contacts terminals creating voltage difference on either side of the photovoltaic cell. The magnitude of this voltage drop is called the open circuit voltage and scales with the intensity of light while remains constant with time for a given intensity. If the terminals of the solar cell are connected together, the light-generated carriers can flow through the external circuit. The higher the open circuit voltage is, the better is the quality of the photovoltaic cell, and hence the more efficient will be the solar cell in converting light into electrical energy.

The ratio of the number of carriers collected by the solar cell to the number of photons of a given energy incident on the solar cell is called quantum efficiency and it can be expressed either as a function of wavelength or as energy. It is one at the particular wavelength if all photons of that wavelength are absorbed and the resulting minority carriers are collected and it is zero for photons with energy below the band gap. However, the quantum efficiency for most solar cells is reduced because of the effects of recombination, where charge carriers are not able to move into an external circuit. The impact of surface passivation and diffusion length on collection probability is important. It is more favorable to place *p*-*n* junction closer to surface rather than bulk, thus the separated carriers have a shorter distance to travel within the cell and as a result a lower chance of recombining.

2.1.1.1 Equivalent circuit of the solar cell

The solar cell can be seen as a current generator, the current is produced by injection from light. To better analyze the electrical behavior of solar cell, the equivalent electrical model based on electrical components is been created. The behavior of these components is well known. This equivalent circuit describes the static behavior of the solar cell. This circuit is composed of a

current source, a *p-n* junction diode and a shunt resistor (R_{SH}) in parallel along with a parasitic series resistor (R_S).

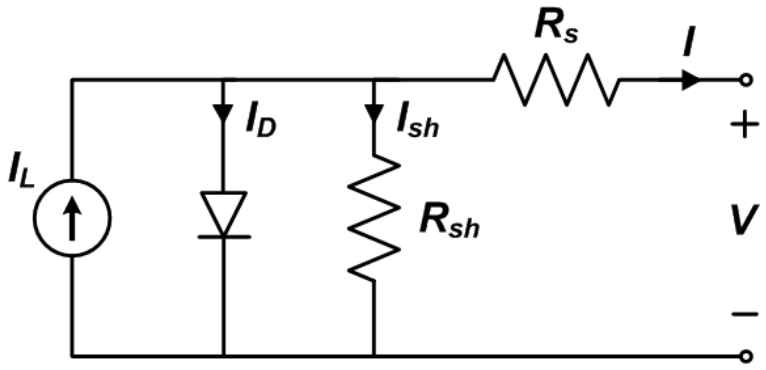

Figure 2-2 Equivalent-circuit model for Solar cells.

Figure 2-2 shows an example of an equivalent circuit of a solar cell with one diode. R_S is the total Ohmic resistance of the solar cell, which is essentially the bulk resistance caused by the fact that a solar cell is not a perfect conductor. For more efficient cells, a smaller R_S value is required. R_{SH} accounts for recombination currents and leakage currents from one terminal to the other due to poor insulation. In this case larger R_{SH} values is required for more efficient cell, this means that the recombination currents and leakage currents are reduced. From the equivalent circuit it is evident that the current produced by the solar cell is equal to:

$$\boldsymbol{I = I_L - I_D - I_{SH}}$$

Where, I, I_L, I_D I_{SH} are output current, photogenerated current, diode current, and shunt current respectively.

The current through these elements is governed by the voltage across them:

$$\boldsymbol{V_j = V + IR_S}$$

Where V_j and V are voltage across both diode and resistor R_{SH} and voltage across the output terminals.

By the Shockley diode equation, the current diverted through the diode is:

$$I_D = I_0 \left\{ exp\left(\frac{qV_j}{nkT}\right) - 1 \right\}$$

Where I_0, n, q, k, T are reverse saturation current, diode ideality factor (1 for an ideal diode), elementary charge, Boltzmann's constant and absolute temperature respectively. At 25°C, KT/q is approximated to 0.0259 volts. By Ohm's law, the current diverted through the shunt resistor is:

$$I_{SH} = \frac{V_j}{R_{SH}}$$

Substituting these into the first equation produces the characteristic equation of a solar cell, which relates solar cell parameters to the output current and voltage:

$$I = I_L - I_0 \left\{ exp\left[\frac{q(V + IR_S)}{nkT}\right] - 1 \right\} - \frac{V + IR_S}{R_{SH}}$$

The [-1] term in the above equation can usually be neglected since the exponential term is usually >> 1.

In principle, the equation can be solve by given a particular operating voltage V and determining the operating current I at that voltage. However, since I appears on both side of equation, the equation has no general analytical solution. Hence, the parameters I_0, n, R_S, and R_{SH} cannot be measured directly, the most common application of the characteristic equation is nonlinear regression to extract the values of these parameters on the basis of their combined effect on solar cell behavior.

Most solar cell parameters can be obtained from simple *I-V* measurements and the performance can be simply demonstrated by few solar cell parameters such as short circuit current (I_{sc}), open circuit voltage (V_{oc}), fill factor (*FF*), power(*W*) and conversion efficiency(η).

The I_{sc} (or I_L) is the current through the solar cell when the voltage across the solar cell is zero and V_{oc} is the voltage across the solar cell when the current through the solar cell is zero and it is the maximum voltage available from the solar cell. One of the most straightforward techniques to estimate R_{SH} and R_S is to measure the slope of *I-V* characteristics as shown in Figure 2-3. R_{SH} also can be estimated from the slope of a reverse biased *I-V* characteristics in the linear region.

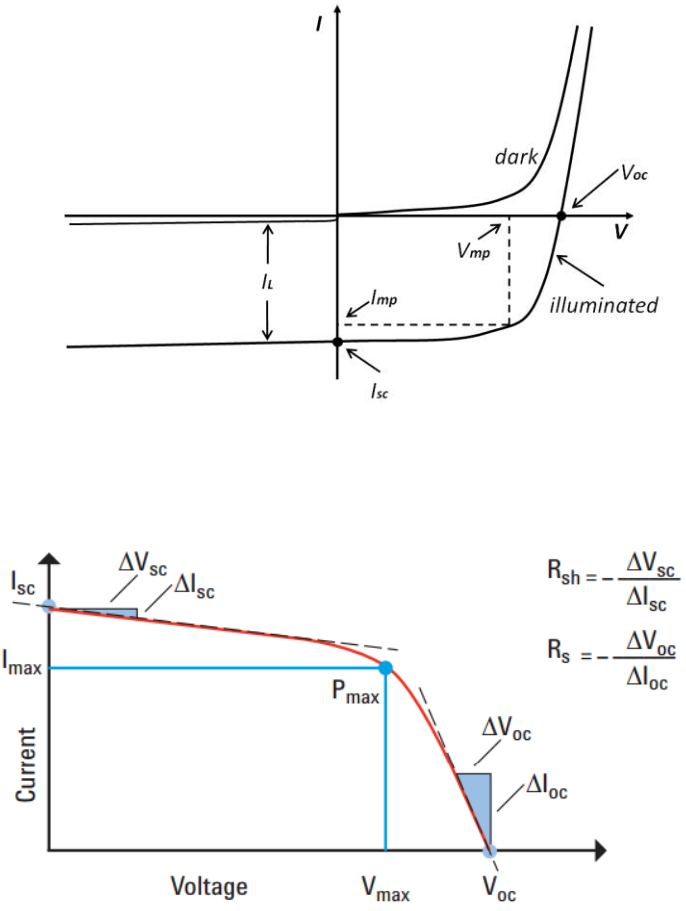

Figure 2-3 Typical IV forward bias characteristics of a solar cell[2].

[2] http://www.azonano.com/article.aspx?ArticleID=3615

The fill factor (*FF*) and the conversion efficiency (η) are metrics used to characterize the performance of the solar cell. The fill factor is defined as the ratio of maximum power point (P_{max}) divided by the product of V_{oc} and I_{sc}. The P_{max} is the condition under which the solar cell generates its maximum power; V_{max} and I_{max} are voltage and current at maximum power point respectively. Fill Factor is essentially a measure of quality of the solar cell and giving by following equation and can also be interpreted graphically as the ratio of the rectangular areas shown in Figure 2-3.

$$\boldsymbol{FF = \frac{V_{max} I_{max}}{V_{oc} I_{SC}}}$$

The conversion efficiency is defined as the ratio of P_{max} to the product of the input light irradiance (*E*) and the solar cell surface area (*A*) or simply Power input.

$$\boldsymbol{\eta = \frac{P_{max}}{E \times A}}$$

2.1.1.2 Type of solar cell

There are a variety of types of solar cells under development. Despite the complicated fabrication process and high cost the majority of solar cells fabricated today are silicon-based solar cells. Silicon-based solar cells types are single crystalline, large-grained poly crystalline and amorphous forms and they dominated PV market by taking 85% of share [4, 5].

Silicon is an abundant material, however its purification is highly expensive and the potential requirement for optimum solar cells exceeds available fabrication process for the high quality, pure silicon crystal lattices high efficiency solar cell. Therefore to have more cost effective solar cells, silicon should be replaced by other materials.

Idea solar cells should possess qualities such as optimum value band gap, direct band gap, homojunction, non toxic and abundant source material, simple and cost effective preparation method and finally good physical and chemical stability.

The maximum possible efficiency of a single junction solar cell under un-concentrated sunlight as a function of the semiconductor band graph can be estimated from the Shockley-Queisser limit graph. This graph is shown in Figure 2-4. If the band gap is too high, most daylight photons cannot be absorbed; if it is too low, then most photons have much more energy than necessary to excite electrons across the band gap, and the rest is wasted.

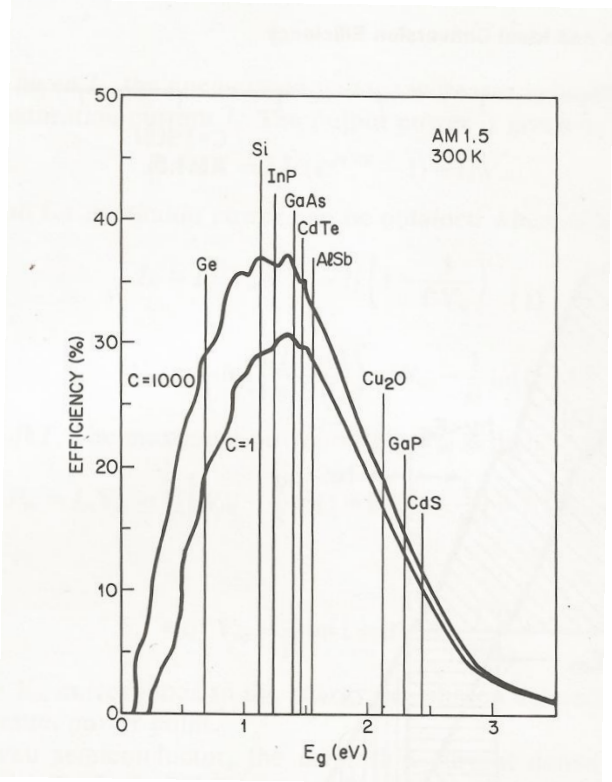

Figure 2-4 Limiting solar cell efficiency as a function of the material bandgap[3].

Lots of efforts is been dedicated to prompt the development of solar cells based on alternative materials to improve conversion efficiency and reduce costs both for fabrication process and for

[3] S.M. Sze, Physics of Semiconductor Devices, Wiley-Interscience 1969

the peripheral components, thereby lowering the cost per Watt of the solar cell. Table 2-1 summarizes the various types of solar cells and the challenges facing them.

Category		Type	Challenges
Silicon		Single crystalline	Development of the device structure and improvement of the crystal quality
		Polly crystalline	
		Amorphous	Multiplying the junctions
Compound	III-V Semiconductor	GaAsInP	Control of the band gap Multiplying the junction
	II-VI Semiconductor	CdTe/CdS – Cu_2S/CdS	
	Chalcopyrite Semiconductor	CIGS	
Organic		Pentancene	Development of the device Development of the materials
Photochemical		Dye sensitized	Development of the materials

Table 2-1 Solar cell types.

2.1.2 Electrochemical cells

Electrochemical deposition, or electrodeposition for short, is well known at the industrial level. Electroplating nickel metal on automotive, copper metal on to circuit boards to provide low resistance interconnection between electronic components and Ni-Fe alloy for magnetic heads has been around for a long time. With the help of this technique a thin film of material can be applied to the surface of an object to change its external properties such as to increase corrosion protection, increase abrasion resistance and even improve decorative quality.

Electrochemical deposition is the process of depositing material onto a conducting surface from a solution containing ionic species (salts). This fabrication technique is been used for plating simple metals, alloys (mixtures of metals) and semiconductors. Recently there is a great research

interest in utilizing this technique to produce semiconductors because of its simplicity, low cost, low-temperature process, control of film quality and possibility of making large area thin films onto conductive substrates.

Electrodeposition cell consists of three electrodes, namely working, reference, and counter electrodes. The process is carried out by passing an electric current between electrodes separated by an electrolyte. The electrodes are connected to a potentiostat which is the instrument which controls the deposition process. This deposition takes place at the electrode-electrolyte interface. The overall electrochemical reaction in a cell consists of two independent half reactions. Each half reaction reacts to the interfacial potential difference at the corresponding electrode namely working or counter electrode (CE). Mostly one half- reaction and the electrode at which it happens is of interest. This electrode is referred as working electrode (WE). To focus on desired reaction, the other half-reaction is standardized by using an electrode with constant composition phases, called reference electrode (RE). The potential of working electrode is fixed.

When a negative potential is applied to the working electrode, the energy of electron at working electrode is increased. When this energy becomes higher than the vacant electronic energy states of species in electrolyte, the electron will transfer into the electrolyte. Hence, the electrons will flow from working electrode into solution and a cathodic current will be established. The cathodic current will cause the reduction of the species in the solution at the surface of the working electrode. Similarly, applying positive potential will lower the energy of the electrons in working electrode and at certain potential, the electrons will flow from solution species to working electrode and an anodic current is formed, which results in the oxidation of the species in the solution. Representation of (a) reduction and (b) oxidation process of a species, A, in solution is given in Figure 2-5. The reactions stop when the equilibrium is achieved. The critical

potential, at which these reactions occurs, is called the standard potential (E_0) for the related species in the solution.

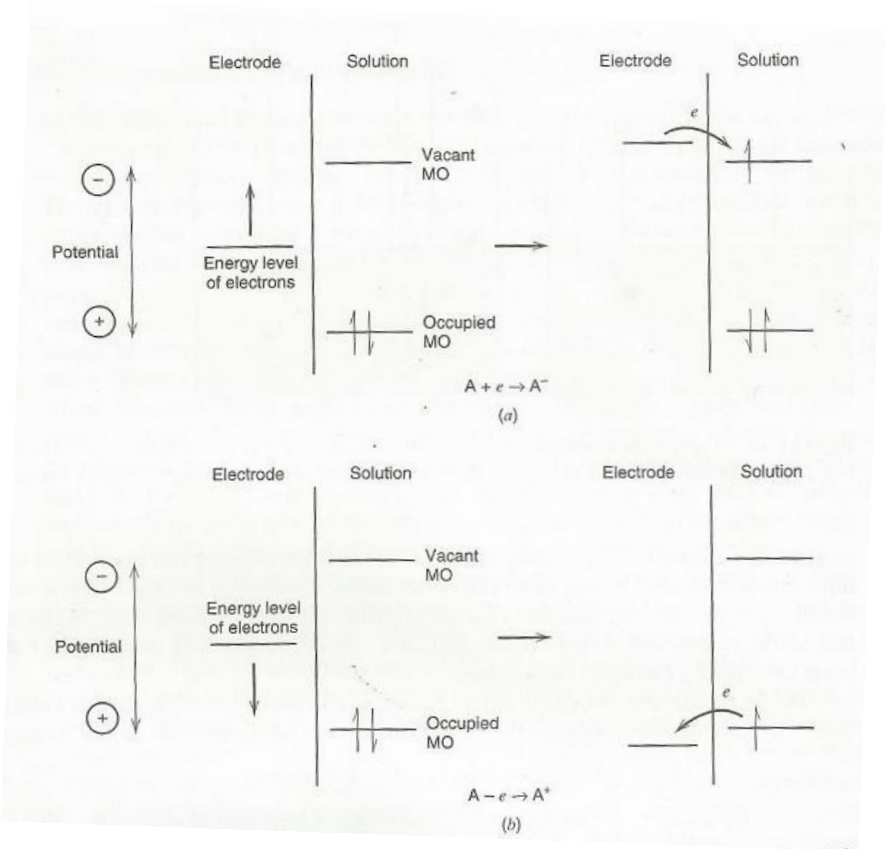

Figure 2-5 Schematic representation of a) reduction and b) oxidation process[4].

In practical electrodeposition, the chemical reaction around the electrode area occurs in a more complicated process. Under applied potential, the ions near the electrode surface will force to rearrange themselves creating an electrical double layer called the Helmholtz double layer, followed by the formation of a diffusion layer. These two layers are referred as the Gouy-Chapman layer. The process describe as follows:

[4] Allen J. Bard, Larry R. Faulkner, Electrochemical Methods: Fundamentals and Applications, John Wiley & Sons, Inc. 2001

- Mass transfer: The hydrated metal ions in the solution migrate towards the working electrode under the influence of current as well as by diffusion and convection.

- Electron transfer: At the working electrode surface, a hydrated metal ion enters the diffused double layer. Then the metal ion enters the Helmholtz double layer where it will be removed of its hydrate envelope.

- Nucleation: chemical reaction precedes and the dehydrated ion is neutralized and adsorbed on the electrode surface.

- Growth: The adsorbed atom then migrates or diffuses to the growth point on the electrode surface.

Therefore an electrode reaction is controlled by many parameters and variables. A summary of these variables is given in Figure 2-6. The key to desirable electrochemical reaction is a proper choice of these parameters. Therefore a large number of trials are required to optimize the process.

Thickness of the electroplated layer on the substrate is determined by the time duration of the plating and layer thickness range is from 0.1 to 30 microns. An electroplated layer is usually composed of a single metallic element although co-deposition of two or more metals is possible under suitable conditions of potential and polarization.

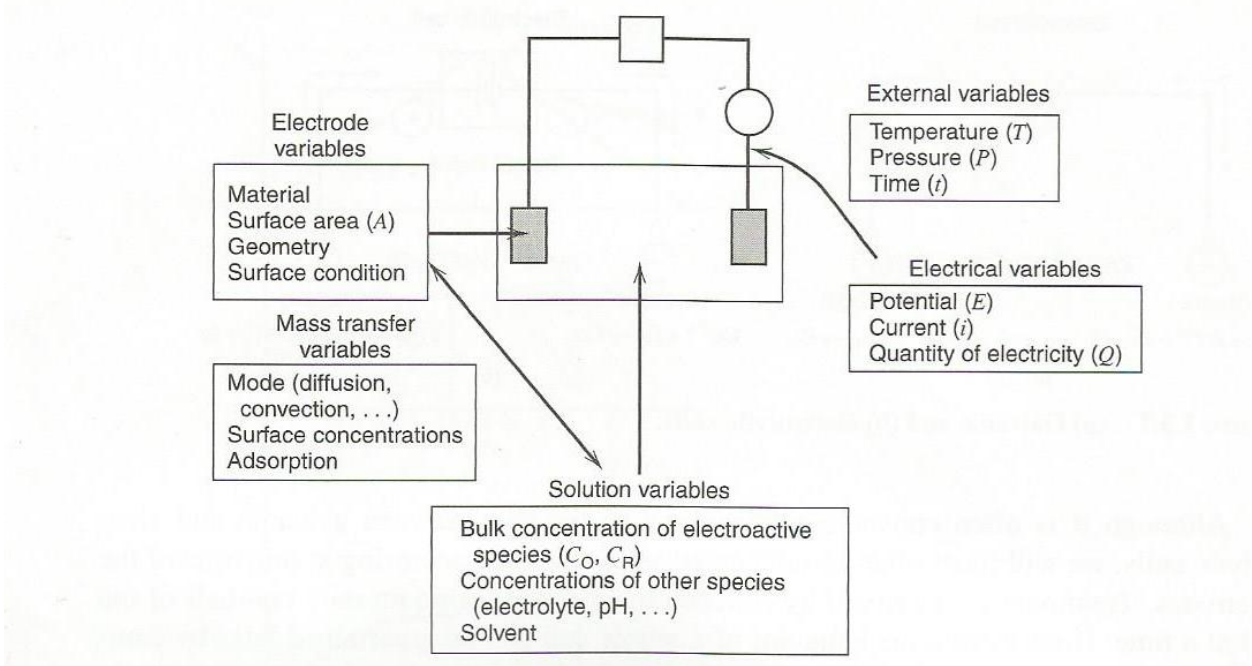

Figure 2-6 Variables affecting electrochemical phase formation[5].

2.1.3 Cyclic voltammetry

Cyclic voltammetry (CV) has become an important and widely used electroanalytical technique in many areas of chemistry. It is widely used for the study of redox processes, for understanding reaction intermediates, and for obtaining stability (the reversibility of a reaction) of reaction products.

A CV system consists of an electrochemical cell, a potentiostat, and a data acquisition system for converting analog waveforms into digital values for processing. Electrochemical cell consists of a working electrode, counter electrode, reference electrode, and electrolytic solution.

The common characteristic of all voltammetric techniques is that they involve the application of a potential (E) to an electrode and the monitoring of the resulting current (i) flowing through the

[5] Allen J. Bard, Larry R. Faulkner, Electrochemical Methods: Fundamentals and Applications, John Wiley & Sons, Inc. 2001

electrochemical cell. In many cases working electrode's potential is varied linearly with time (*t*), both forward and reverse directions (at same scan rate), the reference electrode maintains a constant potential and the current is monitored. The purpose of the electrolytic solution is to provide ions to the electrodes during oxidation and reduction. Thus, all voltammetric techniques can be described as some function of *E*, *i*, and *t*.

The response obtained from a CV can be very simple, and resulting current vs. applied potential curve is predicted for an ideal, reversible system to have the shape shown in Figure 2-7. This Figure shows a CV resulting from a single electron reduction and oxidation. Consider the following reversible reaction: $M^+ + e^- <=> M$. The important parameters in a cyclic voltammogram are the peak potentials (E_{pc} , E_{pa}) and peak currents (i_{pc} , i_{pa}) of the cathodic and anodic peaks, respectively.

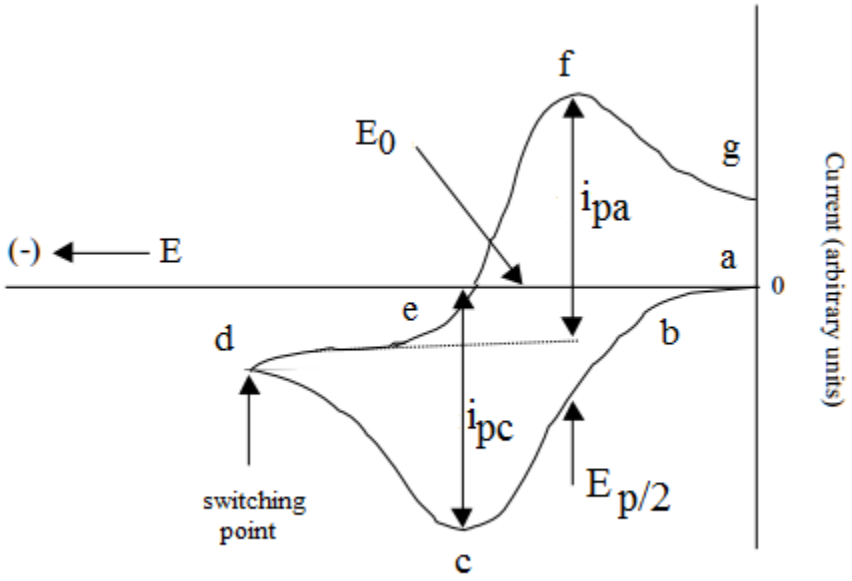

Figure 2-7 Voltammogram of oxidation-reduction process[6]. Potential, E is given vs. Reference electrode.

[6] http://www.basinc.com

The reduction process occurs from (a) the initial potential to (d) the switching potential. In this region the potential is scanned negatively to cause a reduction. The resulting current is called cathodic current (i_{pc}). The corresponding peak potential occurs at (c), and is called the cathodic peak potential (E_{pc}). The E_{pc} is reached when all of the substrate at the surface of the electrode has been reduced. After the switching potential has been reached (d), the potential scans positively from (d) to (g). This results in anodic current (I_{pa}) and oxidation to occur. The peak potential at (f) is called the anodic peak potential (E_{pa}), and is reached when all of the substrate at the surface of the electrode has been oxidized.

The peak current i_p in this voltammogram is given by;

$$\boldsymbol{i_{p=}(2.69\times10^{5})(n^{3/2})\left(AD^{1/2}\right)(v^{1/2})C}$$

where i_p is the peak current (in amperes), n is the number of electrons passed per molecule of analyte oxidized or reduced, A is the electrode area (in cm^2), D is the diffusion coefficient of analyte (in cm^2/sec), v is the potential sweep rate (in volts/sec), and C is the concentration of analyte in bulk solution (in moles/cm^3). The midpoint potential of the two peaks in the voltammogram is given by:

$$\boldsymbol{E_{midpoint}=\frac{\left(E_{p,anodic}+E_{p,cathodic}\right)}{2}=E^{0'}+\frac{RT}{nF}ln\left[\frac{D_R^{1/2}}{D_0^{1/2}}\right]}$$

Where $E^{o'}$ is the redox potential, and D_O and D_R are the diffusion coefficients for the oxidized and reduced halves of that couple. It is frequently reasonable to assume that D_O and D_R are nearly equal, and in such a case the midpoint potential is very nearly equal to the redox potential.

Finally, the separation between the two peaks of the voltammogram is given by:

$$\Delta E_p = \left| E_{p,anodic} - E_{p,cathodic} \right| = 2.3\frac{RT}{nF} = \frac{59}{n} mV \quad (at\ 298\ K)$$

Hence, depending on what is already known about a given system, one could determine the concentration, the diffusion coefficient, the number of electrons per molecule of analyte oxidized or reduced, and/or the redox potential for the analyte, all from a single experiment.

2.1.4 Photoelectrochemical cell

Photoelectrochemistry is a general category encompassing light-induced electrochemical reactions of semiconductors in contact with liquid electrolytes arising from the primary generation of minority carriers. Conceptually, liquid junctions are well suited for semiconductor characterization, since they have almost "contactless" junctions and are most adaptable for on-line characterization.

There are three major components in photoelectrochemical cell (PEC). First is the cell for exposing the semiconductor working surface to the electrolyte while also accommodating auxiliary electrode for controlling the semiconductor potential. Second is the control apparatus, typically a potentiostat and a means for monitoring current. Finally is a light source.

The principle of a photoelectrochemical cell (PEC) based on a single photoanode (*n*-type semiconductor) in a electrolyte with a redox couple (E_{redox}) and a metal counter electrode is shown in Figure 2-8.a. Other configurations of the PEC exist and may involve a single photocathode (*p*-type semiconductor) and a metal counter electrode or a single photoanode and a

photocathode as the counter electrode. In the case of Fig. 2.8.a, the photoanode (*n*-type semiconductor) is characterized by its conduction band (E_{BC}), its valence band, (E_{VB}) in a electrolyte with a redox couple (E_{redox}).

Let us now consider a Photoelectrochemical cell formed by a *n*-type semiconductor, an electrolyte and a metal (platinum or carbon). When a semiconductor is immersed in electrolyte, the charges will flow from one phase to the other to equalize the Fermi level of the semiconductor to the Fermi level of the redox couple. The charge flowing contributes to the formation of the depletion layer, a region on each side of the junction where the charge distribution differs from the bulk material, and band-bending in the semiconductor phase. At equilibrium in the dark the Fermi levels of the three components equalize. When the semiconductor (working electrode) is illuminated with a light having energy *hv* equal or greater than the bandgap, electron-hole couples are generated. These electrons and holes are spatially separated from each other by an electrical field which is created in the semiconductor. This situation gives rise to photopotential, equal to the difference between the Fermi level of the illuminated semiconductor and that of the redox couple in solution. The maximum photovoltage corresponds to the condition where the bands are totally unbended. The corresponding voltage is called flat-band potential, which plays the same role as the point of zero charge in metals.

Under the influence of depletion layer the holes are injected into the solution and the electrons move toward the bulk of the semiconductor and, via an external load, back to the counter electrode, from which they are injected into the solution where they can reduce the oxidised species of the redox couple. The photogenerated holes are swept toward the electrolyte where they can oxidize the reduced species of the redox couple and a photocurrent is generated. Therefore, irradiation on an *n*-type semiconductor will promote an anodic photocurrent. In a *p*-

type semiconductor, the negative space charge region is formed, so under illumination, holes move into semiconductor and electrons move into solution, which generates a cathodic photocurrent. The magnitude of a photocurrent depends on the electrode properties, applied potential, and solution composition, which provide information about the nature of the photo-process.

It should be noted that the photo-generated minority carriers, may oxidize (*n*-type) or reduce (*p*-type) the semiconductor itself, which lead to photocorrosion processes that could rapidly degrade the life of PEC. Therefore an electrolyte composition should be chosen in such ways that make the rate of transport of the photo-generated minority carriers to the redox couple much faster than that of photocorrosion.

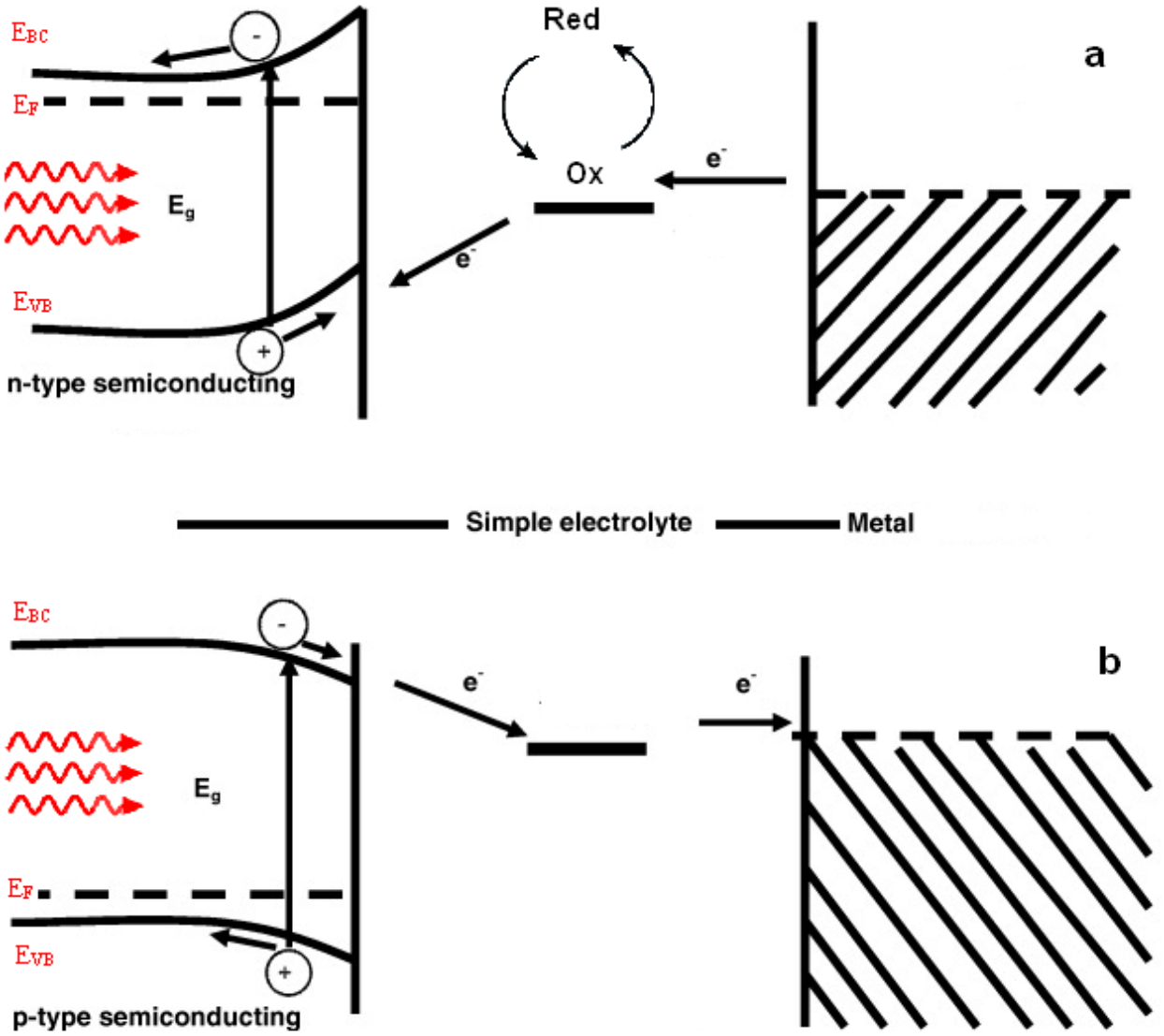

Figure 2-8 Schematic showing the electronic energy levels at the interface between a semiconductor and an electrolyte containing a redox couple and a metal as the counter electrode. a) n-type semiconductor, b) p-type semiconductor[7].

In well-behaved photoelectrochemical cell, the curve of photocurrent vs. applied potential of an *n*-type semiconductor with an electrolyte containing a redox couple (A) is schematically shown in Figure 2-9.

[7] Redraw from: Adv. Nat. Sci.: Nanosci. Nanotechnol. **2** (2011) 023002

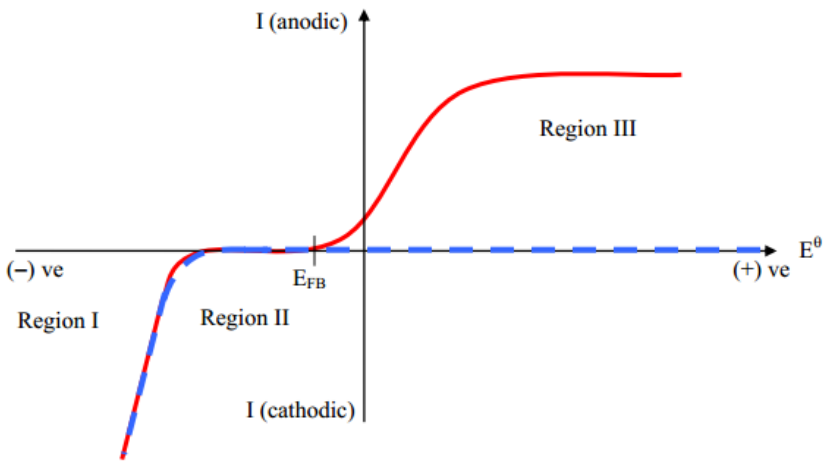

Figure 2-9 Ideal behavior for an n-type semiconductor in the dark (---) and under irradiation (—).

At the flat-band potential there is no current, either in the dark or upon irradiation (Region II), since there is no electric field to separate any generated charge carriers. At potentials negative of the flat-band potential (Region I), an accumulation layer exists, and the electrode can act as a cathode, both in the dark and upon irradiation. At potentials positive of the flat-band potential (Region III), a space-charged layer is thus formed, the width and magnitude of which grows as the potential becomes more positive. Therefore there can be no oxidative (anodic) current in the dark. However, upon irradiation a photocurrent is produced.

2.2 Copper oxide thin film solar cells

Cu_2O crystallizes in a simple cubic structure which the copper atoms arrange in a face-centered cubic (fcc) sublattice and the oxygen atoms in a body-centered cubic (bcc) sublattice. This structure has a lattice constant a_l=4.2696 Å and one sublattice is shifted by a quarter of the body diagonal. In the lattice, each copper atom linearly coordinated by two neighboring oxygens and each oxygen atoms surrounded by four copper atoms, which makes the stoichiometry 2:1.

However, this stoichiometry is not obeyed completely as the ratio of copper and oxygen atoms is slightly different from the ratio in one mole. Therefore the arrangement of atoms in crystalline copper oxide is not perfect. Hence the structure needs to balance itself by the present of defects. In copper oxide crystal, these defects have a form of point defects which are defects that occur only at or around a single lattice point and are not extended in space in any dimension and typically involve at most a few extra or missing atoms. This deviation from stoichiometry, δ in Cu_2O can be identifies either as vacancies, interstitials or both.

Sears et al. 1984 reported that an excess of oxygen, as a result of stoichiometry, is the major active impurity and gives a *p*-doped semiconductor [6]. These defects not only tune the properties of semiconductor but also are involved directly as the active centers in chemical reactions.

Cu_2O is soluble in acid and insoluble in water and has a reddish color [7]. Cu_2O has a molar mass of 143.09 g/mol, density of 6.0 g/cm^3 with melting and boiling points at 1235°C and 1800°C, respectively. High quality natural cuprous oxide crystals with lowest density of structural defect can found in Namibia and Congo [8]. Cu_2O has six atoms per unit cell and thus 3x6 = 18 phonon modes are found, three acoustic and 15 optical phonons [9].

The Cu–O system has two stable oxides: cupric oxide (CuO) and cuprous oxide (Cu_2O). Each oxide has different crystal structures and physical properties. These two oxides are semiconductors with band gaps in the visible or near infrared regions. However cuprous oxide has much better crystallinity, bigger grains and direct bad gap structure. Cu_2O has being frequently studied as absorber for low cost solar cell, even though its optical band gap is not optimum.

Cu_2O is a *p*-type semiconductor with a direct band gap of 2.0–2.2 eV, which is suitable for photovoltaic conversion. Based on the Shockley-Queisser limit, its calculated theoretical electrical power conversion efficiency is approximately 20%; however based on a detailed photon and carrier loss analysis conducted for Cu/Cu_2O cells, it is projected that the ultimate values of the photocurrent for Cu_2O cells would be 12 - 14 mA cm^{-2}. Which indicate that the practical efficiency of around 11%-14% is a realistic achievable goal. This makes it an attractive material for solar cell applications; yet, the experimental efficiencies obtained up to this date are much lower than expectation values [10]. The lack of optimized *p-n* junction is the limiting factor.

The most widely used method of producing Cu_2O is thermal oxidation via the oxidation of copper metal. Copper is abundant material and can be processed by industrially proven low cost methods. Cu_2O thin films can also be prepared by other methods such as anodic oxidation, chemical deposition, sol–gel chemistry, sputtering, electrodeposition, and other gas-phase deposition techniques [11, 12].

Thermal oxidation of copper is a simple and scalable method to produce copper oxide; however the procedure involves the oxidation of high purity copper at an elevated temperature (700-1500^0C). Depending on thickness desire the time range can be from few hours to few minutes followed by high temperature annealing for hours or even days. Copper can be oxidized thermally in air, oxygen or water vapor. Oxidizing in air or oxygen produces CuO and Cu_2O depending on the thermodynamic stability of the oxides. Cu_2O has been identified to be stable at limited ranges of temperatures and oxygen pressure. While water vapor produces more pure Cu_2O phase [13]. In this method Cu_2O with the bulk resistivity in the range of 10^2 -10^4 ohmcm without post treatments can be obtained. This resistivity can further be lowered by oxidizing in

the presence of chlorine gas to below 100 ohmcm. However the purity of the starting Cu_2O material has a significant impact on the quality of Cu_2O. Thermal oxidation process normally shows high carrier concentration and low resistivity [14].

Anodic oxidation of copper surface at constant potential can produce copper oxide; however producing Cu_2O film with high purity in the anodic case is facing serious difficulties. The produced film in this method has a bi-layer structure which consists of Cu_2O as an inner layer and a partly hydrated cupric oxide, $CuO_x(OH)_{2-2x}$ as an outer layer. A pure oxide layer thickness in the 1.5 to 2 μm range is needed for an effective solar cell [15].

Sputtering can be used to deposit copper oxide by sputtering. This method requires use of vacuum technique, as very low pressure in the working space is needed. By varying the rf power during deposition both Cu_2O rich and CuO rich films can be produced. Both the rf power and the oxygen flow rate during deposition affected the electrical sheet resistance of the prepared films. Cu_2O films of resistivity as low as 25 ohmcm have been produced by Drobny et al., using this technique [16, 17].

Chemical vapor deposition (CVD) is a chemical process that produces high-purity solid materials. The produced Cu_2O may be polycrystalline or amorphous depending on the materials and reactor conditions. Chemical vapor deposition has high throughput, high purity, and low-cost of operation. Several important factors such as the deposition temperature, the properties of the precursor, the process pressure, the substrate, the carrier gas flow rate and the chamber geometry affect the quality of the deposited film.

Sol-gel-like dip technique is a simple and low-cost method, with no sophisticated setup; however stoichiometry and phase composition represent a major concern but other aspect such as

crystallite size and distribution, can be easily controlled by a proper choice of the molecular precursors and of the annealing conditions [18].

Electrical properties of Cu_2O, such as carrier mobility, carrier concentration, and resistivity are very dependent on preparation methods. For example thermal oxidation leads to good quality polycrystalline Cu_2O and shows high carrier concentration with the bulk resistivity in the range of 10^2 -10^4 ohmcm while electrodepostion process produces bulk resistivity in the range of 10^4 - 10^6 ohmcm but the grain sizes of the electrodeposits can be controlled easily from 0.1 to 10μm [19]. However the possibility of producing *n*-Cu_2O compensate for this drawback.

Cu_2O semiconductor and its potential for the device application have been recognized since 1920. When silicon, germanium and other potential semiconducting materials were discovered, researcher interest was shifted to these materials and further research on Cu_2O was stopped for two decades. In the 1970s, interest in Cu_2O was revived once again by the photovoltaic community due to its potential application as low cost material for solar cells. Several groups started investigation in metal-Cu_2O solar cells in particular. A Schottky junction solar cell with highest efficiency of 1.8% was fabricated during this time [20]. The best efficient Cu_2O-base heterojunction solar cell was reported recently by Mittiga et al, with efficiency of 2% with the MgF_2/ $ITO_{(sputtering)}$/ $ZnO_{(sputtering)}$/ $Cu_2O_{(oxidation)}$ structure [21]. They concluded that the use of good quality Cu_2O sheets and IBS (ion beam sputtering) room temperature TCO (transparent conducting oxide) deposition can greatly improve the performances of TCO/Cu_2O solar cells.

However, this over all low efficiency is attributed to the lack of *n*-type Cu_2O, which prevents formation of a homogeneous Cu_2O *p*–*n* junction [10, 22] and common conclusion was that the

fabrication of homojunction Cu_2O is the only way to achieve high efficiency Cu_2O-base solar cell due to the fact that homojunction has no interface strain.

In recent years electrodeposition has attracted the researcher because of its simplicity, low cost, low-temperature process (<100^oC) and easy control of film quality onto conductive substrates. This liquid solution, represent other phase of the growth of materials either in bulk form or as thin film. The main advantage of electrodepostion is that the electrical conductivity (*n*-type or *p*-type) can be modify by variation of semiconductor's composition, during the electrodeposition of films [23-25] while none of previously mentioned techniques are able to produce a *n*-type Cu_2O film. The reason for such restriction is not understood yet. It is generally accepted that *n*-type doping is forbidden in the thermodynamic equilibrium because of a self-compensation mechanism. Therefore the concept of the origin of the *n*-type conductivity in Cu_2O should be developed. This will help us to produce optimal *n*-type Cu_2O and hence feasible fabrication of Cu_2O *p-n* junction for higher efficiency photovoltaic application.

Electrodepostion of Cu_2O can be performed either in the potentiostatic mode or, galvanostatic mode. In potentiostatic mode, a potentiostat will accurately control the potential of the counter electrode (CE) against the working electrode (WE) so that the potential difference between the working electrode and the reference electrode (RE) is well defined. In galvanostatic mode, the current flow between the WE and the CE is controlled. The potential difference between the RE and WE and the current flowing between the CE and WE are continuously monitored [11, 18, 26, 27].

Rakhshani et al. [11] prepared *p*-Cu_2O film onto conductive substrates in each three different modes, they used a solution of cupric sulphate, sodium hydroxide and lactic acid and the

composition of the films deposited under all conditions was *p*-Cu_2O with no traces of CuO. The conclusion was that the substrate does not have a major effect on the orientation and the size of the grains; however stirring, concentration and aging of the bath solution all have distinct effects on the deposition parameters. The temperature range was from 25 to 70^oC, they found that deposition temperature had a strong effect on the *p*-Cu_2O grains size, higher temperature results in bigger grains size up to few micrometers; however the orientation of the grains is not effected with change in temperature. Rakhshani et al. [28] also showed that the size of grains could be controlled by the rate of deposition in the galvanostatic mode. Authors found that films deposited galvanostatically in solution of lactic acid (2.7 M), anhydrous cupric sulphate (0.4 M), and sodium hydroxide (4 M) at a temperature of 60 ^oC with pH 9, consisted only of Cu_2O and with highly oriented along the (100) plane parallel to the substrate surface with film resistivity in the range $10^6 – 10^8$ ohmcm.

Mukhopadhyay et al. [27] galvanostatically deposited *p*-Cu_2O at 40–60 °C on copper substrates in solution of cupric sulphate (0.3 M), NaOH (3.2 M) and lactic acid (2.3 M) at pH 9. The deposition kinetics was found to be independent of deposition temperature and linear in the thickness up to about 20 μm. The electrical conductivity of *p*-Cu_2O films was found to vary exponentially with temperature in the 145–300°C range with associated activation energy of 0.79 eV.

Golden et al. [29] electrodeposited *p*-type cuprous oxide by reduction of copper (II) lactate in alkaline solution of 0.4 M cupric sulfate and 3 M lactic acid and concluded that the surface texture of electrodeposited Cu_2O films in bath is affected by bath pH and current density. At a solution pH 9 the orientation of the film is (100), while at a solution pH 12 the orientation changes to (111). The degree of (111) texture for the films grown at pH 12 increased with

applied current density. Other researchers find similar results that at bath pH~9.0, the (100) plane are produced and in higher bath pH~11.0, the (111) are produced [4, 10, 11]. In addition to these preferred orientation Wang et al. in a narrow pH range, ~9.4-~9.9 obtained a third preferred orientation namely (110) [12]. In pH range 8-9, the preferential orientation of Cu_2O deposited film is (200) and as the pH decreases further below 8, the film composition changes from Cu_2O to mix phase of Cu and Cu_2O at pH 7 and to Pure Cu below pH 5 [30].

Zhou and Switzer [31] conducted similar experiment and obtained similar results. They obtained pure four-sided pyramids Cu_2O films at bath pH 9 with applied potential between -0.35 and -0.55 vs. saturated calomel electrode (SCE) or at bath pH 12. Their conclusion was that preferred orientation can be controlled by adjusting the bath pH and/or the applied potential. They also concluded that the grain size in the (111) oriented films are larger than those in (100) films.

Georgieva & Ristov [32] deposited the cuprous oxide (Cu_2O) films using a galvanostatic method from an alkaline $CuSO_4$ bath containing lactic acid and sodium hydroxide at a temperature of 60°C.Authors obtained polycrystalline films of 4–6 μm in thickness with optical band gap of 2.38 eV.

The first *n*-type behavior of Cu_2O by electrodeposition was reported by Siripala and Jaykody [23]. They cathodically deposited *n*-Cu_2O on various metal substrates in solution containing 1mM $CuSO_4$ and small amount of NaOH. Photoconductivity of these films confirmed that the produced film is a *n*-type Cu_2O. However the photoconductivity was changed to *p*-type for the same sample after heat treatment in air at 400^oC for short time. They attributed the *n*-type behavior of Cu_2O to oxygen vacancies created in the crystal lattice and/or additional copper atoms.

On other experiment Siripala et al. [33] used indium tin oxide (ITO) coated glass as substrate and electrodepostion was done in a solution of 0.1 M sodium acetate and 0.016 M cupric acetate for 1.5 h in order to obtain films of thicknesses in the order of 1 μm. They obtained polycrystalline Cu_2O films grain sizes in the order of 1-2 μm. The effect of annealing in air has been studied too and found that there is no apparent change in the crystal structure when heat treated in air at or below 300°C. Annealing above 300°C causes the decomposition of Cu_2O film into a darker film, containing black CuO.

Tang et al. [34] investigated the *n*-type electrochemical deposition of nanocrystalline Cu_2O thin films on TiO_2 films coated on transparent conducting optically (TCO) glass substrates by cathodic reduction in solution consisting of cupric acetate 0.1 M sodium acetate and 0.02 M cupric acetate. The effect of bath temperature was investigated at bath temperature at 0, 30, 45, and 60 °C. Authors found that that growth rates also exhibit significant temperature dependence and the film thickness increases with increasing temperature for the same deposition time.

By selecting a bath temperature of 30 °C and an applied potential of −245 mV (vs. SCE) they investigate the effect of pH and found that it strongly affect the composition and microstructure of the Cu_2O thin films. Authors found that the films deposited at pH < 4 are mostly metallic Cu and only little Cu_2O (according to reaction $Cu^{2+}+2e^{-}\rightarrow Cu$ and the following reaction: $Cu_2O+2e^{-}+2H^{+}\rightarrow 2Cu+H_2O$).

In the region of pH 4 to pH 5.5, the deposited films are mix composite of Cu and Cu_2O, while the films deposited at pH between 5.5 and 6 are pure Cu_2O. Thus they concluded electrodeposition carried out in the pH region 5.5~6 can yield good-quality Cu_2O thin films. In this range pure Cu_2O was deposited at bath temperature between 0 and 30^0C with spherically

shaped grains with 40~50 nm in diameter. Authors found that in order to produce nanocrystalline Cu_2O thin film the bath temperature must be controlled in the range of 0-30^0C. At a temperature of 45°C, a highly branched dendrite formed, and the grain size increased to 200–500 nm. At the temperature above 60°C, a ring-shaped structure with a more porous surface was observed. They also found that heat treatment in air at a temperature above 300 °C causes the oxidation of Cu_2O to CuO. Heat treatment also decreased the resistivity of Cu_2O thin films and optical absorption.

Wijesundera et al. [35] showed that that the single phase polycrystalline Cu_2O can be deposited from 0 to -300 mV (SCE). While at more negative potential co-deposition of Cu and Cu_2O starts and at the deposition potential from -700 mV (SCE) and more negative a single phase Cu thin films are produced. They carried the electrodepostion in an aqueous solution containing sodium acetate and cupric acetate. Single phase polycrystalline Cu_2O thin films with cubic grains of 1–2 μm was produced at the deposition potential around -200 mV (SCE). Authors concluded that the photoactivity of the Cu_2O thin films in a PEC can be improved by depositing microscopic scale random Cu deposits on top of Cu_2O thin films due to the better charge transfer process between Cu_2O and electrolyte.

Jayathileke et al. [36] electrodeposited cuprous oxide thin film in aqueous acetate baths and discovered not only the pH value but also the cupric ion concentration of acetate bath determine the conduction type of the Cu_2O films. The higher concentrations tend to produce *n*-type film and lower concentration produces *p*-type films.

Han et al. [37] [38] studied the effect of doping conditions on electrical properties of *n*-type Cu_2O. For un-doped samples the electrodepostion solution contained $CuSO_4$ and Na lactate and pH was adjusted by adding 4M NaOH. $CuCl_2$ and NaCl were used as the Cl precursor for doped

samples. Different mole concentrations of Cl precursor were used to control the doping level in Cu_2O. They found that the resistivity of Cl-doped Cu_2O is affected by doping conditions such as Cu and Cl concentrations, different Cu and Cl precursors, complexing agent concentration, solution pH and deposition temperature. Thin film *n*-type Cu_2O with resistive as low as 7 Ω-cm with small grain size of around 100nm in Cl-doped, was obtained. Authors suggested that Cl substitution of O in Cu_2O is the reason for excess electrons and thus the *n*-type conductivity. This type of doping enables for much more efficient Cu_2O solar cells by reducing the resistivity to optimum resistivity, which is around 1 Ω-cm for solar cell applications.

Han et al, [39, 40] also studied the effect of bromine doping electrical properties of *n*-type Cu_2O. Bromine doping in Cu_2O significantly reduces the resistivity to as low as 42 Ωcm after vacuum annealing. The deposited Cu_2O film contained larger grain size around ~ 100 μm in linear dimension. They concluded that the large grains and low resistivity will benefit photovoltaic and photochemical cells by reducing carrier recombination as well as carrier scattering at grain boundaries.

The first Cu_2O solar cells of 1% efficiency were fabricated in 1978 at National Science foundation and at the Joint Centre for Graduate Studies. Later on Herion et al, [41] fabricated a Cu/Cu_2O thin-film front wall solar cells using partial thermal oxidation of Cu foil. Open circuit voltages of 0.5 V, and fill factors of 0.45 and efficiencies of 0.4% were obtained. The relatively small fill factor was mainly due to the high series resistance of the cells. These solar cells were limited to Schottky barrier solar cells; i.e., the junction was between *p*-Cu_2O semiconductor and a metal.

When Cu_2O is placed in contact with a metal to form a Schottky barrier, most metals reduce Cu_2O to form a copper-rich region at the interface, to form essentially a Cu/Cu_2O contact. This copper-rich region determines the barrier-height magnitude which is always in the range of 0.7-1.0 eV; regardless of the choice of metal [10]. This oxidation results in low efficiencies in the order of 1%.

Since by that time researchers have not succeeded in producing *n*-type Cu_2O, the homojunction cell structure could not be fabricated. Therefore researches were focused on heterojunction cells. A heterojunction solar cell is fabricated by depositing *n*-type semiconductor of suitable band gap on Cu_2O.

Later on Herion et al,[42] fabricated metal oxide/cuprous oxide heterojunction solar cells prepared by ion etching of a Cu_2O substrate using air as the sputtering gas. Two types of heterojunction solar cells namely CuO/Cu_2O and ZnO/Cu_2O were prepared. They concluded that ZnO/Cu_2O heterojunction is essentially Cu/Cu_2O Schottky cell since Zn reduces Cu_2O to Cu. The fabricated *p*-Cu_2O/*n*-ZnO photovoltaic device showed poor photovoltaic performance of 0.11% conversion efficiency [43].

Other researchers shift their interest towards transparent conducting oxide. Georgieva & Ristov fabricated ITO/Cu_2O solar cell by depositing graphite paste on the rear of the Cu_2O layer with values of the open circuit voltage V_{oc} of 340 mV and the short circuit current density I_{sc} of 245 $\mu A/cm^2$[32].

Tanaka et al. [44] prepared various transparent conducting oxide (TCO)-cuprous oxide (Cu_2O) heterojunction such as indium oxide (In_2O_3), tin oxide (SnO_2) and multi-component oxides like aluminium-zinc oxide (AZO) and aluminium- zinc-indium-tin-oxide (AZITO) and ZnO. The

electrical and photovoltaic properties measured on these heterojunction devices prepared by a pulsed laser deposition showed poor results. The best results obtained with AZO-Cu_2O devices prepared at 150 ^{O}C and measured under air mass 2 (AM2). Illumination with an open-circuit voltage of 0.4 V, a short-circuit current density of 7.1 mA/cm^2, a fill factor of 0.4 and an energy conversion efficiency of 1.2%.

Mittiga et al., [21] prepared ITO/ZnO/Cu_2O solar cell with efficiency of 2%. This is the best solar cell, to date using transparent conducting oxide (TCO) thin films. The TCO films have been grown by ion beam sputtering on good quality Cu_2O sheets prepared by oxidizing copper at a high temperature.

Wijesundera, [45] potentiostatically electrodeposited *n*-Cu_2O thin films in an acetate bath (0.1M sodium acetate and 0.01 M cupric acetate) on Ti/CuO electrodes in order to fabricate the *p*-CuO/*n*-Cu_2O heterojunction. The Ti/CuO/Cu_2O/Au heterojunction gave the open circuit voltage (V_{oc}) of~210 mV, short circuit current (J_{sc}) of~310μA cm^2, fill factor (*FF*) of~0.26 and efficiency (η) of ~0.02% under the white light illumination of 90 mW cm^{-2}.

Katayama et al, [46] prepared Cu_2O/ZnO solar cells by electrodeposition of ZnO on tin-oxide-coated glass followed by galvanostatic deposition of Cu_2O to form Cu_2O/ZnO/ITO solar cells with a short-circuit photocurrent density of 2.08 mA cm^{-2},an open-circuit voltage of 0.19 V, a fill factor of 0.295 and conversion efficiency of 0.117%. Cu_2O film was deposited at current densities of -0.1 to -0.4 mA cm^{-2} from alkaline copper (II) sulfate solution containing malic acid as a complexing agent at pH 9.0. The low efficiency was contributed to defects induced by mismatch between the lattice parameters at the heterojunction.

Septina et al, [47] fabricated a Cu_2O/AZO heterojunction was fabricated by electrodeposition of a Cu_2O film on glass substrates coated with F-doped SnO_2 from an alkaline electrolyte solution (pH 12.5) containing copper (II) sulfate and lactic acid. The Cu_2O film deposited at −0.6 V (vs. Ag/AgCl) at 60 °C showed good electrical rectification. The deposited film had the band gap of 1.9 eV. The solar cell prepared by these parameters had the best performance with 0.60% conversion efficiency.

Cheng and his co-worker showed that preparing nanostructured Cu_2O/ZnO by the electrodeposition will increased *p–n* heterojunction area and then the enhanced charge carriers collection ability. Their cavity-like nano-patterns solar cell showed a efficiency of 0.51% with a V_{oc} of 0.24 V, a J_{sc} of 6.33 mA cm^{-2}, and a FF of 34.5 [48].

These heterojunction cells have low conversation efficiency, much lower than the theoretical efficiency limit of the Cu_2O solar cell. The above low efficiencies can be attributed to parasitic current losses due to the injection of minority carriers across the junction. Poor interface quality due to the crystal lattice mismatch and different crystal orientation is a main cause of these parasitic current losses.

With successful preparation of *n*-type Cu_2O, a homogeneous Cu_2O *p–n* junction could be fabricated, and common conclusion is that the fabrication of homojunction Cu_2O with consistence crystal orientation is the only way to achieve high efficiency Cu_2O-base solar cell due to the fact that homojunction has no interface strain [10, 49-51].

Despite this conclusion, fabrication of *p-n* Cu_2O homojunction solar cells has been very limited; so far only four Cu_2O homojunction have been reported to date [22, 49, 50, 52]. Han et al, fabricated Cu_2O *p-n* homojunction by a two-step sequential electrodeposition process. a 0.8 μm

n-type Cu_2O film was first electrodeposited on a ITO coated glass substrate in an aqueous solution containing 0.01 M copper acetate and 0.1 M sodium acetate at solution pH 5.2. The deposition potential was -0.1 V and deposition temperature 60 °C. In second step a *p*-type Cu_2O film with 3.0 µm thickness was then directly deposited on *n*-type Cu_2O in an aqueous solution containing 0.4 M copper sulfate and 3 M sodium lactate at solution pH 13.0. The deposition potential was -0.5 V and deposition temperature 60 °C. They achieved efficiency of 0.15 % in a Cu_2O substrate solar cell with an area of 0.01 cm^2. They also concluded that solution pH has significant effect on the flat-band voltage and hence on open-circuit voltage. Increase in solution pH will lower the open-circuit voltage. They also found that the open-circuit voltage of the cells increases linearly with the thickness of the *p*-type Cu_2O layer, while the short-circuit current remains almost the same. The low efficiency solar cells was largely attributed to the high resistivity of both *p*-type and *n*-type Cu_2O. Therefore, they suggested doping in both *p*-type and *n*-type Cu_2O to reduce their resistivity in order to increase the efficiency [50].

Other group suggested that tuning the homojunction interface crystal orientation and forming a pyramid-like textured surface can increase the efficiency [49, 51].

2.2.1 *p*-type materials

Cu_2O having *p*-type conductivity could be produced by different methods. In electrodepostion method the most common materials for preparing *p*-type Cu_2O are copper sulfate ($CuSO_4$), sodium lactate ($NaC_3H_5O_3$, 60% w/w aqueous solution) and NaOH [11, 53]. *p*-type Cu_2O could also be prepared from a solution of copper acetate, trioctylamine ($C_{24}H_{51}N$), and oleic acid($C_{18}H_{34}O_2$) [54].

2.2.2 *n*-type materials

For electrodepostion method the most common materials for preparing *n*-type Cu_2O is aqueous solution of copper acetate and sodium acetate [33]. *n*-type Cu_2O is also prepared from Copper(II) acetate ($Cu(OOCCH_3)$, copper(II) nitrate trihydrate ($Cu(NO_3)$ and acetic acid (CH_3COOH) [55]. Immersing polished and ultrasonically cleaned copper plates in HCl solution of pH 3 at 40^oC for several hours also produce a *n*-type Cu_2O [56]. Our attempt to prepare *n*-type Cu_2O with this method was not successful. Siripala and Kumara also observed *n*-type behavior by dipping a polished copper plated in 0.5 M $CuSO_4$ stirred solution (pH=4). The pH was adjusted by mixture of NaOH and H_2SO_4 solution [57].

References

[1] http://www.iea.org/aboutus/faqs/renewableenergy.

[2] N. S. Lewis and D. G. Nocera, "Powering the planet: Chemical challenges in solar energy utilization," *Proceedings of the National Academy of Sciences,* vol. 103, pp. 15729-15735, October 24, 2006 2006.

[3] http://www.iea.org/Textbase/npsum/solar2011SUM.pdf.

[4] V. Avrutin*, et al.*, "Semiconductor solar cells: Recent progress in terrestrial applications," *Superlattices and Microstructures,* vol. 49, pp. 337-364, 2011.

[5] A. Goetzberger*, et al.*, "Photovoltaic materials, history, status and outlook," *Materials Science and Engineering: R: Reports,* vol. 40, pp. 1-46, 2003.

[6] W. M. Sears and E. Fortin, "Preparation and properties of Cu2O/Cu photovoltaic cells," *Solar Energy Materials,* vol. 10, pp. 93-103, 1984.

[7] F. Yang*, et al.*, "Identification of 5–7 Defects in a Copper Oxide Surface," *Journal of the American Chemical Society,* vol. 133, pp. 11474-11477, 2011/08/03 2011.

[8] S. Heinrich*, et al.*, "Condensation of excitons in Cu 2 O at ultracold temperatures: experiment and theory," *New Journal of Physics,* vol. 14, p. 105007, 2012.

[9] C. Sandfort, "Acoustic and optical phonon scattering of the yellow 1S excitons in Cu2O - A high resolution spectroscopy study," *Dissertation,* 2010.

[10] L. C. Olsen*, et al.*, "Experimental and theoretical studies of Cu2O solar cells," *Solar Cells,* vol. 7, pp. 247-279, 1982.

[11] A. E. Rakhshani*, et al.*, "Electrodeposition and characterization of cuprous oxide," *Thin Solid Films,* vol. 148, pp. 191-201, 1987.

[12] L. C. Wang*, et al.*, "Electrodeposited copper oxide films: Effect of bath pH on grain orientation and orientation-dependent interfacial behavior," *Thin Solid Films,* vol. 515, pp. 3090-3095, 2007.

[13] J. Liang*, et al.*, "Thin cuprous oxide films prepared by thermal oxidation of copper foils with water vapor," *Thin Solid Films,* vol. 520, pp. 2679-2682, 2012.

[14] Y. Abdu and A. O. Musa, "COPPER (I) OXIDE (Cu2O) BASED SOLAR CELLS - A REVIEW " *Bayero Journal of Pure and Applied Sciences,* vol. 2, p. 5, December 2009 2009.

[15] M. Seo*, et al.*, "Composition and Structure of Anodic Oxide Films on Copper in Neutral and Weakly Alkaline Borate Solutions," *Bulletin of the Faculty of Engineering, Hokkaido University,* vol. 102, 1981.

[16] V. F. Drobny and D. L. Pulfrey, "Properties of reactively-sputtered copper oxide thin films," *Thin Solid Films,* vol. 61, pp. 89 - 98, 1979.

[17] A. A. Ogwu*, et al.*, "Electrical resistivity of copper oxide thin films prepared by reactive magnetron sputtering," *Journal of achievements in Materials and Manufacturing Engineering,* vol. 24, pp. 172-177, 2007.

[18] M. T. S. Nair*, et al.*, "Chemically deposited copper oxide thin films: structural, optical and electrical characteristics," *Applied Surface Science,* vol. 150, pp. 143-151, 1999.

[19] N. A. Economou*, et al.*, "Photovoltaic cells of electrodeposited cuprous oxide," *In: Photovoltaic Solar Energy Conference, Luxembourg,* pp. 1180-1185, 1978.

[20] L. C. Olsen*, et al.*, "Explanation for low-efficiency Cu2O Schottky-barrier solar cells," *Applied Physics Letters,* vol. 34, pp. 47-49, 1979.

[21] A. Mittiga*, et al.*, "Heterojunction solar cell with 2% efficiency based on a Cu2O substrate," *Applied Physics Letters,* vol. 88, pp. 163502-2, 2006.

[22] K. Han and M. Tao, "Electrochemically deposited p–n homojunction cuprous oxide solar cells," *Solar Energy Materials and Solar Cells,* vol. 93, pp. 153-157, 2009.

[23] W. Siripala and J. R. P. Jayakody, "Observation of n-type photoconductivity in electrodeposited copper oxide film electrodes in a photoelectrochemical cell," *Solar Energy Materials,* vol. 14, pp. 23-27, 1986.

[24] W. P. Siripala, "Electrodeposition of n-type Cuprous Oxide Thin Films," *ECS Transactions,* vol. 11, pp. 1-10, February 8, 2008 2008.

[25] L. Xiong*, et al.*, "p-Type and n-type Cu2O semiconductor thin films: Controllable preparation by simple solvothermal method and photoelectrochemical properties," *Electrochimica Acta,* vol. 56, pp. 2735-2739, 2011.

[26] A. E. Rakhshani and J. Varghese, "Galvanostatic deposition of thin films of cuprous oxide," *Solar Energy Materials,* vol. 15, pp. 237-248, 1987.

[27] A. K. Mukhopadhyay*, et al.*, "Galvanostatic deposition and electrical characterization of cuprous oxide thin films," *Thin Solid Films,* vol. 209, pp. 92-96, 1992.

[28] A. E. Rakhshani and J. Varghese, "Surface texture in electrodeposited films of cuprous oxide," *Journal of Materials Science,* vol. 23, pp. 3847-3853, 1988/11/01 1988.

[29] T. D. Golden*, et al.*, "Electrochemical Deposition of Copper(I) Oxide Films," *Chemistry of Materials,* vol. 8, pp. 2499-2504, 1996/01/01 1996.

[30] T. Mahalingam*, et al.*, "Galvanostatic deposition and characterization of cuprous oxide thin films," *Journal of Crystal Growth,* vol. 216, pp. 304-310, 2000.

[31] Y. Zhou and J. A. Switzer, "Electrochemical deposition and microstructure of copper(I) oxide films," *Scripta Materialia,* vol. 38, pp. 1731–1738, 1998.

[32] V. Georgieva and M. Ristov, "Electrodeposited cuprous oxide on indium tin oxide for solar applications," *Solar Energy Materials and Solar Cells,* vol. 73, pp. 67-73, 2002.

[33] W. Siripala*, et al.*, "Study of annealing effects of cuprous oxide grown by electrodeposition technique," *Solar Energy Materials and Solar Cells,* vol. 44, pp. 251-260, 1996.

[34] Y. Tang*, et al.*, "Electrodeposition and characterization of nanocrystalline cuprous oxide thin films on TiO2 films," *Materials Letters,* vol. 59, pp. 434-438, 2005.

[35] R. P. Wijesundera*, et al.*, "Growth and characterisation of potentiostatically electrodeposited Cu2O and Cu thin films," *Thin Solid Films,* vol. 500, pp. 241-246, 2006.

[36] K. Jayathileke*, et al.*, "Electrodeposition of p-type, n-type and p-n Homojunction Cuprous Oxide Thin Films," *Sri Lankan Journal of Physics,* vol. 9, pp. 35-46, 2008.

[37] X. Han*, et al.*, "Characterization of Cl-doped n-type Cu2O prepared by electrodeposition," *Thin Solid Films,* vol. 518, pp. 5363-5367, 2010.

[38] X. Han and M. Tao, "Solution-based n-type doping in Cu2O and its implications for 3rd-generation cells " in *Photovoltaic Specialists Conference (PVSC), 2009 34th IEEE*, 2009, pp. 002086-002089.

[39] K. Han*, et al.*, "Enhanced crystal grain size by bromine doping in electrodeposited Cu2O," *Thin Solid Films,* vol. 520, pp. 5239-5244, 2012.

[40] X. Han*, et al.*, "n-Type Cu2O by Electrochemical Doping with Cl," *Electrochemical and Solid-State Letters,* vol. 12, pp. H89-H91, April 1, 2009 2009.

[41] J. Herion*, et al.*, "PREPARATION AND ANALYSIS OF Cu2O THIN-FILM SOLAR CELLS.," *Journal of Applied Metalworking,* pp. 917-924, 1979 1979.

[42] J. Herion*, et al.*, "Investigation of metal oxide/cuprous oxide heterojunction solar cells," *Solar Energy Materials,* vol. 4, pp. 101-112, 1980.

[43] I. Masanobu*, et al.*, "Electrochemically constructed p-Cu2O/n-ZnO heterojunction diode for photovoltaic device," *Journal of Physics D: Applied Physics,* vol. 40, p. 3326, 2007.

[44] H. Tanaka*, et al.*, "Electrical and optical properties of TCO–Cu2O heterojunction devices," *Thin Solid Films,* vol. 469–470, pp. 80-85, 2004.

[45] R. P. Wijesundera, "Fabrication of the CuO/Cu2O heterojunction using an electrodeposition technique for solar cell applications," *Semiconductor Science and Technology,* vol. 25, p. 045015, 2010.

[46] J. Katayama*, et al.*, "Performance of Cu2O/ZnO Solar Cell Prepared By Two-Step Electrodeposition," *Journal of Applied Electrochemistry,* vol. 34, pp. 687-692, 2004/07/01 2004.

[47] W. Septina*, et al.*, "Potentiostatic electrodeposition of cuprous oxide thin films for photovoltaic applications," *Electrochimica Acta,* vol. 56, pp. 4882-4888, 2011.

[48] K. Cheng*, et al.*, "Interface engineering for efficient charge collection in Cu2O/ZnO heterojunction solar cells with ordered ZnO cavity-like nanopatterns," *Solar Energy Materials and Solar Cells,* vol. 116, pp. 120-125, 2013.

[49] C. M. McShane*, et al.*, "Effect of Junction Morphology on the Performance of Polycrystalline Cu2O Homojunction Solar Cells," *The Journal of Physical Chemistry Letters,* vol. 1, pp. 2666-2670, 2010/09/16 2010.

[50] K. Han*, et al.*, "Fabrication and characterization of electrodeposited Cu2O p-n homojunction solar cells," in *Photovoltaic Specialists Conference (PVSC), 2010 35th IEEE*, 2010, pp. 003334-003337.

[51] H. M. Wei*, et al.*, "Photovoltaic Efficiency Enhancement of Cu2O Solar Cells Achieved by Controlling Homojunction Orientation and Surface Microstructure," *The Journal of Physical Chemistry C,* vol. 116, pp. 10510-10515, 2012/05/17 2012.

[52] C. M. McShane and K.-S. Choi, "Junction studies on electrochemically fabricated p-n Cu2O homojunction solar cells for efficiency enhancement," *Physical Chemistry Chemical Physics,* vol. 14, pp. 6112-6118, 2012.

[53] L. Wang and M. Tao, "Fabrication and characterization of p-n homojunctions in cuprous oxide by electrochemical deposition," *Electrochemical and Solid-State Letters,* vol. 10, pp. 248-250, 2007.

[54] B. D. Yuhas and P. Yang, "Nanowire-Based All-Oxide Solar Cells," *Journal of the American Chemical Society,* vol. 131, pp. 3756-3761, 2009/03/18 2009.

[55] C. M. McShane and K.-S. Choi, "Photocurrent Enhancement of n-Type Cu2O Electrodes Achieved by Controlling Dendritic Branching Growth," *Journal of the American Chemical Society,* vol. 131, pp. 2561-2569, 2009/02/25 2009.

[56] C. Jayewardena*, et al.*, "Fabrication of n-Cu2O electrodes with higher energy conversion efficiency in a photoelectrochemical cell," *Solar Energy Materials and Solar Cells,* vol. 56, pp. 29-33, 1998.

[57] W. Siripala and K. P. Kumara, "A photoelectrochemical investigation of the n- and p-type semiconducting behaviour of copper(I) oxide films," *Semiconductor Science and Technology,* vol. 4, p. 465, 1989.

Chapter 3 OBJECTIVE

Photovoltaic limited efficiency and the high cost of silicon solar cells are key issues for solar cell to become an alternative to the use of readily available fossil fuels. Therefore the development of new cost effective and non-toxic photovoltaic materials and energy efficient processes is essential. Transition metal oxides have a great potential to fulfill these requirements. Among them cuprous oxide (Cu_2O) has potential alternative to silicon due to its, non-toxicity and simple low-cost fabrication process from abundantly available materials. Cu_2O has direct band-gap energy of 2.0 eV and a relatively high absorption (~10^4 cm^{-1}) coefficient in the visible region. Its calculated theoretical electrical power conversion efficiency is approximately 20 % [1]. However limited understanding of the conductivity the *n*-type of Cu_2O semiconductor as well the difficulty in doping and the lack of *n*-type Cu_2O has hindered the efficient production of homojunction Cu_2O based photovoltaic cells.

Cuprous oxide is a non-stoichiometric naturally *p*-type semiconductor due to point defects such as copper excess vacancy in comparison to oxygen. Since the principles of photovoltaic relies on a *p*-*n* junction, hetero-junction Cu_2O photovoltaic cells such as ZnO/Cu_2O , CdO/Cu_2O and ITO/Cu_2O has been fabricated during the past decades, i.e., ZnO, CdO and ITO as a *n*-type material and Cu_2O as a *p*-type active material. These heterojunction cells have low conversation efficiency, with the highest efficiency of less than 2% [2]. Few publications [3-6] have demonstrated the feasibility of Cu_2O homojunction for photovoltaic applications and optimum efficiency which was claimed was around 1% [5]. Until now there are no systematic studies which evaluate the relations between the physico-chemical properties and the electrodeposition

and annealing parameters of *p*-Cu_2O and *n*-Cu_2O. These aspects are very important if we want to improve the efficiency of *p-n* Cu_2O homojunction solar cells.

The objective of the present study was to carefully evaluate the correlations between the physico-chemical properties and the electrodeposition and annealing parameters of *p*-Cu_2O and *n*-Cu_2O. This will help to identify optimum preparation parameters for high efficiency homojunction *p-n* Cu_2O solar Cell. For the first time this work will present a new approach to improve the photocurrent response due to a specific preparation of the *n*-Cu_2O. The feasibility of a *p-n* Cu_2O homojunction thin film solar cell will be also demonstrated.

References

[1] L. C. Olsen*, et al.*, "Experimental and theoretical studies of Cu2O solar cells," *Solar Cells,* vol. 7, pp. 247-279, 1982.

[2] A. Mittiga*, et al.*, "Heterojunction solar cell with 2% efficiency based on a Cu2O substrate," *Applied Physics Letters,* vol. 88, pp. 163502-2, 2006.

[3] K. Han and M. Tao, "Electrochemically deposited p–n homojunction cuprous oxide solar cells," *Solar Energy Materials and Solar Cells,* vol. 93, pp. 153-157, 2009.

[4] K. Han*, et al.*, "Fabrication and characterization of electrodeposited Cu2O p-n homojunction solar cells," in *Photovoltaic Specialists Conference (PVSC), 2010 35th IEEE*, 2010, pp. 003334-003337.

[5] C. M. McShane and K. S. Choi, "Junction studies on electrochemically fabricated p-n Cu2O homojunction solar cells for efficiency enhancement," *Physical Chemistry Chemical Physics,* vol. 14, pp. 6112-6118, 2012.

[6] C. M. McShane*, et al.*, "Effect of Junction Morphology on the Performance of Polycrystalline Cu2O Homojunction Solar Cells," *The Journal of Physical Chemistry Letters,* vol. 1, pp. 2666-2670, 2010/09/16 2010.

Chapter 4 EXPERIMENTAL METHODS AND ORGANISATION OF THE ARTICLES

Abstract. In this chapter the key experimental methods are introduced and data analysis methods are explained.

4.1 Experimental Methods

4.1.1 Scanning Electron Microscopy (SEM)

For understanding the morphology of prepared films, it is important to investigate the surface structure. Scanning electron microscopy (SEM) analysis was performed to provide micro- and nano-scale information on morphology and composition of thin film. The SEM measurements were conducted by using a FEI JEOL JSM-7600TFE scanning electron microscope. This microscope is equipped with a Field Effect Gun (FEG) for the observation of non-conducting samples and its lateral resolution is given as 1.4 nm at 1 kV and 1.0 nm at 15 kV.

Figure 4-1 shows a typical diagram to explain processes in the SEM. Electrons with high energy are accelerated towards the sample surface from the filament source. The scattered electrons provide surface topography information. In addition, X-ray emission from the sample is caused by electron excitation (inner electrons) after electron impact. Energy dispersive X-ray spectroscopy (EDX) is an analytical technique for surface elemental analysis. By exposing the material to high energy electrons (15 keV in the present work) excitation (inner electrons) after electron impact EDX can be measured. This process excites the atoms and consequently some of the core electrons move from the ground state (unexcited state) to a higher energy level or they are emitted leaving an electron hole. Then there are two possibilities: (i) either an electron from

an outer, higher-energy shell falls back into this hole causing characteristic X-ray emission lines (EDX) or (ii) a second electron is emitted when the electron drops into the ground state to refill the position (Auger effect, only for light elements). The difference in energy between the higher energy shell and the lower energy shell may be released in the form of characteristic X-rays in EDX. Energy dispersive spectrometer can be used to count the energy of the X-rays emitted from a specimen. Because of the energy of the X-ray is characteristic for the difference in energy between the two atomic shells, the type of element and the approximate concentration can be determined. In this study we will use these methods of analysis to determine the morphology and the chemical composition of the electrodeposited Cu_2O. The SEM will be used to determine the grains size of the electrodeposited thin films in various experimental conditions. The effect of these experimental electrode position and heat treatment conditions will be evaluated using these methods.

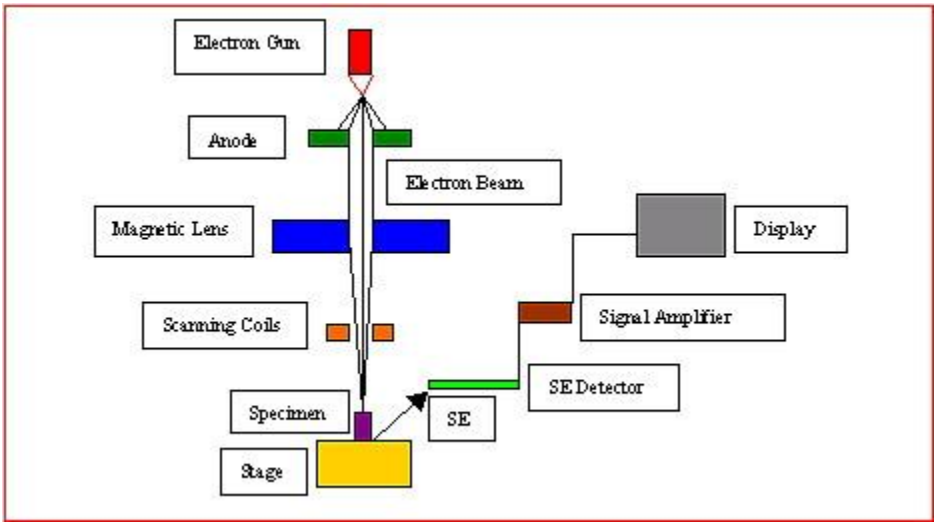

4-1 Schematic illustration of SEM[8].

[8] http://nanoart21.org/sem.html

4.1.2 X-ray Diffraction (XRD) Techniques

X-ray crystallography is a fundamental experimental techniques used for determining the atomic and molecular structure of a crystal. X-ray diffraction is a non-destructive rapid analytical technique primarily used for phase identification of a crystalline material which can yield the unique fingerprint of unit cell dimensions by Bragg reflections associated with a crystal structure. One can regard a crystal structure as being built of layers, or planes, which each act as a semi-transparent mirror. X-rays with a wavelength similar to the distances between these planes can be reflected such that the angle of reflection is equal to the angle of incidence.

The X-ray region is located in the section of the electromagnetic spectrum in the wavelength range between 0.1-100 Å. Like all electromagnetic waves, X-rays can be viewed as both of flow of photon particles and a wave of energy and they can be characterised by their energy. The energy is given by the product of the inverse wavelength (λ), the Planck constant (h), and the frequency (υ)

$$E = h\upsilon \qquad (1)$$

$$\upsilon = {}^{c}/_{\lambda} \qquad (2)$$

Here c is the speed of light, h is the Planck constant. From equation (1) and (2) the photon energy can be calculated (eq. 3).

$$E = \frac{hV}{\lambda} \qquad (3)$$

Thus, X-ray wavelengths are short and they have comparably higher energy. X-rays can be produced when high energy electrons emitted from a hot filament (cathode) strike a heavy

metallic target (anode). Usually, the cathode can be maintained at a potential of 30 to 50 kV relative to the anode. The electrons librated from the heated filament and accelerated by high voltage towards the metal target.

A crystal structure can be regard as building of layers, or planes, which each act as a semi-transparent mirror. X-rays with a wavelength similar to the distances between these planes can be reflected reinforce one another in certain direction according to Bragg's law of diffraction.

$$n\lambda = 2d\ \sin\theta \qquad (4)$$

where *n* is an integer, *d* is the spacing between the adjacent crystal planes, θ is the angle between incident X-ray beam and scattering plane, and λ is the wavelength of incident X-ray. These diffracted X-rays are then detected, processed and counted. By changing the geometry of the incident rays, the orientation of the centered crystal and the detector, all possible diffraction directions of the lattice should be attained. Figure 4-2 illustrates the interaction of the electromagnetic wave and the crystal planes.

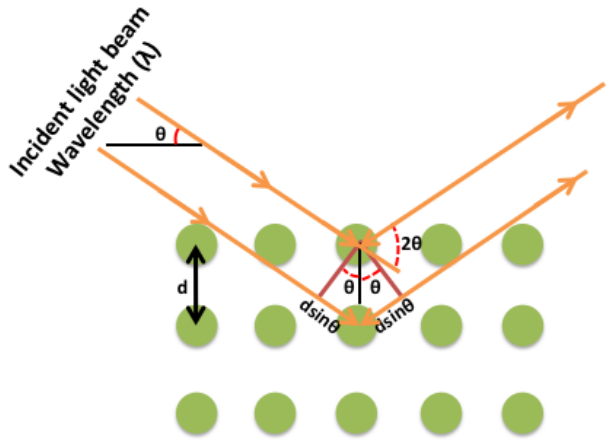

4-2 Schematic drawing illustrating X-ray diffraction and Bragg's Law[9].

[9] http://cnx.org/content/m46154/1.2/

In this work the purity and crystal phases of each Cu_2O layers were examined by X-ray diffraction (XRD). XRD data acquisition was done using a Philips X'Pert diffractometer equipped with Cu Kα radiation (λ = 1.5406 Å) (at 50 kV and 40 mA) in a scan range (2θ) from 20° to 90° and data analysis was carried out using the Panalytical X'pert Highscore Plus program. The high resolution of the equipment (min step 0.0001° in detector and omega, best instrumental resolution ~0.003° in omega & omega/2theta) will allow us to determine properly the detection of the XRD the main patterns of the electrodeposited films for various experimental conditions.

4.1.3 Current-Voltage Characterisation

A photovoltaic cell may be represented by the equivalent circuit model described in section 2.1.1.1 and shown in Figure 2-2, consisting of a photon current source (I_L), a diode, a series resistance (R_s), and a shunt resistance (R_{sh}).

Critical PV cell performance parameters, such as the equivalent cell shunt and series resistance and the electrical conversion efficiency and fill factor, may be determined from I-V measurements. The cell must be maintained at a constant temperature and a radiant source with a constant intensity and a known spectral distribution must be used.

This test involves generating the forward biased I-V curve between the two points ($V_1 = 0$, $I_1 = I_{sc}$) and ($V_2 = V_{oc}$, $I_2 = 0$). The parameters V_{oc} and I_{sc} can be directly determined from the curve and I_{mp}, V_{mp}, P_{max}, FF, and η are easily calculated. Additional analytical techniques may be used to determine R_s and R_{sh}.

The reverse bias I-V curve test is performed in the dark between 0V and the level where breakdown begins to occur. In this region, the slope of the current-voltage characteristic can be used to estimate the shunt resistance (R_{sh}).

4.1.4 Photocurrent characterization

The optical properties of the films were determined by photocurrent characterization carried out in a custom built three-electrode electrochemical cell based on Photoelectrochemical cell (PEC) described in section 2.1.4. A Pt mesh, Ag/AgCl reference electrode, and the Cu_2O film were used as the counter, reference, and working electrode, respectively. The illumination switch was controlled manually to chop the light in certain time intervals. For photocurrent measurements, using Princeton Applied Research potentiostat, the electrolyte was an aqueous solution of 0.5 M sodium acetate. To avoid false signals rising from oxygen reduction, the electrolyte was continuously purged with N_2 to remove oxygen.

The conversion of photon of light into electrical energy was characterized by solid-liquid junction called Photo-electrochemical cell (PEC). The PEC consists of the Cu_2O film semiconductor deposited on ITO coated class as the working electrode, a carbon rod electrode as counter electrode and Ag/AgCl reference electrode. The electrolyte was sodium hydroxide at pH 8.5. A xenon lamp was used to illuminate the semiconductor surface through the electrolyte to get an equivalent of 100 mW/cm^2 at the semiconductor surface. The PEC was characterized by measuring current voltage characteristics in dark as well as under illumination in the same cell used for photocurrent characterization.

4.2 Organisation of Articles

This thesis consists of the following two articles;

1. Electrochemically deposited *n* and *p* type Cu_2O thin films and their characterization for photovoltaic applications.
2. Photocurrent enhancement of *n*-type Cu_2O fabricated under different gas atmospheres in the electrolyte.

Chapter 5 ARTICLE 1: ELECTROCHEMICALLY DEPOSITED *n* AND *p* TYPE Cu_2O THIN FILMS AND THEIR CHARACTERIZATION FOR PHOTOVOLTAIC APPLICATIONS

S. M. Shahrestani and O. Savadogo

Laboratory of New Materials for Electrochemistry and Energy

École Polytechnque de Montréal, Canada, H3C 3A7

Submitted to the Materials Research Bulletin, on November, 2013

Abstract

Polycrystalline *p*-Cu_2O and *n*-Cu_2O thin films were electrodeposited in aqueous electrolytes on copper sheet or Indium tin oxide (ITO) coated glass. The effect of the electrodeposition parameters on the resistivity and the photo-response of the films were determined. The best electrolyte and potential for the electro-deposition of *n*-Cu_2O was determined for the first time. A two-step electrodeposition process is implemented to fabricate *p-n* homojunction cuprous oxide on ITO substrate which was used as a transparent conductive oxide for the homojunction Cu_2O solar cell. The photovoltaic performance of a *p-n* Cu_2O homojunction solar cell was determined. The short circuit current and open circuit voltage are respectively determined as 235 microA/cm^2 and 0.35 Volt. The fill factor (*FF*) and the cell conversion efficiency of light to electricity are determined to be respectively 0.305 and 0.082%.

Key Words: Electro deposition, *p* and *n* type Cu_2O thin films, homojunction, photovoltaic solar cells

5.1 Introduction

Despite the tremendous progress in all aspects of production of Si-based solar cells and the rapid decrease of production cost for PV modules from $5 per peak watt at the beginning of the 1990s to $2.5 per peak watt in 2010, or $0.7 per kWh, this remains effectively too high[1]. A cost level of $0.50 per peak watt would make solar light conversion very attractive for large-scale application of solar light conversion devices. This will also make solar cell more competitive than fossil fuel resources for various large applications. A total solar cell cost of $130 m^{-2} with a light conversion efficiency of 50% is necessary to reach this peak watt cost. There is no current solar cell technology which meets these two requirements. From basic scientific principles, these requirements are feasible but the development of related commercial devices is facing major scientific as well as engineering development challenges.

Thin-film materials and nanomaterials are based on material layers the thicknesses of which range from monolayer's of nanometers to several micrometers. Among them various transition metal oxides including cuprous oxide (Cu_2O) have a great potential as an alternative to Si-based solar cell. Cuprous oxide has direct band-gap energy of 2.0 eV, a relatively high absorption coefficient in the visible region. Cu_2O is an abundant and low cost material satisfying economical and environmental requirement necessary for large scale applications [2]. Its calculated theoretical electrical power conversion efficiency is approximately 22%; however practical efficiencies of around 11%-14% are a realistic achievable goal [3, 4]. This makes it an attractive material for solar cell applications; yet, the experimental efficiencies obtained up to this date are much lower than expectation values. The best efficient Cu_2O-base heterojunction solar cell was reported recently by Mittiga et al. with efficiency of 2% [5]. This low efficiency is attributed

to the lack of *n*-type Cu_2O, which prevents formation of a homogeneous Cu_2O *p*–*n* junction [3, 6]. Cuprous oxide is non-stoichiometric naturally *p*-type semiconductor due to point defects. Sears et al. 1984 reported that an excess of oxygen, as a result of stoichiometry, is the major active impurity and gives a *p*-doped semiconductor [7]. Others attributed *p*-type conductivity to presence of Cu vacancies [8-10].

Cu_2O thin films are prepared by various methods such as thermal oxidation, anodic oxidation, chemical deposition, sol–gel chemistry, sputtering, electrodeposition and other gas-phase deposition techniques [11-13]. All these methods produces *p*-type Cu_2O semiconductor.

The first *n*-type behavior of Cu_2O was reported by Siripala and Jaykody. They implement electrodepostion techniques to produce *n*-Cu_2O thin films. They attributed the *n*-type behavior of Cu_2O to oxygen vacancies and/or additional copper atoms [14].

Electrodeposition is simple, low cost and low-temperature process. Control of film quality and possibility of making large area thin films onto conductive substrates can be achieved easily by electrodepostion. In electrodeposition, the electrical conductivity (*n*-type or *p*-type) can be modify more easily by variation of semiconductor's composition during the electrodeposition of films [14-18]. However better understanding of point defects and doping process is required to produce optimal *n*-type Cu_2O and hence feasible fabrication of Cu_2O *p*-*n* junction for higher efficiency photovoltaic application.

It has been reported that the structural properties, such as the crystal orientation, grain size, surface texture of electro-deposited Cu_2O films in acetate bath is affected by bath pH and applied potential. At bath pH~9.0, the (100) planes are produced and in higher bath pH~11.0, the (111) planes are produced [13, 19, 20]. In addition to these preferred orientation a narrow pH range,

~9.4-~9.9 showed a third preferred orientation namely (110) [13]. At higher bath pH, Cu ions diffuse to the surface, form the Cu vacancies and hence produce *p*-type films, while at lower pH values the oxygen vacancies will produce *n*-type conductivity [14, 21-23]. However, why pH can influence vacancy type, and thereby the conduction type of Cu_2O, is not yet explained clearly**.** Moreover the resistivity of *n*-type Cu_2O film produced by electrodepostion techniques remains high in the range of ($10^6 – 10^8$ ohm/cm) [6, 17].

The objective of the present study was to carefully prepare *p*-type and *n*-type Cu_2O thin films by simply adjusting the pH of the copper (II) acetate aqueous solution. Photoelectrochemical characterization confirmed that Cu_2O films deposited in acidic and alkaline media show *n*-type and *p*-type behavior, respectively. We have systematically investigated the deposition conditions.

5.2 Experimental methods

5.2.1 Preparation of Cu_2O

5.2.1.1 Preparation of working electrode

Two different substrates were used as the working electrodes for the electrodeposition of Cu_2O. One was transparent conducting oxide - ITO (indium tin oxide) on glass substrate with a sheet resistance of 18Ω/cm. The other one was Copper foil with a thickness of 18 µm.

Prior to the film deposition, ITO/glass and Cu foil were degreased in ultrasonicated acetone for 15 minutes, rinsed in de-ionized water. The degreasing process is to remove dirt, loose particles, grease, oil, and other surface organic contaminants by immersion of the working sample into a bath of solvent. Ethanol and isopropanol can also be used as cleaning solvent. The

ultrasonic source will create very high frequency cavitation of the solvent forming thousands of small bubbles which then collapse. This constant formation and collapsing action scrubs the surface of sample, helping to remove insoluble soils and particulates. For more efficient results this process was carried out at temperature of 50 °C. After degreasing process, the samples are rinsed in de-ionized water.

After cleaning process, chemical etching was performed on samples to remove inorganic contamination and native oxides on sample surface. ITO/glass and Cu foil were etched chemically, in diluted hydrochloric acid (HCl) and nitric acid respectively for 2 minutes, and finally rinsed in de-ionized water.

5.2.1.2 Preparation of solution

Two different electrolyte solutions were used for Cu_2O electrochemical deposition. For the electro-deposition of *p*-type Cu_2O, the electrolyte was the aqueous solution of 0.4 M copper sulfate and 3M sodium lactate ($NaC_3H_5O_3$, 60% w/w aqueous solution) [11]. Copper sulfate was first dissolved in de-ionized water then 3M sodium lactate was added to the solution. Sodium lactate works as the complexing agent to stabilize the Cu^{2+} ion at high pH values and prevent it to precipitate when NaOH is added to the solution. For *n*-type Cu_2O, the electrolyte solution was the aqueous solution of 0.01M copper acetate and 0.1M sodium acetate [15]. Sodium acetate was introduced as a background electrolyte into solution to remove migration effect and also acts as a conductor to help the passage of current thought the solution. All chemicals were from commercial sources. They were used without further purification. All solutions in this study were prepared from de-ionized water.

5.2.1.3 Electro-deposition parameters and procedure

A single-compartment, three-electrode electrochemical cell, as illustrated in Figure 5.1, was used for film deposition. Electrodeposition was carried out with a Princeton Applied Research potentiostat 273A. The commercial Ag/AgCl (4M KCl) and Pt mesh were used as the reference and counter electrode, respectively. The electrolyte was kept in a water-jacked cell and the temperature was controlled between 30°C and 70 °C by a Polystat circulation water bath. The electrodeposition was carried out in the potentiostatic mode at different applied potential values with respect to the reference electrode. The applied potential window was chosen from cyclic voltammetry (CV) or linear voltammetry (LV). After deposition, the films were rinsed in de-ionized water and dried at room temperature.

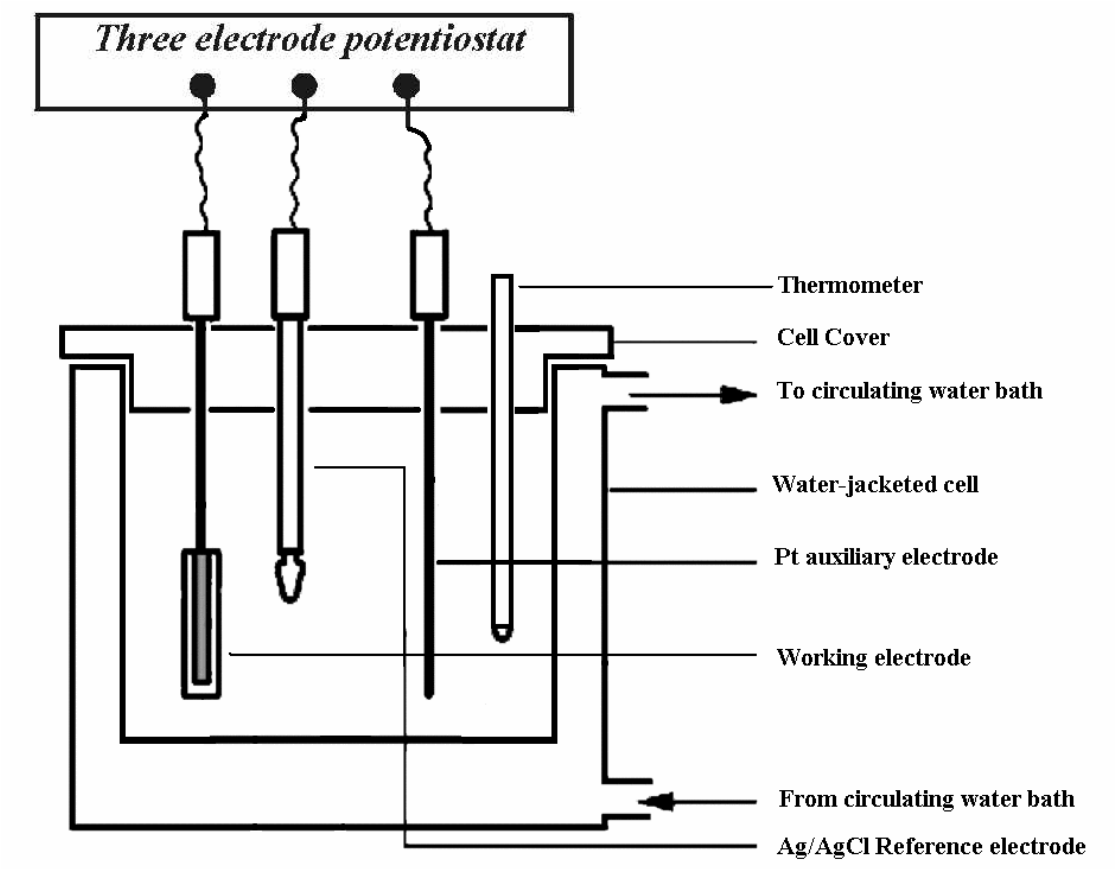

Figure 5-1 Schematic representation of the electrochemical cell used in this study.

5.2.2 Characterization

Linear voltammetry (LV) at slow scan rate was used for the initial characterization and identifying the electrochemically redox processes. LV measurements were performed in the same single-compartment, three-electrode electrochemical cell used for electrodeposition. The potential was applied between the reference electrode and the working electrode and the current was measured between the working electrode and the counter electrode. The linear voltammetry was performed prior to each deposition for each new solution with different pH.

To investigate the influence of bath pH on voltammetric curve, baths with different pH values were prepared. The pH of the bath was controlled by adding different amounts of NaOH in the electrolyte. As an example, the temperature of the bath was fixed at 60 °C in the solution containing 0.4M copper sulfate and 3M sodium lactate. A shift in the peak cathodic peak potential to negative values was noticed when the pH increases.

The surface morphology of the films was studied using FEI JEOL JSM-7600TFE scanning electron microscope (SEM). The purity and crystal phases of each Cu_2O layers were examined by X-ray diffraction (XRD). XRD data acquisition was done using a Philips X'Pert diffractometer equipped with Cu Kα radiation (λ = 1.5406 Å) (at 50 kV and 40 mA) in a scan range (2θ) from 20° to 90°. The optical properties of the films were determined by photocurrent characterization carried out in a custom built three-electrode electrochemical cell. A Pt mesh, Ag/AgCl reference electrode, and the Cu_2O film were used as the counter, reference, and working electrode, respectively. The illumination switch was controlled manually to chop the light in certain time intervals. For photocurrent measurements, using Princeton Applied Research potentiostat, the electrolyte was an aqueous solution of 0.5 M sodium acetate. To avoid

false signals raising from oxygen reduction the electrolyte was continuously purged with N_2 to remove oxygen.

The conversion of photon of light into electrical energy was characterized by solid-liquid junction called Photo-electrochemical cell (PEC). The PEC consists of the Cu_2O film semiconductor deposited on a ITO coated class as the working electrode, a carbon rod electrode as counter electrode and a Ag/AgCl reference electrode. The electrolyte was sodium hydroxide at pH 8.5. A xenon lamp was used to illuminate the semiconductor surface through the electrolyte to get an equivalent of 100 mW/cm^2 at the semiconductor surface. The PEC was characterized by measuring current voltage characteristics (I-V) in dark as well as in light in the same cell used for photocurrent characterization.

I-V measurements were performed to determine the resistivity of *p*-type Cu_2O films. Due to highly conductive substrate (copper substrate) it was difficult to characterize the electrical properties of *p*-type Cu_2O films by standard Four-point probe measurements. Therefore a circular Cu electrode was placed on top of Cu_2O films. A voltage was sweep between the substrate and the top electrode and the current was measured at room temperature with the Princeton Applied Research potentiostat 273A. From the slope of I-V curve, the area of top electrode, and the thickness of deposited film, the resistivity was determined.

$$\boldsymbol{\rho = \frac{V \times A}{d \times I}} \qquad (\mathbf{1})$$

Where ρ is the resistivity of the Cu_2O film, A is the area of the top electrode, d is the thickness of the Cu_2O film, V is the applied voltage, and I is the measured current. The thickness of Cu_2O film was estimated from the following equation assuming that two electrons are consumed for

the formation of one molecule of Cu_2O or Cu and that no parallel charge transfer other than that leading to deposition of Cu_2O or Cu is taking place at the deposition potential.

$$\boldsymbol{d = \frac{M}{nA\sigma Ne} Q} \qquad (\mathbf{2})$$

Where *d, n, A, Q, M, σ, N and e* are film thickness, number of electron in the electrochemical reaction (2 for Cu^{2+}), area, total charge passed during deposition, molecular weight of the deposit, mass density of the film, Avogadro's number and electron charge respectively. In the calculation it was assumed that only a single phase of Cu_2O or Cu was deposited and the density of Cu_2O film was 6 g/cm^3. The thickness of film where there is co-deposition of Cu_2O and Cu could not be estimated with this formula.

5.3 Results and discussion

5.3.1 *p*-Cu_2O

A linear voltammetry performed in a bath pH 12.5 in shown in Figure 5.2. This Voltammogram was performed in a deposition solution at bath temperature of 60 °C between 0. 05 and -1.0 V vs. Ag/AgCl at a scan rate of 10 mV/s. Two cathodic regions are absorbed, the first region placed around -0.2 to -0.6 V vs. Ag/AgCl and second region around -0.8V. The first peak is attributed to the reduction of Cu^{2+} to Cu^{+} and hence to Cu_2O and the second peak to the formation of copper according to the following respective reactions.

$$\boldsymbol{2Cu^{2+} + H_2O + 2e^- \Rightarrow Cu_2O + 2H^+} \qquad (\mathbf{3})$$

$$Cu^{2+} + 2e^{-} \Rightarrow Cu \qquad (4)$$

This is in agreement with previous works [20, 23-25]. These results show clearly that the deposition potential of *p*-Cu_2O should be in the range of -0.15 V to -0.6 V, although this range depends on the bath temperature.

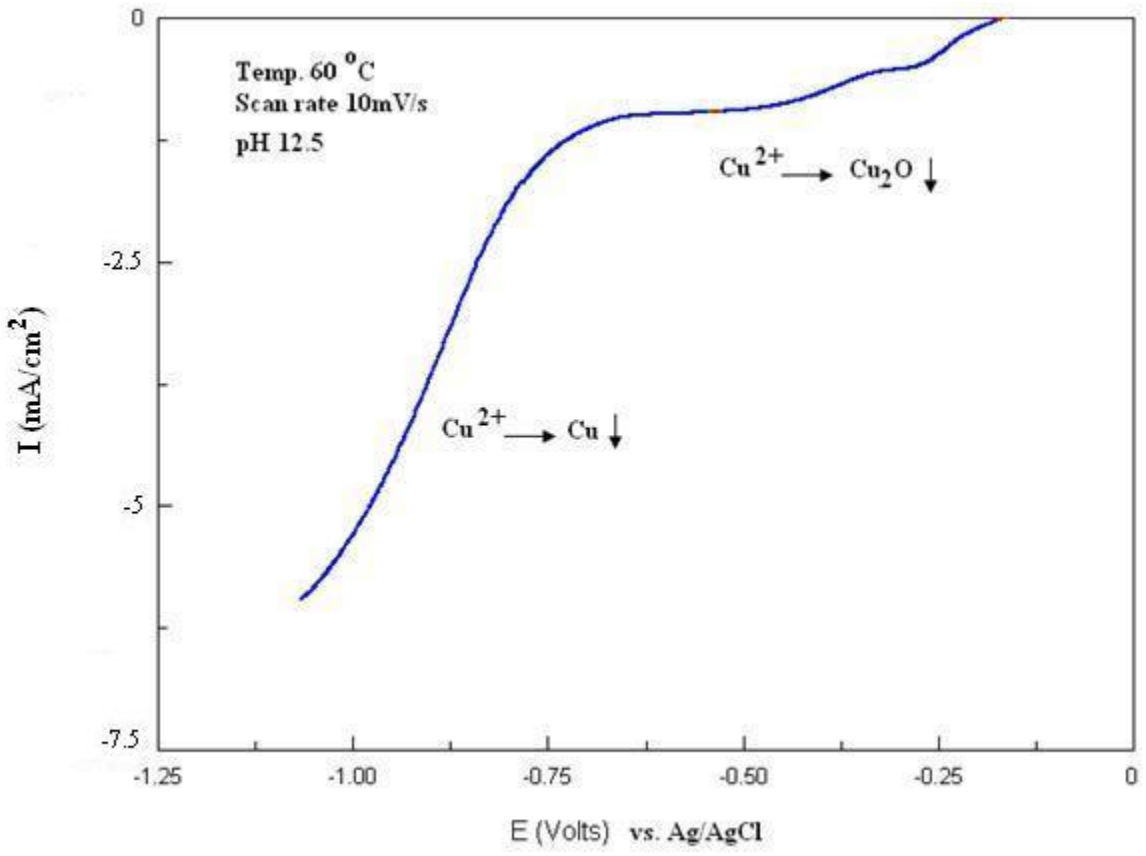

Figure 5-2 Linear voltammogram of solution containing 0.4M copper sulfate and 3 M sodium lactate on copper foil substrate with given parameters.

Figure 5.3 shows that the deposition current increases with the pH of the deposition bath. The pH change was controlled by adding different amounts of NaOH. The cathodic current peaks are

shifted to the negative potential side when the pH of the bath increases. This indicates that the window of potentials to electrodeposits Cu_2O is more important at high pH values.

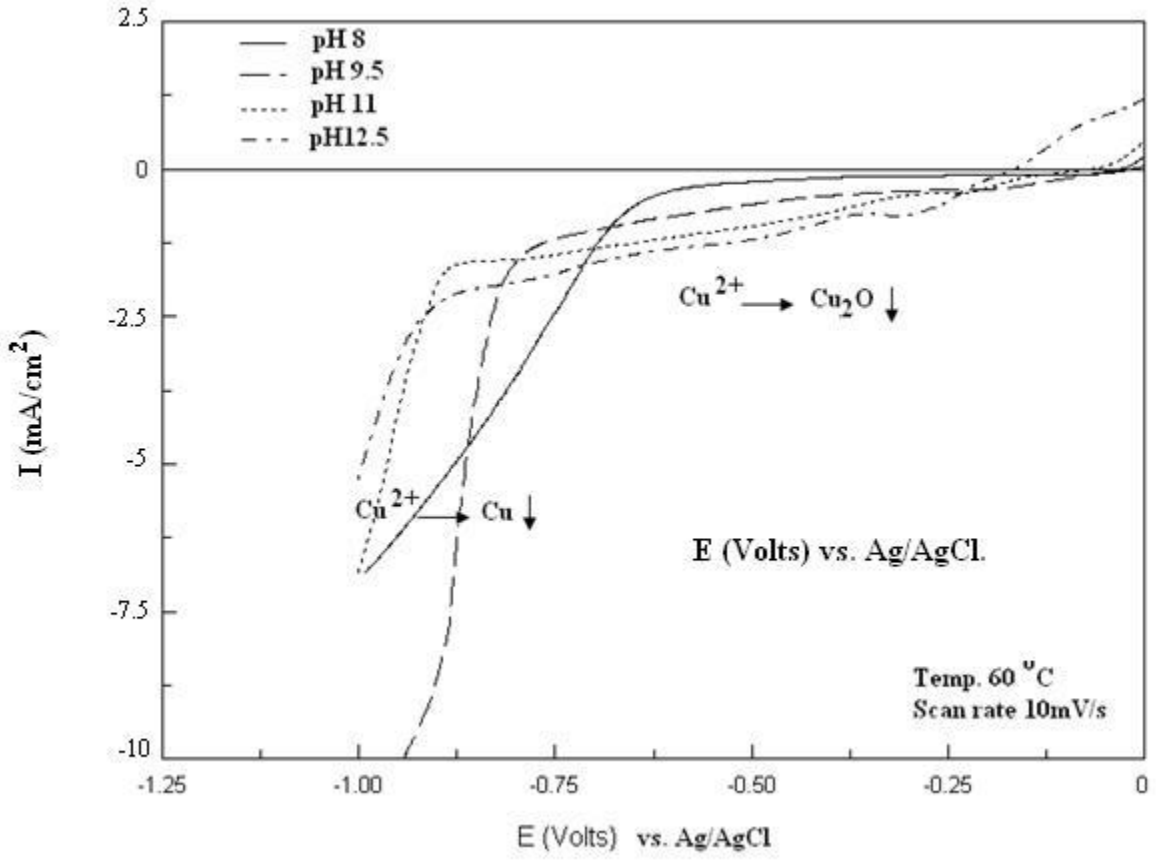

Figure 5-3 Voltammetric curves of a copper foil in an electrochemical cell containing 0.4M copper sulfate and 3 M sodium lactate at different bath pH (pH was adjusted by adding 1M NaOH).

Figure 5.4 shows the voltammetric curves obtained using the solution of 0.4M copper sulfate and 3M sodium lactate at pH 9 and temperatures from 50 to 80^{o}C. The electro-deposition current increases and the cathodic peaks are slightly shifted to the negative potential side when the temperature increases. Therefore, the electro-deposition current increases with the temperature. This might be due to the improvement of the electro-deposition rate with the increase of the temperature.

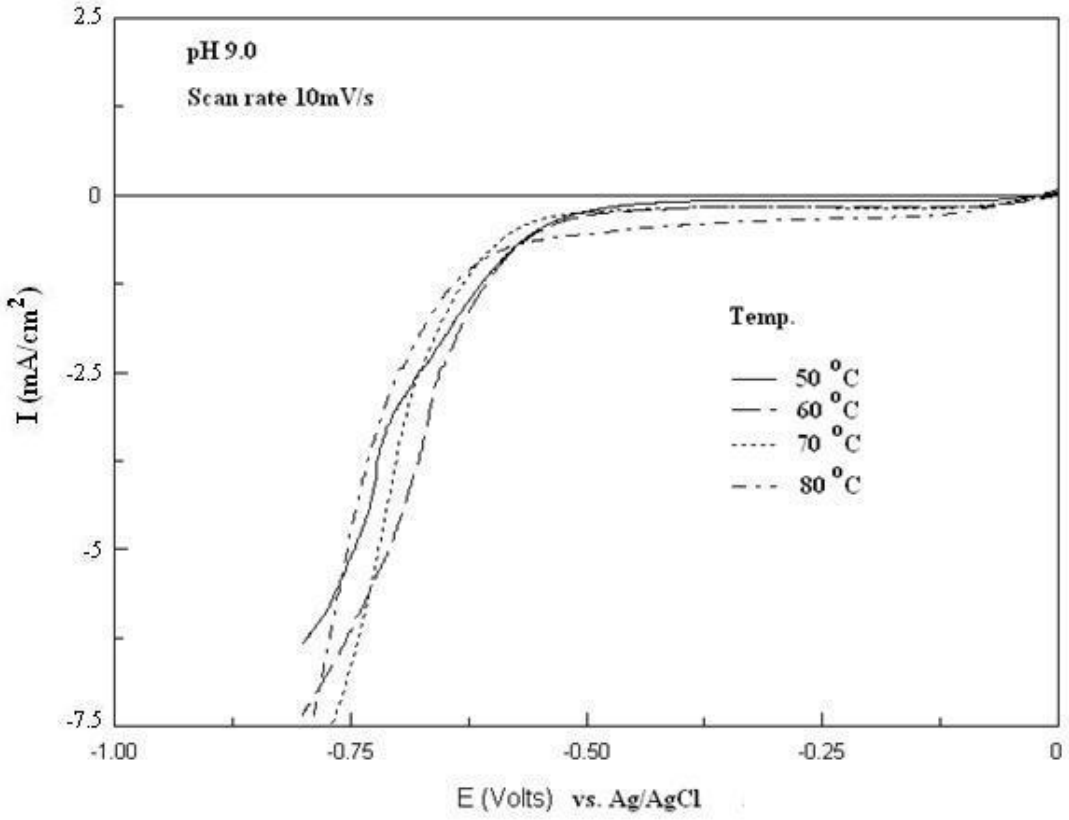

Figure 5-4 Voltammetric curves of a copper foil in an electrochemical cell containing 0.4M copper sulfate and 3 M sodium lactate at a pH of 9 and different temperatures.

Accordingly, to determine the effect of the pH of the bath on the properties (crystal shape and orientation, surface morphology, and photo-response) of the electrodeposited films, several samples were electro-deposited respectively in an aqueous solution containing 0.4M copper sulfate and 3 M sodium lactate at a potential between -0.3 V and -0.6 V vs. Ag/AgCl reference electrode and at pH between 8.5 and 13. As shown in Figure 5.3, the electro-deposition potential between -0.3 V and -0.6V may allow the deposition of Cu_2O without copper deposition which appears at higher negative potential and current densities. Reproducible experimental results we got in this study have also shown that making *p*-Cu_2O electro-deposition close to this potential of -0.3 V ensures a reasonable deposition rate of the film, since we did not obtained any film for

deposition performed at -0.2 V. This is supported by the following results on the growth rate with time.

To determine the effect of the pH of the electrodeposition electrolyte on the electrodeposited films properties, several samples were electrodeposited in an aqueous solution containing 0.4M copper sulfate and 3 M sodium lactate by selecting the applied potential at a fixed value of -0.3 V versus the Ag/AgCl reference electrode and different pH values between 8.5 and 13. This fixed deposition potential is chosen according to voltammetric curves for having reasonable deposition rate.

X-ray Diffraction method (XRD) was used to further investigate the structure of the Cu_2O films. For this purpose, samples were electro-deposited at a potential of -0.3 V and cupper sulfate based electrolyte with pH varying from 9 to 13. We have verified experimentally that all the samples deposited at this potential and the various pH (from 9 to 13) are composed of pure Cu_2O without any traces of CuO deposits on the films. All samples deposited at selected pH range of 9 to 13 were crystalline. An example of the XRD patterns is shown in Figure 5.5 for the films deposited at pH 9 and pH 13.

The quality of the films we obtained experimentally in this work (chemical composition, morphology, reproducibility of preparation of the films, etc.) indicates that the appropriate *p*-Cu_2O films are obtained when the pH is between 9 and 13 and deposition potential range is between -0.3 to -0.6 Volt vs. Ag/AgCl.

Figure 5.6.a shows the growth rate of *p*-type Cu_2O as a function of the deposition time for several samples were electro-deposited using electrolyte of at pH 11.6. For all samples the electro-deposition potential was -0.32V. Film thickness was determined from careful weighing

method using a density of 6.0 gcm^{-3}. The details of these calculations are given in annex A. The thickness of the Cu_2O layer increases with the electro-deposition time between 10 and 30 minutes. Experimentally, we have obtained that when the electro-deposition time is less than 3 minutes no film is obtained. Consequently thicknesses before 5 minutes were not determined.

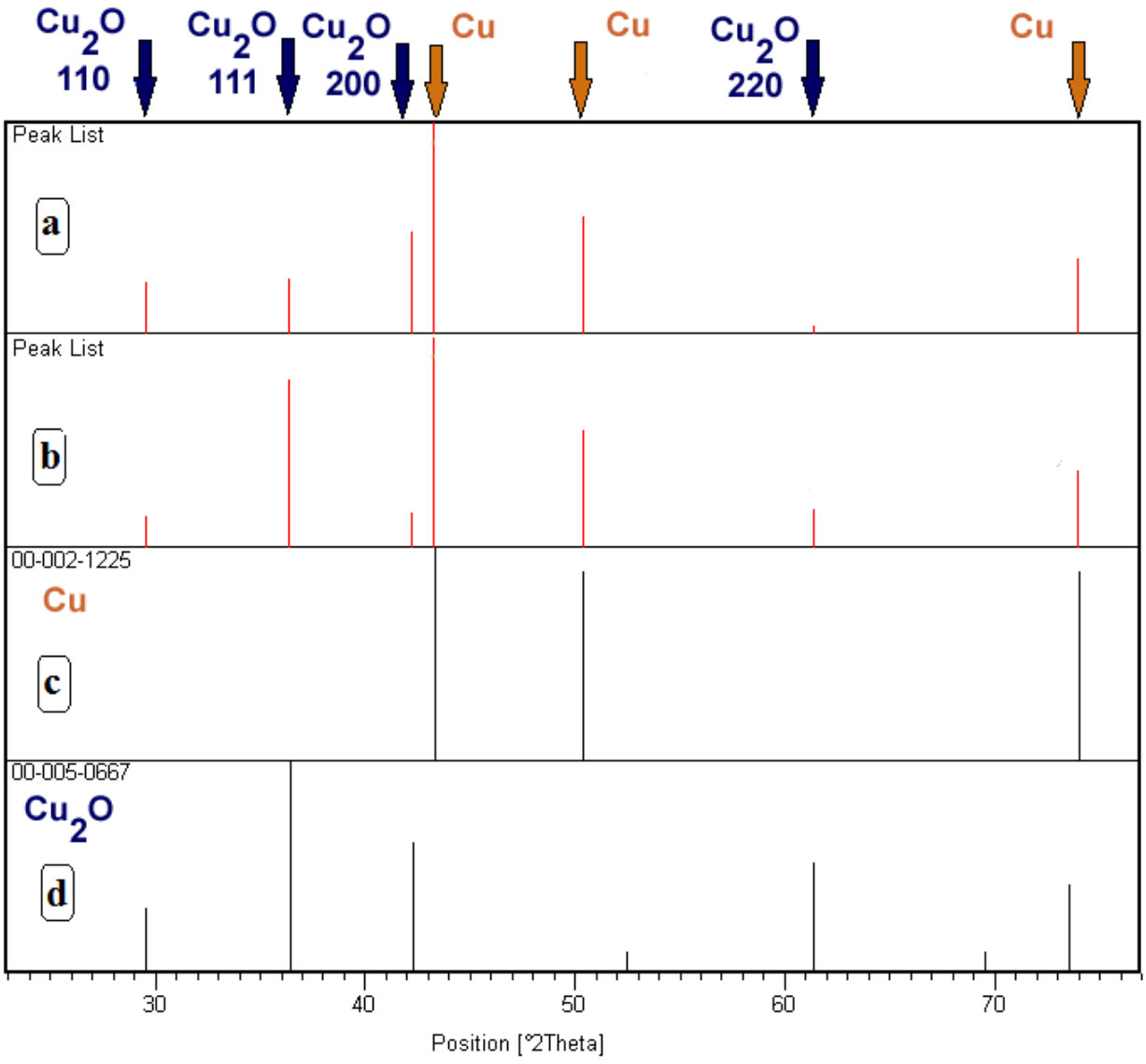

Figure 5-5 XRD spectra of electrodeposited Cu_2O film obtained using bath containing 0.4M copper sulfate and 2 M sodium lactate. The electro-deposition potential and pH is respectively -0.3 Volt a) pH 9 and b) ph 13. c) Reflections of Cu substrate according to the JCPDS card (2-1225). d) Reflections of Cu_2O according to the JCPDS card (5-0667).

The variation of the thickness (named *Y* in microns) of the electro-deposited *p*-Cu_2O of the sample with time (named *x* in minutes) are in the form:

$$\boldsymbol{Y = 1.51 \ln x - 1.4} \qquad (\mathbf{5})$$

In first approximation, this type of curve is an indication that the deposition is limited by the diffusion of the species involved in this electro-deposition process or by their mass transfer process at the electrode surface. This is supported by the experimental results we have obtained and which have shown the non significant variation of the *p*-Cu_2O thickness with the applied current density (from -0,5 to -2 mA/cm^2 the thickness variation is less than 10%) for the same electro-deposition potential.

In comparison Figure 5.6.b the growth rate of *n*-type Cu_2O (the *n*-type electro-deposition will be discussed in paragraph 3.2) as a function of the electro-deposition time for several samples using electrolyte of at pH 5.5. In Figure 5.6.b the variation of the thickness (named *Y* in microns) with time (named *x* in minutes) is in the form:

$$\boldsymbol{Y = 2.087 \ln x - 7.54} \qquad (\mathbf{6})$$

In first approximation, this type of curve is an indication that the deposition is limited by the diffusion of the species involved in this electro-deposition process or by their mass transfer process at the electrode surface.

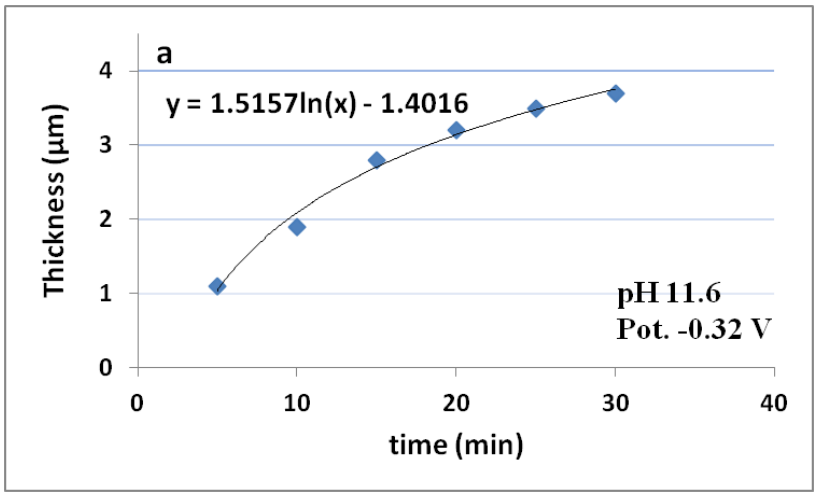

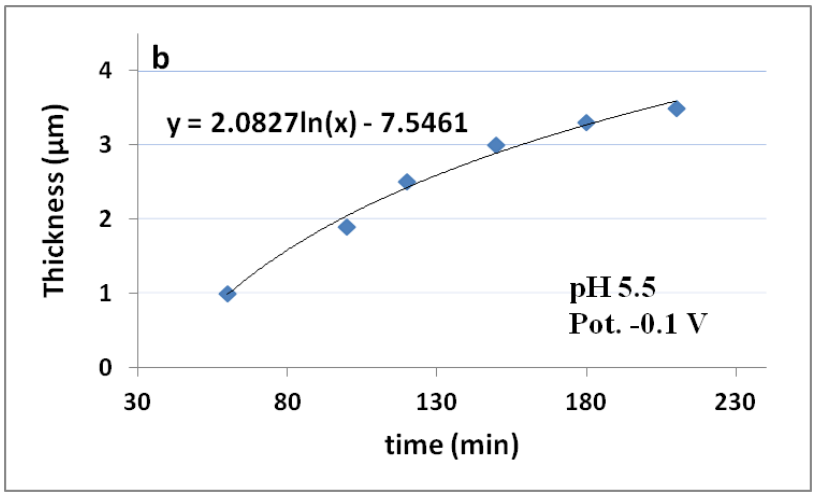

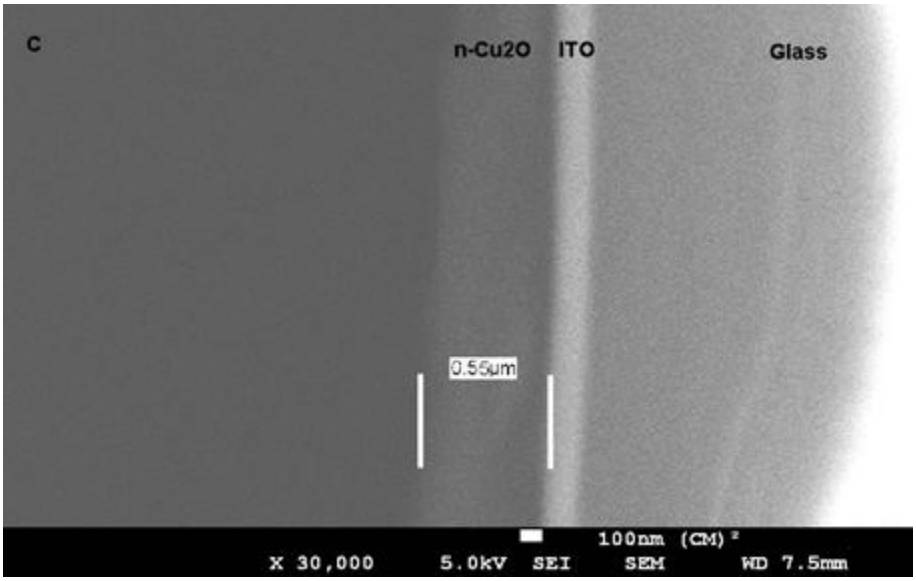

Figure 5-6 Thickness vs deposition time of a) *p*-type Cu_2O deposited at 60 °C in solution pH 11.6; b) *n*-type Cu_2O deposited at 60 °C in solution pH 5.5. c) SEM of *n*-type Cu_2O film deposited on ITO, deposition time 50 min.

The relations (5) and (6) show also clearly that the Faradic law e.g. the linear variation between the deposited mass and the deposition time is not obtained. This might indicate that the side reactions as the hydrogen evolution reaction are also involved during the Cu_2O electrodeposition. The side reactions are more important at higher deposition time. However if we consider the reaction rate as

$$\boldsymbol{r = \frac{I}{nFA}} \qquad (7.a)$$

Where, *r*, *I*, *n*, *F* and *A* are the reaction rate, the current, number of electrons involved in the reaction, The Faraday number (~96500 coulombs per mole) and the electrode area respectively. Trough the classical Faraday law, the reaction rate represents (mol/sec.area), and is an index of mass per time or thickness per time formation rate because the mass is proportional to the thickness. For a constant current density (*i/A*) during a fixed deposition time, the relation between the thickness and the deposition time must be linear. But, in this study (Figs. 5.6), it is not the case because the value (current density) is not a constant with the deposition time; Here the voltage was the constant parameter, and therefore, the current density might change with respect to the change of the deposited film resistance.

$$\boldsymbol{d = \frac{ItM}{\rho nF}} \qquad (\boldsymbol{7.b})$$

Where *d*, *I*, *t*, *M* and ρ are the thickness, the current density, the deposition time, the molar mass and the density of the deposited film respectively.

As the thickness or/and sides reactions are increasing with time, consequently the total resistivity or/and the current due to side reactions increase as well. Therefore when the resistivity or/and side reactions increases, for a constant voltage, total useful current for the film deposition will

decrease. Hence, reaction rate which is a variable of the useful current density for the film deposition will decrease during the time causing the decrease in the thickness with time.

This thickness of the film was also evaluated by SEM. The *n*-Cu_2O film was deposited on ITO substrate for 50 minutes. Using the classical Faraday Law between the thickness and the deposition time for *n*-Cu_2O films, the thickness of this deposited film calculated as 0.6µm. A cross section SEM image (Figure 5-6.c) was taken from this sample. Based on the SEM image obtained from the film; the thickness was measured as 0.55µm. Therefore there is an agreement between the theoretical and the experimental values of the thickness of the *n*-Cu_2O films.

Comparison of Figure 5.6.a and Figure 5.6.b shows that to get the same thickness, the deposition time of *n*-Cu_2O at pH 5.5 is around 9 times higher than that of *p*-type Cu_2O at pH 11.6. As an example the thickness of *p*-Cu_2O deposited during 10 minutes is around 2 microns and to get the same thickness for *n*-Cu_2O the electro deposition time is 90 minutes. This significant difference between the two rates of deposition is not well know and is under active investigation.

Figure 5.7 shows the SEM images of the Cu_2O films electro-deposited at a temperature of 60^oC and an applied potential of -0.4 V vs. Ag/AgCl for: a) pH = 8.5; b) pH= 9.5 and c) pH= 12. There is a noticeable differences in crystal shape and grain size when the pH changes.

The grain size increases with the pH of the electro-deposition bath. Even the real mechanism of the dependence of grain size on the pH is not currently well elucidated; we may argue it might due to a preferential orientation of the grains depending of the value of the pH. This might help in the grain size variation with the pH. This is in agreement with the work of Zohu et al. [20] that attributed the change in grain size to the preferred orientation, and preferred orientation because specific crystallographic plane have different growth rate which changes with the pH.

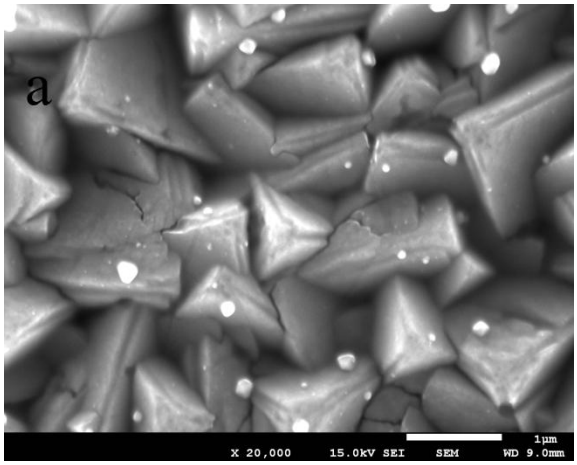

Figure 5-7 SEM images of Cu_2O film electro- deposited at -0.4 vs Ag/AgCl and at 22°C; The pH of the electro-deposition bath was 12. The electro-deposition of the film was done at constant charge of 1.35 coulombs.

SEM pictures form samples prepeared under an applied potential of -0.4V vs. Ag/AgCl and 60°C reveled differenct surface morphology and crystal size for different pH bath. Films depsotioed at pH 8.5 exposed the crystal grains in the shape of 4-sided pyramids in a relatively uniform size distribution. This texture is attributed to [100] preferred orientation plane by measuring the intensity ratio I(111)/I(200) obtained from XRD patterns [32]. Films deposited at pH 9.5 exposed the crystal grains shape in the form of triangular prisms, with less uniform distributation when compared to the 4-sided pyramids shape in [100] plane. This texture is related to a [110] preferred orientation plane. Films deposited at pH 12 exposed the cyrstal grains with a large size 3-faced pyramid shape. This plane texture is related to [111] preferred orientation. These results support well that the pH has important effect on the crystal orientation which in turn has an impact on the grain size.

Figure 5.7 and Figure 5.8 shows the effect of the electro-deposition temperature on the SEM images of the surface morphology of the samples fabricated at -0.4 V vs. Ag/AgCl. The electro-deposition of each film was done at constant charge of 1.35 coulombs to allow a film thickness of 1 micron approximately. We can see cracks and defects in Figure 5.7 for sample

electrodeposited at 22^{o}C. This is an indication that the electro-deposition of *p*-Cu_2O at room temperature is not an optimized electro-deposition temperature. From the SEM image of Figure 5.8 it is clear that film prepared at 60^{o}C has better crystallinity with less cracks and defects in crystals. These results support well that the electro-deposition at 60^{o}C is one of the optimum conditions for the fabrication of *p*-Cu_2O.

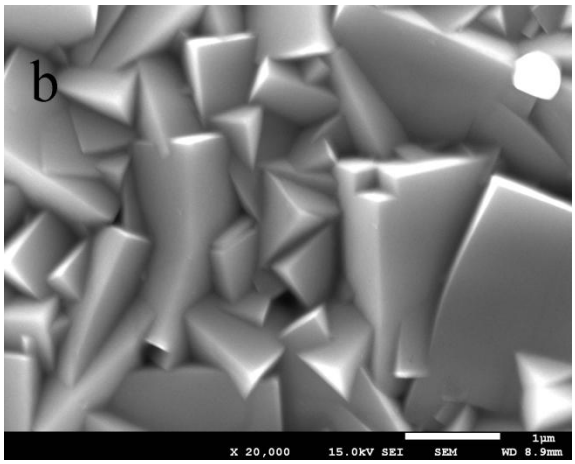

Figure 5-8 SEM image of Cu_2O film electro- deposited at -0.4 vs Ag/AgCl and at 60^{o}C; The pH of the electro-deposition bath was 12. The electro-deposition of the film was done at constant charge of 1.35 coulombs.

Figure 5.9 shows the Scanning electron micrographs at high magnification (x20 000) of the electrodeposited Cu_2O films prepared respectively at 5 different potentials. This helps to analyze the effect of the electro-deposition potential on the composition, orientation, and crystallite shape and grain size of the p-Cu_2O films. The samples were prepared on ITO in solution containing 0.4M copper sulfate and 3M sodium lactate. The electrolyte pH and temperature were fixed at 12 and 60^{o}C respectivily. The applied potential range was -0.3 to -0.7 V versus Ag/AgCl. In each case, the deposition time was controlled with a potentiostat (PAR 273A) which fixed the value of 1.35 coulombs as the total amount of charge passed during each electro-deposition. This ensures equal film thickness of about 1 µm for all prepared samples. SEM characterization reveled that all films were pyramidal in shape. Pure crystalline Cu_2O was obtained at deposition potential of -

0.3 to -0.6 V. However the degree of texture changes with the applied potential. A decrease in grain size has been observed when the applied potential changes more negative values from -0.3 to -0.7 V versus Ag/AgCl as shown in Figure 5.9. From the SEM image on our samples, the surface morphology became coarser and coarser when the potential for the electro-deposition of Cu_2O films progressively changes from -0.3 to -0.7 V vs Ag/AgCl. The dependence of grain size on depostion potential can be attributed to the change of depostion rate at different depostion potentials. The Cu_2O film deposited at -0.3 was 3-faced pyramid shape and relatively large, about 3.5µm (Figure 5.9.a). With the increase toward negative potential the crytals size becomes smaller and smaller, and cyrtals being more uniformaly distributed (Figure 5.9.b to 5.9.e). However, significant bumps appear on the surface of Cu_2O when the film is depostied at -0.7 V vs Ag/AgCl. These bumps are attributed to Cu metal. Therefore at this potential nano-sized Cu and crystalline Cu_2O are co-deposited. This is supported by the SEM images done lower magnification which shows some allots of Cu deposits on the sample.

Figure 5.10 shows the SEM images at low magnification (x5 000) of films morphlogy deposited at -0.7 V versus Ag/AgCl. Figure 5.10.a shows relative nano-sized Cu metal nanocubes(white particles) nucleated on the Cu_2O facets.

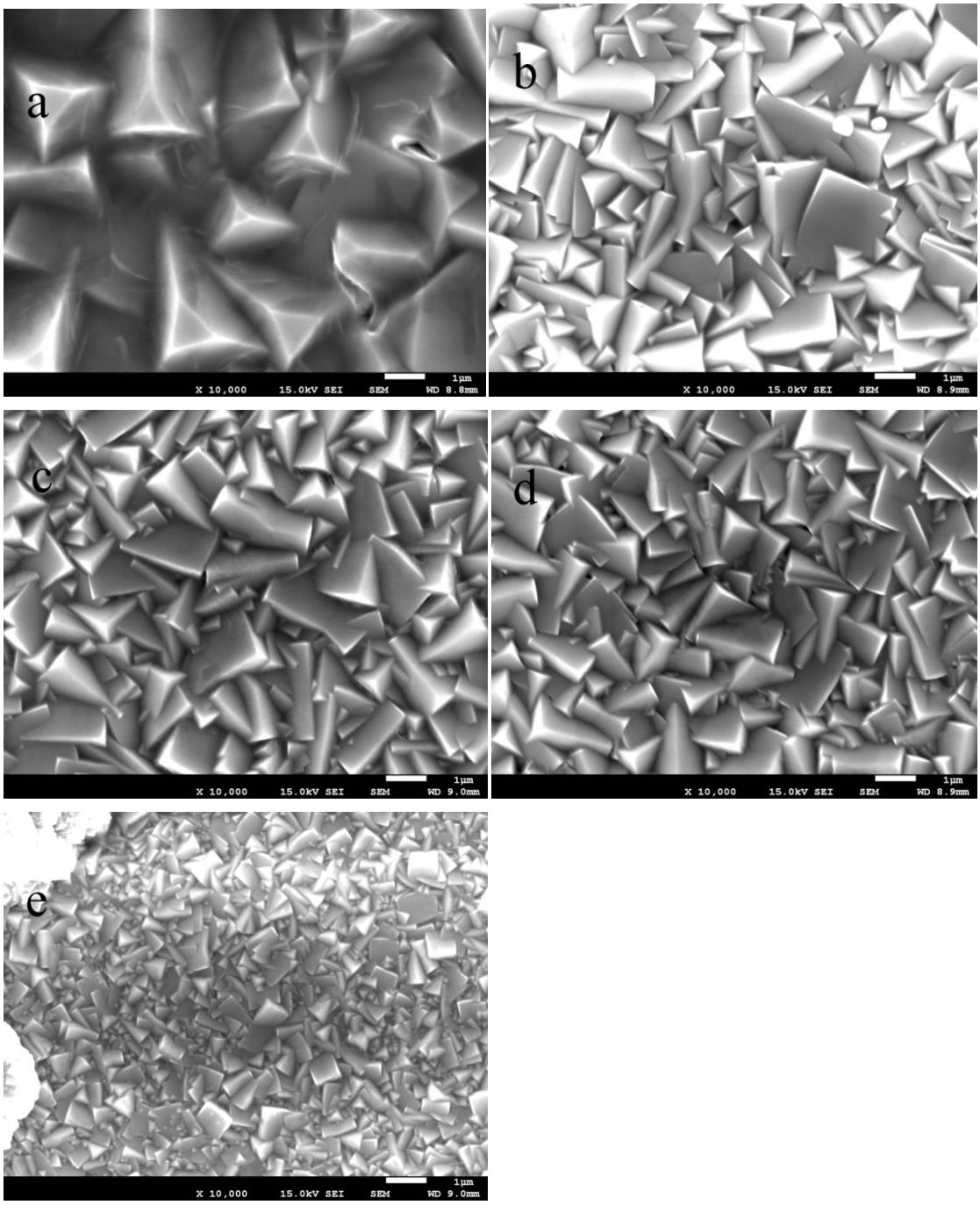

Figure 5-9 Scanning electron micrographs of the electrodeposited Cu_2O films prepared with at different potentials a) -0.3, b) -0.4, c) -0.5, d) -0.6, e)-0.7 V vs. Ag/AgCl. The pH of the electro-deposition bath was 12. The electro-deposition of each film was done at constant charge of 1.35 coulombs.

Other noticeable result was that films eletro-deposited at -0.3 V appeared to be less bright and bigger grain size than those electro-deposited at lower potentials. Films electro-deposited at -0.6 V had smaller grain size brighter appearance than other samples. Therefore the grain size

due to multiple reflection and scattering of light from the grains can determine the film brightness.

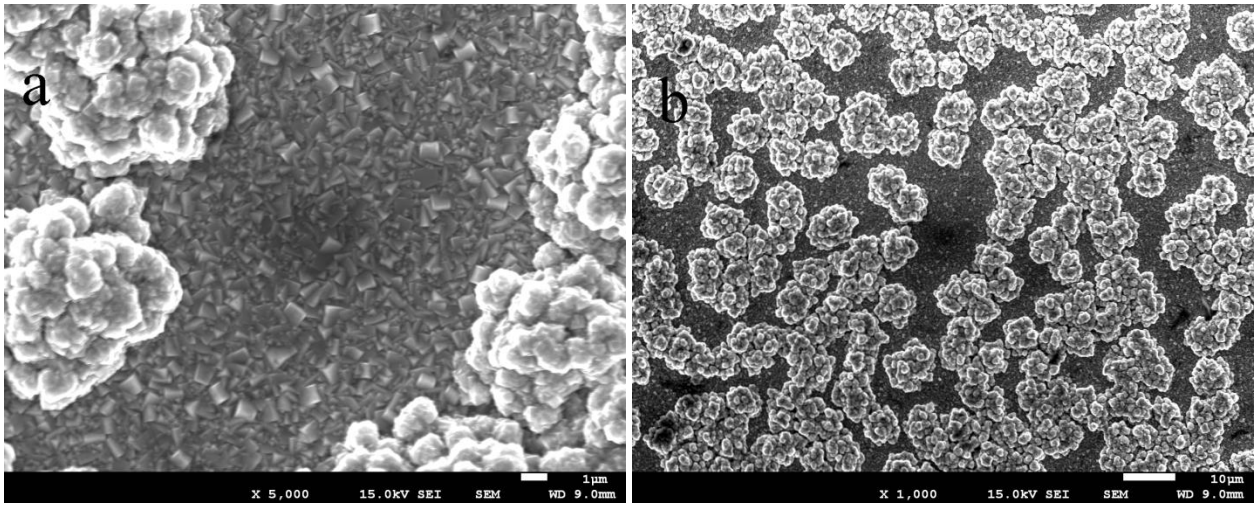

Figure 5-10 Scanning electron micrographs of the electrodeposited Cu_2O films prepared at potentials -0.7 vs. Ag/AgCl, b) the same sample with lower magnification(x 1000). The pH of the electro-deposition bath was 12. The electro-deposition of each film was done at constant charge of 1.35 coulombs.

After the electro-deposition, we verify if the fabricated films respond under light illumination and if this response is in the cathodic (*p*-type semiconductor) potentials or in the anodic (*n*-type semiconductor) potentials. Figure 5.11 shows the current-voltage curve (inset curve) under dark and illumination of the *p*-Cu_2O based photoelectrochemical cell (PEC). Under illumination the cathodic current increases significantly in comparison to the dark current. The fabricated films are sensitive to illumination and a photo current can be measured. This response of the films under cathodic polarization confirms the p-type of the films. The photocurrent measurements under applied potentials were carried out in the photo electrochemical cell described in the experimental section.

Figure 5.11 shows photocurrent characteristics under chopped illumination of the polarization curve of electrodeposited *p*-type Cu_2O/Cu. The photocurrent is generated in cathodic region. This indicates that Cu_2O films obtained under above experimental conditions are *p*-type cuprous

oxide. On this curve, the magnitude of the PEC photo current of Cu_2O films (film electro-deposited at -0.3 V and at pH=13) increases from less cathodic potential (-0.2V to more cathodic potential (-0.7 V). The electrolyte used for the photoelectrochemical cell measurement was: 0.5 M sodium acetate in deionised water (pH 9). As an example the photocurrent at the polarized potential of -0.3 Volt is 20µA and -0.65 V this photocurrent is around -300 µA.

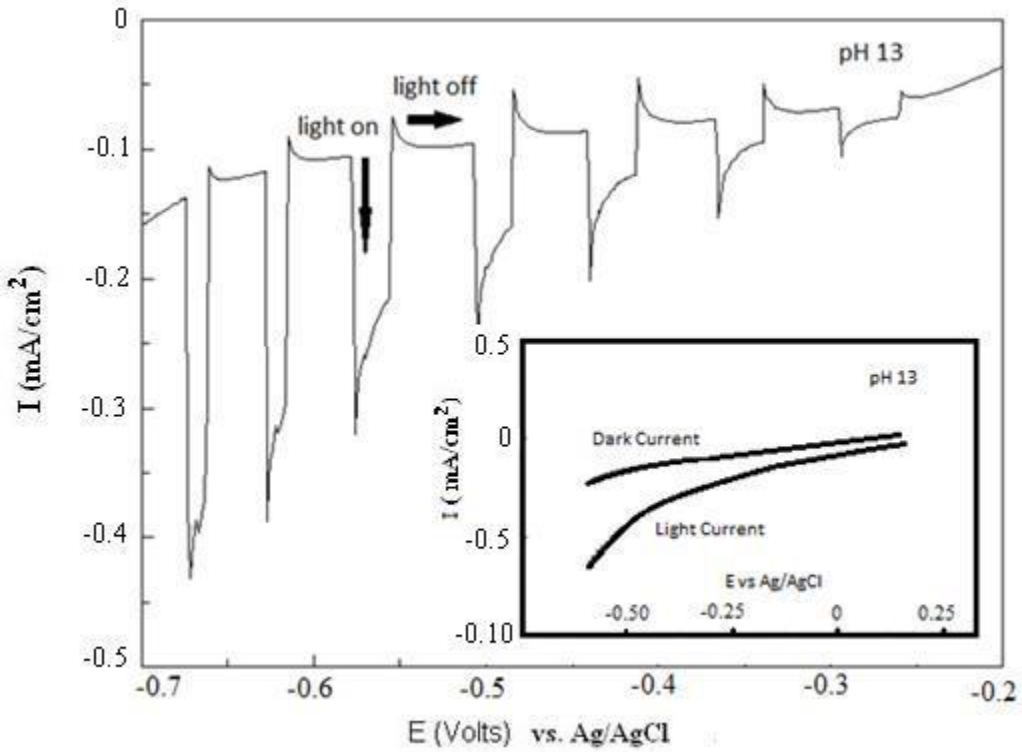

Figure 5-11 Photocurrent characteristics under chopped illumination of electrodeposited *p*-type Cu_2O/Cu. Inset shows dark and light current-voltage characterization of Cu_2O thin film in PEC cell prepared at pH 13.

This may be due to an increse of the band bending (difference between the polarisation potential and the flat band potential: $V_{polarisation} - V_{fb}$) when the polarisation potential ($V_{polarisation}$) increases to more negative values which allow the charge transfer process between Cu_2O and electrolyte. Tha flat band potential was meausred from the analysis of the capacitance-potential data via the Mott–Schottky (M–S) expression [26-28].

$$\frac{1}{C^2} = \frac{2}{\varepsilon\varepsilon_0 e N_A A^2}\left(-V + V_{fb} - \frac{kT}{e}\right) \qquad (7)$$

Where C is the interfacial capacitance (i.e., capacitance of the semiconductor depletion layer), ε is the dielectric constant of Cu_2O (can be taken as 8.6,[29]), ε_0 is the permittivity of free space (8.85×10^{-12} F/m), N_A is the density (cm^{-3}) of acceptors in Cu_2O, A is the electrode area, V_{ap} is the applied potential, k is the Boltzmann constant (1.38×10^{-23} J/K), T is the absolute temperature (298 K) and e is the electronic charge (1.6×10^{-19} C). The intercept (V_0) of a plot of $1/C^2$ versus the applied potential (in the reverse bias regime) on the potential axis affords a value for the flat-band potential; V_{fb} after the small thermal correction, kT/e is made:

$$V_{fb} = V_0 + \frac{kT}{e} \qquad (8)$$

The flat band potential obtained here is +0.15 Volt/Ag/AgCl at pH = 9 and and -0.43 at pH = 13 (by adding sodium hydroxyde in the electrolyte) is in agreement with the V_{fb} of p-Cu_2O obtained in [13]. The Cu_2O film/electrolyte capacitance was measured at different DC potential applied to the Cu_2O/electrolyte interface and for each DC applied potential an AC input signal of 10 mV was applied to the interface. The variation of the interface capacitance (C) on the DC potential was measured for various frequencies in the frequency range, 5–100000 Hz using a Solatron 1280 Model system.

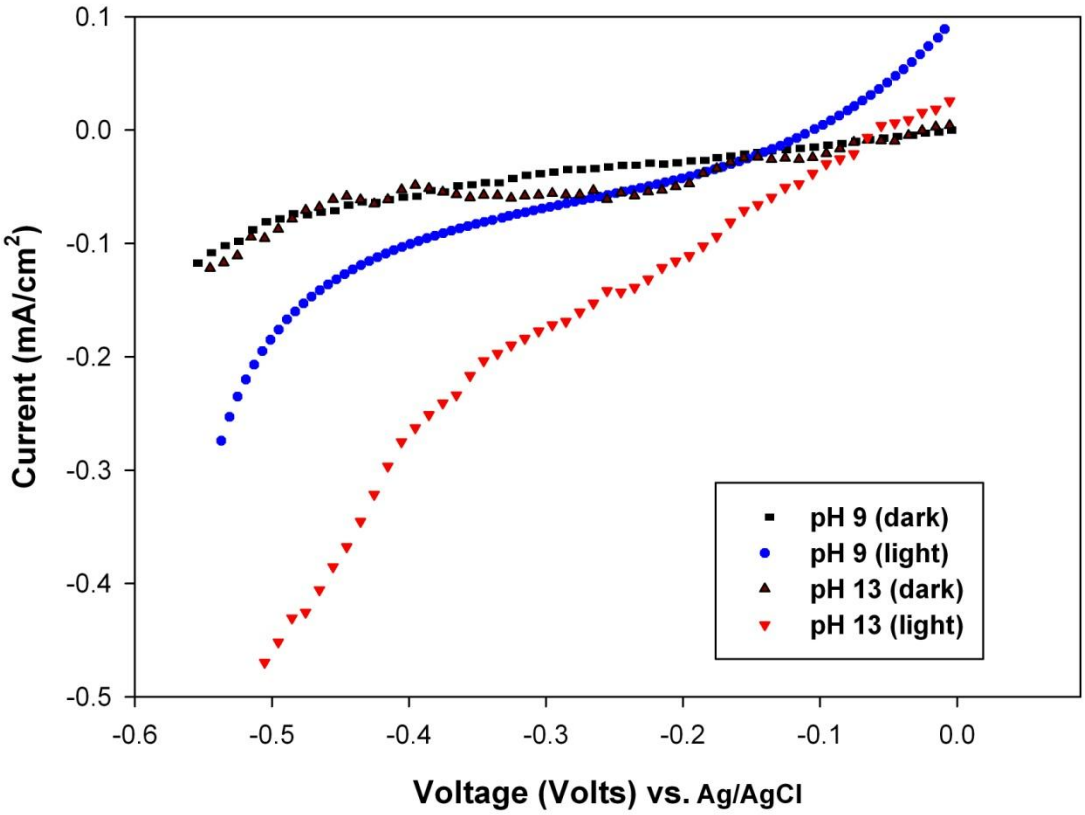

Figure 5-12 Current-voltage characteristics under dark and illumination of electro-deposited p-type Cu_2O/Cu, at pH 8.5 and 13. The electrodeposition time and temperature is respectively 60 minutes and 50°C.

Figure 5.12 shows the current-voltage (I-V) polarization curve under dark and under illumination of a PEC cell based on *p*-Cu2O films variation of the photocurrent exhibited by a sample electrodeposited at pH 13 (dashed lines) is significantly higher than those of the sample electrodeposited at pH 9. This might be related to a more important band bending and/or less recombination effect of the carriers under illumination for samples prepared at high pH and/or the preferential orientation of the crystal. The determination of the variation of the film resistivity with the pH of the electrolyte of the sample electro deposition might help to understand this behavior.

In order to determine the dependence of the effect of the pH of the electrolyte of the electrodeposition on the electrical properties of the electrodeposited *p*-type Cu_2O films, we study the variation of the conductivity of the samples which been fabricated at various pH values from 9.0 to 13.0 by adding different amounts of NaOH in the basic electrolyte of 0.5 M sodium acetate in deionised water. The deposition potential was fixed at -0.4 V vs. Ag/AgCl for all these samples. The deposition time was 60 minutes.

Current-voltage curves (I-V) of the *p*-Cu_2O films were performed using the schematic structure of Cu/Cu_2O of Figure 5.13. The Cu_2O film was deposited on copper substrate. After deposition without any heat treatment a copper tape was placed on top of deposited film as the top electrode. The voltage sweep between -0.5 and +0.5 V was applied between Cu film and top electrode. From the slope of I-V curve of each sample, and using equation (1) the resistivity of the film was calculated because we know the surface area of the top *p*-Cu_2O and the thickness of deposited film.

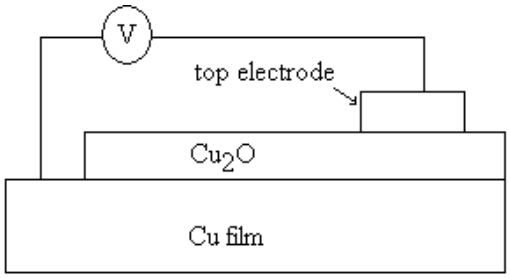

Figure 5-13 Schematic of Cu/Cu_2O structure for current-Voltage characterization.

Figure 5.14a shows that the variation of the resistivity of samples with the pH of the electrolyte used to fabricate them. The resistivity of the film decreases as pH increases. As an example the resistivity of the film prepared at pH 9 is about $5x10^7$ Ωcm whereas those prepare at pH 13 is $4x10^5$ Ωcm. Consequently the smallest resistivity was obtained at pH 13.0, which is lower by

two orders of magnitude than of film prepared at pH 9.0. We have also shown above that samples prepared at pH 13 have crystal with preferential orientation of (111) which appears at pH 13, while preferential orientation of samples prepared at pH 9.0 is (100). This supports the idea that the improvement in photocurrent at pH 13 is related to the significant decrease of the carriers recombination and low resistivity for electrodeposited films at pH 13.

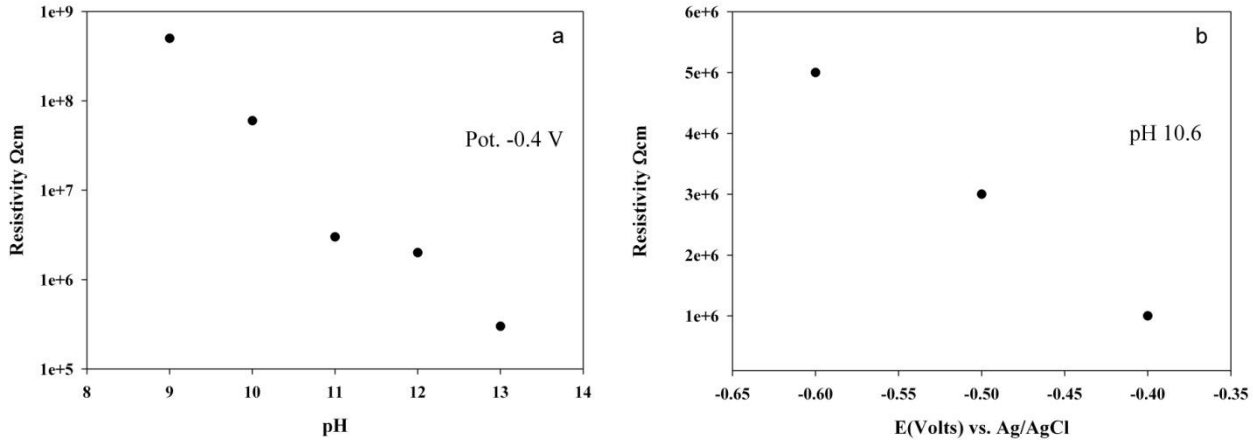

Figure 5-14 Resistivity of *p*-Cu_2O films as a function of the pH of the electro-deposition electrolyte and the potential of the electro-deposition a) Variation of the resistivity of the films with pH of the electro-deposition electrolyte from 9 to 13 and a constant potential of -0.4 Volt; b) variation of resistivity with electro-deposition potential of the films from -0.3 to -0.6 V and a constant electro-deposition electrolyte pH 10.6.

Figure 5-14b shows also that the resistivity of the film decreases when the electro-deposition potential increases from more negative to more positive values. This might be due to the decrease of the grain size when the electro-deposition potential becomes more negative [20]. From Figures 5-14a and Figure 5-14b the optimized low resistivity of the *p*-Cu_2O can be obtained by the electro-deposition of the *p*-Cu_2O films at pH 13 and at a potential of -0.4 or -0.3 V. Some preliminary results we obtained have shown that combing these parameters and the proper heat treatment of the films have allowed a resistivity in the range of 100 Ωcm. This is result is not yet reproducible and is not used the *p-n* junction fabrication. This is particularly

important because the high resistivity of the *p*-Cu_2O films is the most important limitations for their utilization in solar cell applications. It is anticipated that doping Cu_2O with an appropriate agent will contribute to decrease significantly the resistivity of the films and could be lower to appropriate level of 1 Ωcm for industrial solar cells.

5.3.2 *n*-Cu_2O

The objective of this part of the work is to identify the optimum conditions of the electro-deposition of *n*-Cu_2O which experimental parameters of fabrication are missing in the literature. Consequently, our electro-deposition electrolyte was based on an acetate bath containing 0.01 M copper acetate and 0.1 M sodium acetate. A voltammogram of copper foil electrode containing this electrolyte was firstly done in view to identify the electro-deposition conditions of *n*-Cu_2O. Figure 5.15 shows voltammetric curves of a copper foil substrate obtained in 0.01 M copper acetate and 0.1 M sodium acetate. The electrolyte temperature was 60°C at various pH. This voltammetric curve revealed that the electro-deposition potential should be more positive than -0.25 V. For a given potential and temperature, the corresponding current in this range are lower than that of a *p*-type Cu_2O deposition. This makes the rate of electro-deposition of *n*-Cu_2O significantly lower than those of *p*-Cu_2O Therefore to compensate this lower deposition rate of *n*-Cu_2O longer electro-deposition time, e.g. 120 minutes, was chosen for the electro-deposition of *n*-type Cu_2O. To investigate the influence of the pH of the electrolyte on the voltammetric curve, different values of the pH were prepared by adding appropriate amount in the 0.01 M copper acetate and 0.1 M sodium acetate.

Figure 5.16a shows a shift to more positive potentials of the cathodic peak corresponding to the Cu deposition when the electrolyte pH decreases. This indicates that the acidic electrolyte favors the electro-deposition of copper over the Cu_2O deposition. Figure 5.16.a shows also that the cathode current increased with the cathode potential. The cathodic currents in this region are slightly shifted to the negative potentials with an increase of the pH of the electrolyte. Figure 5.16.b shows the voltammetric curves obtained for the temperature range of 30 to 60 ^{o}C in the solution of the 0.01 M copper acetate and 0.1 M sodium acetate at pH 5.5. The current increased and cathode peaks are slightly shifted to the negative potential side when the temperature increases. In the regions of the *n*-Cu_2O (between -0.25 and 0.05 V/Ag/AgCl) the current density increases with the temperature due to the improvement of the activation of the Cu^{2+} e. g. more diffusion of these ions at the support surface at high temperature. Therefore when the electrolyte pH increases, the potentials shifted to more negative values for a given current. This variation is on the order of -0.125 Volt per unit of pH variation (between pH 5.5 and pH 6.6) at a current density of -1.25mA.cm^{-2}. This variation might be attributed to the improvement of the deposition of copper when the pH increases in this range of acid pH. On the other hand, the current increases with the pH for a given potential. As an example at -0.625 V, the variation of the current is in the order of 0.5 mA.cm^2 per unit of pH when pH between 5.5 and 6.6. This increase of the current with the pH is in agreement of the improvement of the copper deposition.

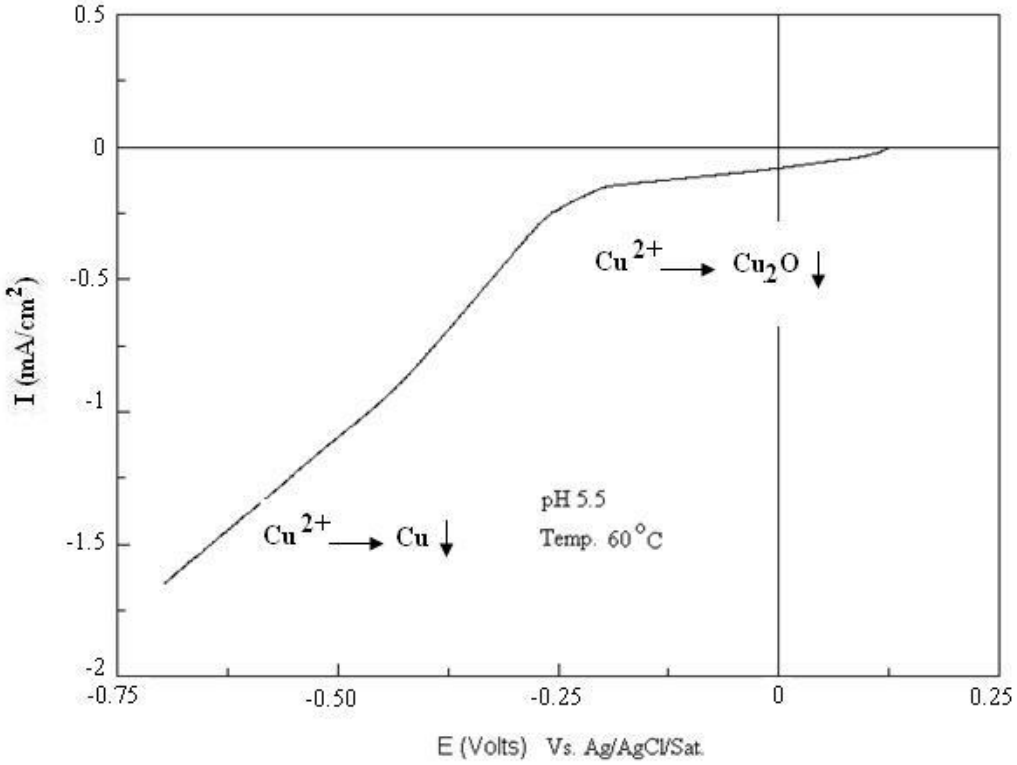

Figure 5-15 Linear voltammogram of copper foil substrate electrode contacting the electrolyte of 0.01 M copper acetate and 0.1 M sodium acetate.

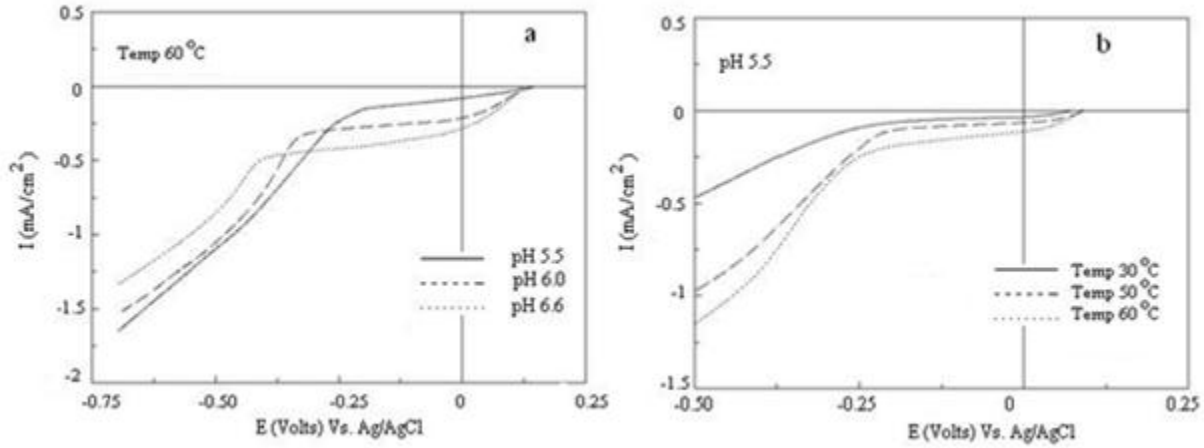

Figure 5-16 Linear voltammogram of the solution containing 0.01 M copper acetate and 0.1 M sodium acetate, (a) on copper foil substrate with given parameters. (b) at different pH (pH was adjusted by adding acetic acid).

From the results obtained above on linear voltammogram, we may conclude that the best parameters for the electro-deposition of Cu_2O in acidic media are: The electro-deposition

potential between -0.25 and 0.05 V; the electrolyte pH between 4.5 to 6.5 and the electro-deposition temperature of 60^{o}C.

Figure 5.17 shows the Current-voltage curves of an as-deposited and an annealed sample in vacuum for 80 min at 150 °C. After annealing in vacuum for 80 minutes at 150^{o}C, the current in the dark of the films is smaller than that of the as-deposited films. The photocurrent of the annealed films is significantly enhanced in comparison to those of samples which are not annealed. This improvement of the photo-response for annealed films must be due to a decrease of the carrier's recombination centers of the films after annealing. This is supported by the resistivity measurement on as-deposited and annealed film.

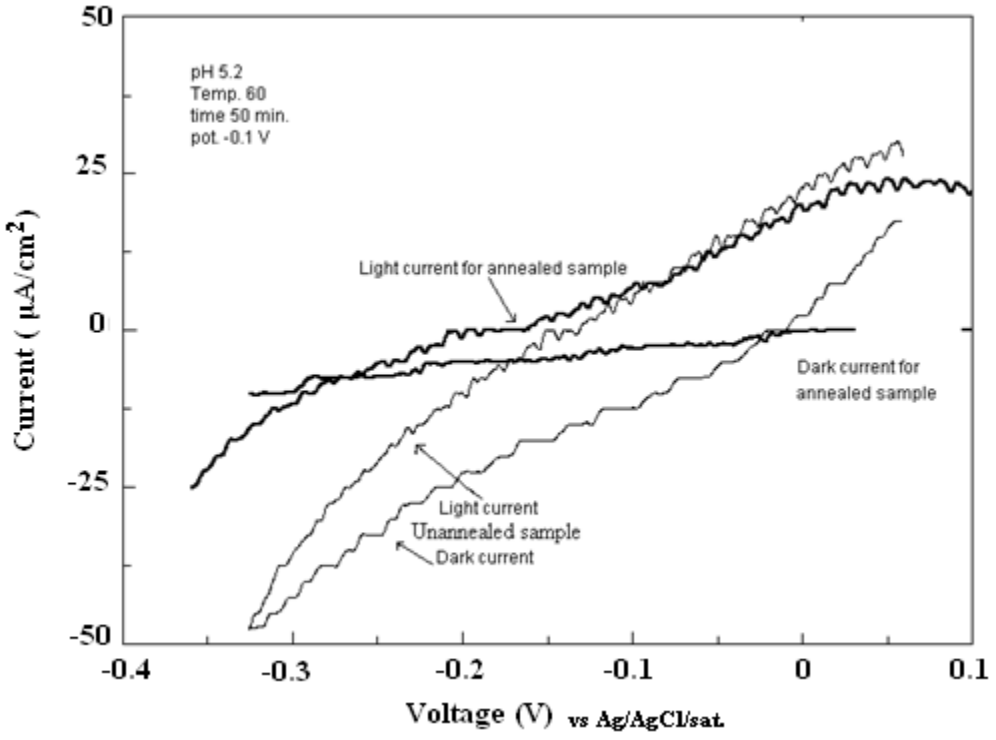

Figure 5-17 Current-voltage characteristics in as-deposited and annealed sample in vacuum for 80 min at 150 °C.

Figure 5.18 shows the variation of the resistivity of *n*- Cu_2O films as a function of pH, before and after heat treatment in air for 80 min at 150 °C. For a given pH, the resistivity of annealed samples is about one order of magnitude lower than those of the as-deposited sample. This may indicate the presence of fewer defects in annealed films than in as-deposited films and consequently the annealed films might exhibit higher photo-response than annealed film. The resistivity of the as-deposited and annealed films increases (about one order of magnitude per unit of pH from pH 4 to 6) with the pH of the electro-deposition electrolyte. In comparison to Figure 5.14 (resistivity of *p*-Cu_2O), the resistivity of the *n*-Cu_2O (figure 5.18) is slightly lower than those of *p*-Cu_2O. These results are different from those obtained elsewhere [6] where the resistivity of the *n*-Cu_2O was slightly higher than the *p*-Cu_2O and the resistivity of *n*-Cu_2O decreases when the pH increases. These differences are attributed to the difference in the experimental conditions (electrolyte composition and voltage used) we used in this work in comparison to those used in [6].

These results can be compared to those obtained elsewhere [15, 30, 31]. In particular it was shown that electro-deposited *p*-Cu_2O film heated at 350°C for 30 min reduced the electrical resistivity from 10^6 ohm.cm to 10^3 ohm.cm [31]. Our results show that we can get similar results if the as-deposited samples are heated at only 150 ^oC during 80 minutes. We keep the heating temperature lower than 300^oC because our experimental results have shown that heating *n*-Cu_2O at temperature higher than 300^oC will change the conductivity from *n*-type Cu_2O to *p*-type and the films become cupric oxide (CuO). This is in agreement with previous results [15]. Accordingly better electrodeposited *n*-Cu_2O films are obtained with the experimental conditions which integrate annealing at temperature lower than 300^oC as we found in this work.

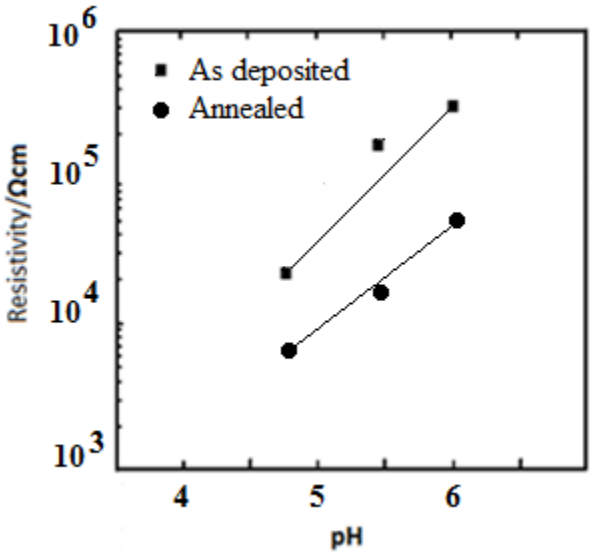

Figure 5-18 Resistivity of *n*-Cu_2O films as a function of pH from 4.8 to 6, before and after heat treatment in air for 80 min at 150 °C.

For a better understanding of the effect of the pH and potential on the photo response of the films, a set of thin films were electro-deposited on Cu foil substrate in the electrochemical cell containing 0.01 M copper acetate and 0.1 M sodium acetate at various pH controlled from 5.8 to 4.9 with different amounts of acetic acid. Another set of thin films were deposited on copper foil under various applied potentials vs. Ag/AgCl between +0.05 and -0.25 V 60°C.

Figure 5.19 shows the photocurrent characteristics under chopped illumination of the polarization curve of electrodeposited *n*-Cu_2O/Cu at 0.0 V Ag/AgCl and pH 5.6. Only anodic photocurrent is obtained. No cathode photocurrent is observed. This curve represents the typical behavior of the *n*-type semiconductor. This indicates that *n*-Cu_2O films are obtained from these above experimental conditions of preparation of the cuprous oxide. On this curve, the magnitude of the PEC photo current of *n*-Cu_2O films is almost constant (1 $\mu A/cm^2$ in the range of of potential between -0.013 V and +0.01 V vs. Ag/AgCl. The electrolyte used for the

photoelectrochemical cell measurement was: 0.1 M sodium acetate in deionised water which pH was 8.5.

Thin *n*-Cu_2O films electro-deposited at fixed potential and various pH values showed different magnitude of the photocurrent. Our experimental results have also shown that the films prepared at pH 5.5 produced higher photocurrent (1 $\mu A/cm^2$) comparing to the films prepared at pH 4.8(0.5 $\mu A/cm^2$). Both films were electro-deposited at 60°C and ~-0.1 V vs. Ag/AgCl. Current-voltage characteristics (I-V) in dark as well as in light were preformed on prepared samples. All samples prepared in the pH range of 4.8-6.3, produced anodic current under illumination, confirming their *n*-type conductivity.

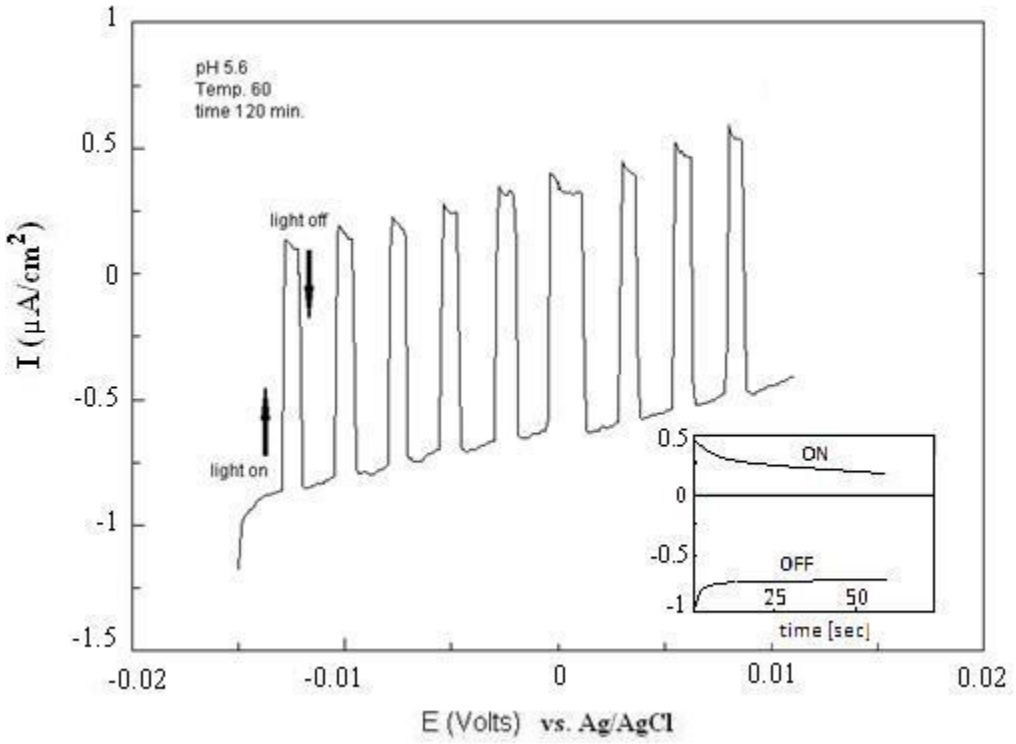

Figure 5-19 Current-voltage characteristics under chopped illumination of electrodeposited n-type Cu_2O/Cu at 0.0 V vs. Ag/AgCl and pH 5.6. The inset shows respective photocurrent density for electrode held at 0V vs. Ag/AgCl in dark and light illumination.

Figure 5.20 show the photoresponse of a PEC based on *n*-Cu_2O/Cu contacting 0.1 M sodium acetate in deionised water at pH 8.2. The *n*-Cu_2O thin films were electro-deposited at respectively 0.0 V; -0.8 V and -0.25 V vs. Ag/AgCl and a pH value of 5.5. The photo current (I_{Ph}) increases when the electro-deposition potential of the films becomes more negative: I_{Ph} (at 0.0 V) < I_{Ph} (at -0.08 V < I_{Ph} (at -0.25 V). Accordingly the highest photoresponse for pH 5.5 were obtained for Cu_2O deposited at -0.25 V vs. Ag/AgCl. This might be attributed to a decrease of the crystal defects when the electro-deposition potential of the films becomes more negative. These defects might be the sites of recombination of the carriers under illumination and their concentration might decrease when the electro-deposition potential of the films is more negative.

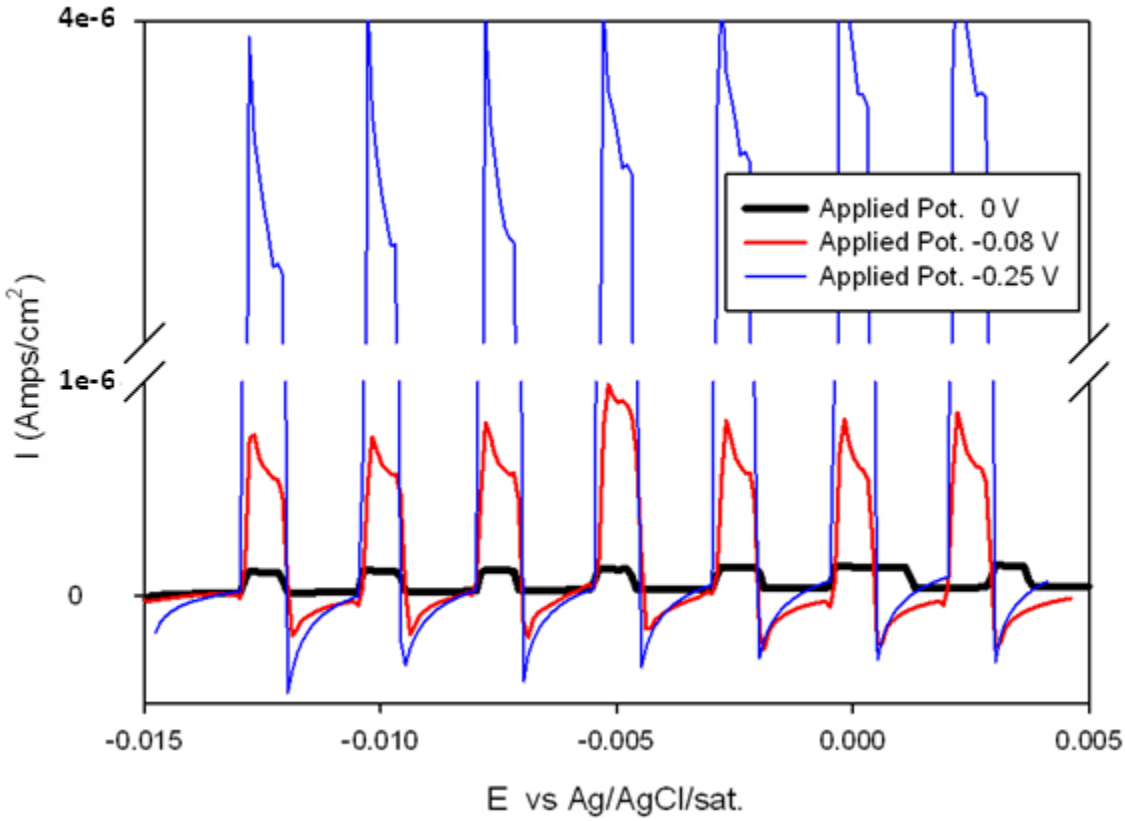

Figure 5-20 Current-voltage characteristics under chopped illumination of electrodeposited n-type Cu2O/Cu, for a pH of 5.5 and different electro-deposition potential (0.0 V; -0.08 V and -0.25 V vs. Ag/AgCl).

5.3.3 *p-n* homojunction Cu_2O solar cell

A two-step electro-deposition process is implemented to fabricate *p-n* homo junction cuprous oxide on Indium tin oxide (ITO) substrate which was used as a transparent conductive oxide for the homo junction Cu_2O solar cell. The electro-deposition of *p*-Cu_2O and *n*-Cu_2O was performed potentiostatically without stirring in a single-compartment, three-electrode electrochemical cell. The working electrode for cell was ITO substrate, the reference electrode was Ag/AgCl and the counter electrode was a platinum mesh.

The working electrode (ITO) immersed into a solution with bath pH of 12.5 containing 0.4M copper sulfate and 3M sodium lactate. Cu_2O film is deposited at a potential of -0.6 V (vs. Ag/AgCl/4M KCl) at 60^oC. The deposition time was controlled by amount of charge deposited. The amount of charge deposited kept at 0.82 C-cm^{-2} to ensure the deposition thickness of 1µm *p*-Cu_2O film.

After the deposition, *p*-Cu_2O film was annealed in air at 300^oC for 30 minutes. Right after heat treatment the substrate with *p*-type cuprous oxide is put into a solution with bath pH of 6.3 containing 0.01 M copper acetate and 0.1 M sodium acetate. To determine the optimized deposition conditions of *n*-Cu_2O on *p*-Cu_2O, liner voltammetry was obtained. The voltammogram shown in Figure 5.21 reveals that parameters for deposition of *n*-Cu_2O on *p*-Cu_2O are different than those previously obtained on copper foil substrate or ITO substrate. There is noticeable shift in cathodic peak towards positive potential and decrease in deposition rate. This potential shift is due to the potential barrier between ITO and *p*-Cu_2O. The electrolyte for depositing *n*-Cu_2O was 0.01 M copper acetate and 0.1 M sodium acetate at pH 6.3.

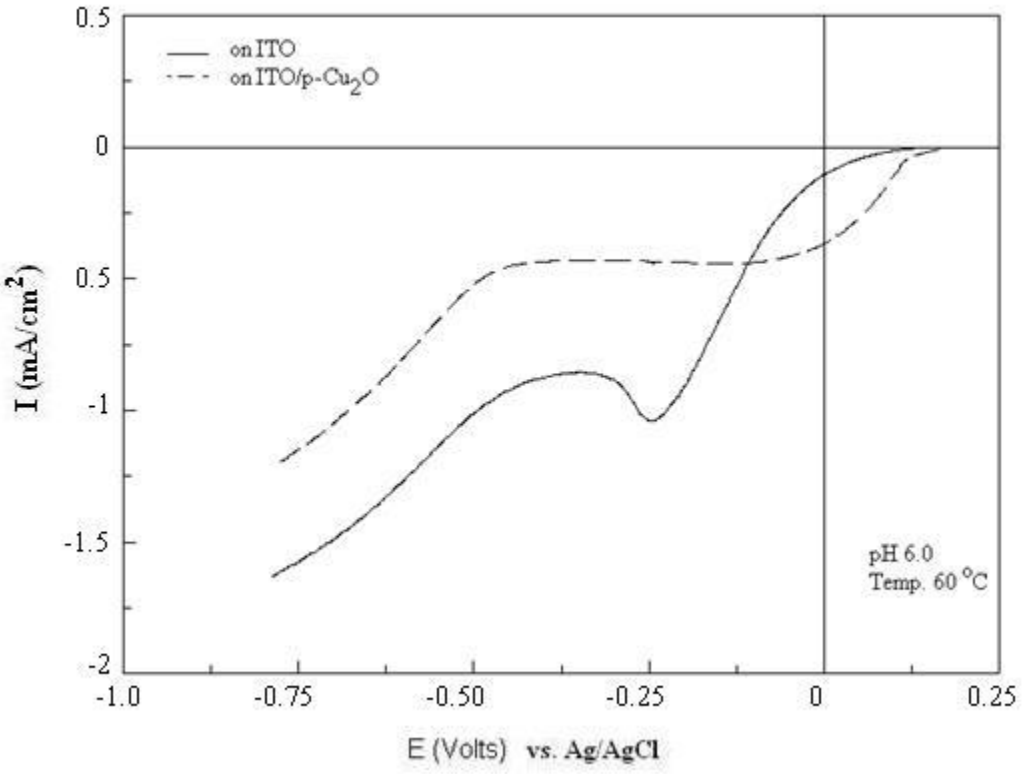

Figure 5-21 Linear voltammogram of solution containing 0.02 M copper acetate and 0.1 M sodium acetate on ITO and ITO/ *p*-Cu_2O substrate with given parameters.

Therefore the electrodeposition of *n*-Cu_2O on *p*-Cu_2O was performed based on new voltammogram obtained on *p*-Cu_2O. The applied potential was fixed to 0V (vs. Ag/AgCl), the deposition time was controlled by amount of charge deposited. The amount of charge deposited kept at 0.38 C-cm^{-2} to ensure the deposition thickness of 450 nm for *n*-Cu_2O film. After the deposition, *n*-Cu_2O film was annealed in air at 120^{o}C for 20 minutes. The back Cu contact used to assemble the solar cell (cell: ITO/*p*-Cu_2O/*n*-Cu_2O/Cu).

The current-voltage (I-V) curves under dark and illumination of a fabricated cell: ITO/ *p*-Cu_2O/*n*-Cu_2O/Cu illuminated through the ITO substrate are shown in Figure 5.22. This curve of the *p*-Cu_2O/*n*-Cu_2O homojunction shows clearly a behavior which is similar to those of the I-V polarization curves of the *p*-*n* solar cell junction. Under illumination, electrons diffuse to *n*-Cu_2O

region, whereas holes diffuse to the *p*-Cu_2O region under influence of applied eclectic field. As a result, a photocurrent is generated. The short circuit current and open circuit voltage are respectively determined as 235 microA/cm^2 and 0.35 Volt. The fill factor (*FF*) and the cell conversion efficiency of light to electricity are determined to be respectively 0.305 and 0.082%. However obtained efficiency is not in desirable range. This could be due high resistivity of films, weak contact between top electrode and *n*-Cu_2O film and also weak junction between *p*-Cu_2O and *n*-Cu_2O films. There are also measuring errors such as lead contact resistance and deviations from AM1.5 which cause errors in I_{sc}, and optical losses such as surface reflection and rear surface reflection. All these source of losses with definitely have a impact on this low efficiency. However our results on cell performances in this work are close to those obtained in [6].

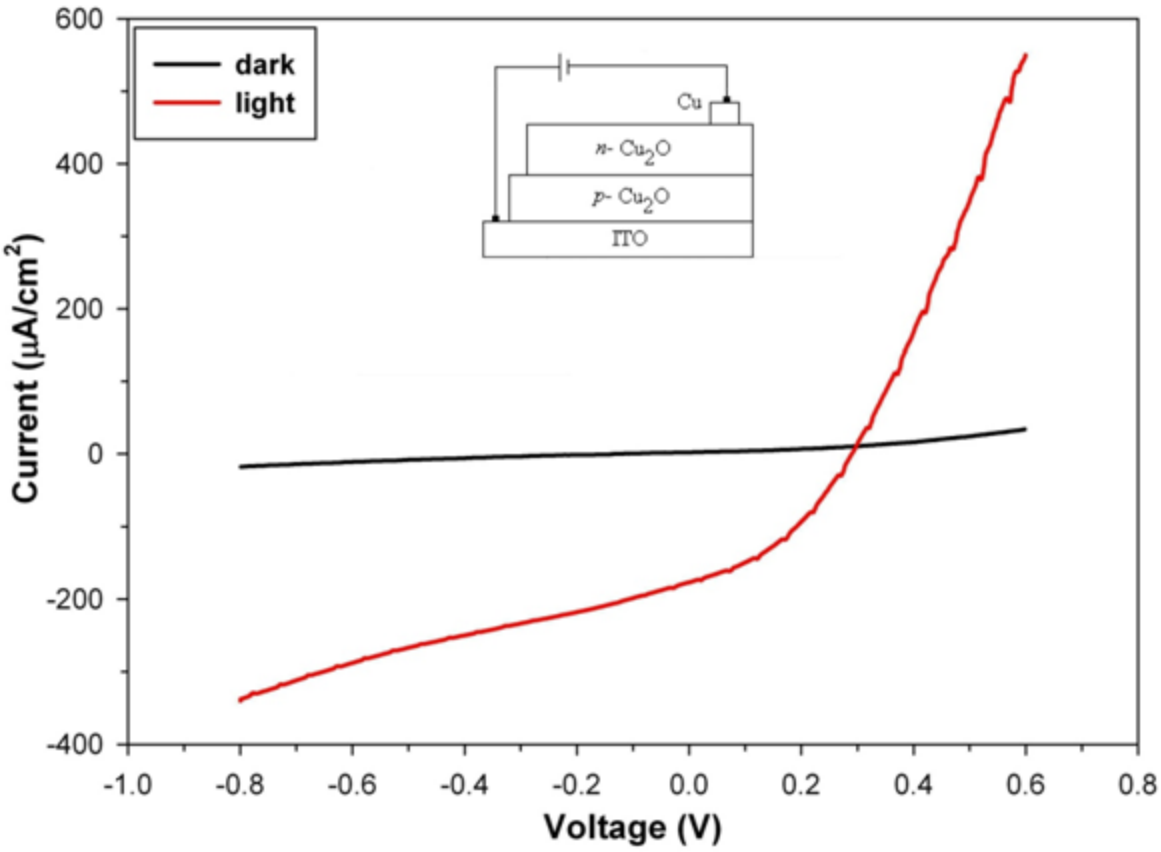

Figure 5-22 I-V characteristics of ITO/ *p*-Cu_2O/*n*-Cu_2O/Cu. Inset: an illustration of testing configuration.

5.4 Conclusion

Polycrystalline *p*-Cu_2O thin films were electrodeposited in aqueous solutions based on aqueous solution containing 0.4M copper sulfate and 3 M sodium lactate at a potential between -0.3 V and -0.7 V vs. Ag/AgCl reference electrode and at pH between 8.5 and 13. *p*-type conductivity was obtained in alkaline media (pH > 8). Resistivity was decreasing with increase in pH value. At pH 9 the resistivity of the film is $5x10^7$ Ωcm whereas those prepare at pH 13 it is $4x10^5$ Ωcm. It was found that the optimum parameters for deposition of *p*-Cu_2O are; higher pH and more negative potential at 60^{o}C. *n*-type conductivity was obtained in acidic media (pH 4.8–6.5) in solution containing copper acetate sodium acetate. The optimum parameters for deposition of *n*-Cu_2O are more negative potential and 60^{o}C. Furthermore the prepared films were annealed. The annealed films showed enhancement in current-voltage characteristics. For annealed films the resistivity ranged from $5x10^3$ at ph 4.8 to $5x10^4$ at pH 6.4.

On successful production of *n*-type and *p*-type Cu_2O films, a homojunction *p*-*n* Cu_2O solar cell was fabricated by two-step electro-deposition process. Indium tin oxide (ITO) substrate was used as a transparent conductive oxide for the homojunction *p*-*n* Cu_2O solar cell. The photovoltaic characterization was performed. The short circuit current and open circuit voltage are respectively determined as 235 microA/cm^2 and 0.35 Volt. The fill factor (*FF*) and the cell conversion efficiency of light to electricity are determined to be respectively 0.305 and 0.082%. However obtained efficiency is not in desirable range. This could be due to weak contact between top electrode and *n*-Cu_2O film and also weak junction between *p*-$Cu_2O$and *n*-Cu_2O films.

The future work will be focused on the:

1) Improvement the film resistivity by doping *p*-$Cu_2O$and *n*-Cu_2O films. It is anticipated that doping Cu_2O with an appropriate agent will contribute to decrease significantly the resistivity of the films and could be reached to appropriate level of 1 Ωcm for industrial solar cells. Our approach is to dope *n*-Cu_2O film with iodide (I). Copper iodide (CuI) can be used as a source of doping and can be introduced in the electrodepostion bath. Therefore co-deposition of Iodide in Cu_2O could be investigated.

2) Improvement of the junction between *p*-$Cu_2O$and *n*-Cu_{2O} films and contact between the film and top electrode.

References

[1] O. Savadogo, Thin-Film Semiconductors Deposited in Nanometric Scales by Electrochemical and Wet Chemical Methods for Photovoltaic Solar Cell Applications, in: Photoelectrochemical Materials and Energy Conversion Processes, Wiley-VCH Verlag GmbH & Co. KGaA, 2010, pp. 277-350.
[2] B.P. Rai, Cu2O solar cells: A review, Solar Cells, 25 (1988) 265-272.
[3] L.C. Olsen, F.W. Addis, W. Miller, Experimental and theoretical studies of Cu2O solar cells, Solar Cells, 7 (1982) 247-279.
[4] L.C. Olsen, R.C. Bohara, M.W. Urie, Explanation for low-efficiency Cu[sub 2]O Schottky-barrier solar cells, Applied Physics Letters, 34 (1979) 47-49.
[5] A. Mittiga, E. Salza, F. Sarto, M. Tucci, R. Vasanthi, Heterojunction solar cell with 2% efficiency based on a Cu[sub 2]O substrate, Applied Physics Letters, 88 (2006) 163502-163502.
[6] K. Han, M. Tao, Electrochemically deposited p–n homojunction cuprous oxide solar cells, Solar Energy Materials and Solar Cells, 93 (2009) 153-157.
[7] W.M. Sears, E. Fortin, Preparation and properties of Cu2O/Cu photovoltaic cells, Solar Energy Materials, 10 (1984) 93-103.
[8] J. Liang, N. Kishi, T. Soga, T. Jimbo, M. Ahmed, Thin cuprous oxide films prepared by thermal oxidation of copper foils with water vapor, Thin Solid Films, 520 (2012) 2679-2682.
[9] M. Seo, T. Iwata, N. Sato, Composition and Structure of Anodic Oxide Films on Copper in Neutral and Weakly Alkaline Borate Solutions, Bulletin of the Faculty of Engineering, Hokkaido University, 102 (1981).
[10] V.F. Drobny, D.L. Pulfrey, Properties of reactively-sputtered copper oxide thin films, Thin Solid Films, 61 (1979) 89 - 98.
[11] A.E. Rakhshani, A.A. Al-Jassar, J. Varghese, Electrodeposition and characterization of cuprous oxide, Thin Solid Films, 148 (1987) 191-201.
[12] A.E. Rakhshani, J. Varghese, Galvanostatic deposition of thin films of cuprous oxide, Solar Energy Materials, 15 (1987) 237-248.
[13] L.C. Wang, N.R. de Tacconi, C.R. Chenthamarakshan, K. Rajeshwar, M. Tao, Electrodeposited copper oxide films: Effect of bath pH on grain orientation and orientation-dependent interfacial behavior, Thin Solid Films, 515 (2007) 3090-3095.
[14] W. Siripala, J.R.P. Jayakody, Observation of n-type photoconductivity in electrodeposited copper oxide film electrodes in a photoelectrochemical cell, Solar Energy Materials, 14 (1986) 23-27.
[15] W. Siripala, L.D.R.D. Perera, K.T.L. De Silva, J.K.D.S. Jayanetti, I.M. Dharmadasa, Study of annealing effects of cuprous oxide grown by electrodeposition technique, Solar Energy Materials and Solar Cells, 44 (1996) 251-260.
[16] L. Xiong, S. Huang, X. Yang, M. Qiu, Z. Chen, Y. Yu, p-Type and n-type Cu2O semiconductor thin films: Controllable preparation by simple solvothermal method and photoelectrochemical properties, Electrochimica Acta, 56 (2011) 2735-2739.
[17] X. Han, K. Han, M. Tao, Characterization of Cl-doped n-type Cu2O prepared by electrodeposition, Thin Solid Films, 518 (2010) 5363-5367.
[18] W. Siripala, Electrodeposition of n-type cuprous oxide thin films, in: Next Generation Photovoltaics and Photoelectrochemistry - 212th ECS Meeting, October 7, 2007 - October 12, 2007, Electrochemical Society Inc., Washington, DC, United states, 2008, pp. 1-10.
[19] C. Jayewardena, K.P. Hewaparakrama, D.L.A. Wijewardena, H. Guruge, Fabrication of n-Cu2O electrodes with higher energy conversion efficiency in a photoelectrochemical cell, Solar Energy Materials and Solar Cells, 56 (1998) 29-33.

[20] Y. Zhou, J.A. Switzer, Electrochemical deposition and microstructure of copper(I) oxide films, Scripta Materialia, 38 (1998) 1731–1738.
[21] M. Nolan, S.D. Elliott, The p-type conduction mechanism in Cu2O: a first principles study, Physical Chemistry Chemical Physics, 8 (2006) 5350-5358.
[22] W. Wang, D. Wu, Q. Zhang, L. Wang, M. Tao, pH-dependence of conduction type in cuprous oxide synthesized from solution, Journal of Applied Physics, 107 (2010) 123717-123714.
[23] K. Jayathileke, W. Siripala, J. Jayanetti, Electrodeposition of p-type, n-type and p-n Homojunction Cuprous Oxide Thin Films, Sri Lankan Journal of Physics, 9 (2008) 35-46.
[24] X. Han, M. Tao, Solution-based n-type doping in Cu2O and its implications for 3rd generation cells, in: Photovoltaic Specialists Conference (PVSC), 2009 34th IEEE, 2009, pp. 002086-002089.
[25] K. Mizuno, M. Izaki, K. Murase, T. Shinagawa, M. Chigane, M. Inaba, A. Tasaka, Y. Awakura, Structural and Electrical Characterizations of Electrodeposited p-Type Semiconductor Cu2O Films, Journal of The Electrochemical Society, 152 (2005) C179-C182.
[26] R. Krishnan, "Fundamentals of Semiconductor Electrochemistry and Photoelectrochemistry," in *Encyclopedia of Electrochemistry*, ed: Wiley-VCH Verlag GmbH & Co. KGaA, 2007.
[27] O. Savadogo, Correlation between the flat band potential of semiconductors and solvent donor numbers, Material Research Bulletin 23, (1988), pp. 1451–1458
[28] O. Savadogo, Correlation between the flat band potential and electron affinity of semiconductors: (1) equation including the effect of the solvent donor numbers, Materials Reserach Bulletin 25, (1988), pp. 1209–1217
[29]E. C. Heltemes, "Far-Infrared Properties of Cuprous Oxide," *Physical Review,* vol. 141, pp. 803-805, 1966.
[30] T. Mahalingam, J.S.P. Chitra, J.P. Chu, S. Velumani, P.J. Sebastian, Structural and annealing studies of potentiostatically deposited Cu2O thin films, Solar Energy Materials and Solar Cells, 88 (2005) 209-216.
[31] T. Mahalingam, J.S.P. Chitra, J.P. Chu, H. Moon, H.J. Kwon, Y.D. Kim, Photoelectrochemical solar cell studies on electroplated cuprous oxide thin films, Journal of Materials Science: Materials in Electronics, 17 (2006) 519-523.
[32] S. Bijani*, et al.*, "Low-Temperature Electrodeposition of Cu2O Thin Films: Modulation of Micro-Nanostructure by Modifying the Applied Potential and Electrolytic Bath pH," *The Journal of Physical Chemistry C,* vol. 113, pp. 19482-19487, 2009/11/12 2009.

Chapter 6 ARTICLE 2: PHOTOCURRENT ENHANCEMENT OF *n*-TYPE Cu_2O THIN FILMS ELECTRODEPOSITED UNDER DIFFERENT GAS ATMOSPHERES IN THE ELECTROLYTE

S. M. Shahrestani and O. Savadogo

Laboratory of New Materials for Electrochemistry and Energy

Department of Chemical Engineering

Program of Metallurgy and Materials

École Polytechnque de Montréal, Canada, H3C 3A7

Submitted to the Journal of Electroactive Materials, on November, 2013

Abstract

n-type Cu_2O thin films electrodeposited under different gas atmospheres in the electrolyte was achieved. The photocurrent response of the electrodeposited sample changes with the type of gas introduced in the electrolyte during the electrode deposition process. It was found that for Cu_2O samples electrodeposited at a given time, nitrogen bubbling leads to films which exhibit more photocurrent than those fabricated from argon bubbling or not bubbling each of these gases. The photocurrent response also increases with the gas bubbling time. The morphology of the films changes from porous (no bubbling with nitrogen) to more dense film (bubbling with nitrogen). This photocurrent changes also with nitrogen bubbling time. It was concluded that the type of the bubbling gas (nitrogen and argon) and time has no effect on the chemical composition of the sample.

Key words: *n*-type Cu_2O, electrodeposition, effect of gas bubbling, nitrogen, photocurrent enhancement

6.1 Introduction

Copper oxide semiconductors are promising alternative to silicon-based solar cells because Cu_2O is a non-toxic, abundant and low cost material satisfying economical and environmental requirement necessary for large scale applications [1]. Cu_2O is a potential high efficiency solar cell with direct band gap energy of 2.0 eV, which is close to the ideal energy gap (about 1.5 eV), and well matched with solar spectrum. Its calculated theoretical electrical power conversion efficiency is approximately 20 % [2]. However limited understanding of conductivity type of Cu_2O semiconductor and lack of efficient n-type Cu_2O has hindered the efficient production of Cu_2O based photovoltaic cells.

The best efficient Cu_2O-base heterojunction solar cell was reported recently by Mittiga et al. with efficiency of 2% [3]. This low efficiency is attributed to the lack of a homogeneous Cu_2O *p–n* junction [2, 4]. The common conclusion is that the fabrication of homojunction Cu_2O is the only way to achieve high efficiency Cu_2O-base solar cell. In this case abrupt structural discontinuities or sever interface structures is not expected to cause interface strain.

In the Cu_2O lattice, each copper atoms linearly coordinated by two neighboring oxygen and each oxygen atoms surrounded by four copper atoms, which makes the stoichiometry 2:1. However, this stoichiometry is not obeyed completely as the ratio of copper and oxygen atoms is slightly different from the ratio in one mole. Therefore the arrangement of atoms in crystalline copper

oxide is not perfect. This deviation from stoichiometry, δ in Cu_2O can be identifies either as vacancies, interstitials or both.

Recently, *n*-type thin film Cu_2O is been produced by electrodepostion [4-7]. Electrodeposition is a simple and inexpensive technique to deposit Cu_2O films on a conductive substrate. Other techniques such as thermal oxidation, anodic oxidation, chemical deposition, sol–gel chemistry, sputtering, and other gas-phase deposition techniques produce p-type conductivity due to the presence of Cu vacancies [8-11]. Sears et al. 1984 reported that an excess of oxygen, as a result of stoichiometry, is the major active impurity and gives a *p*-doped semiconductor [12]. The origin of *n*-type conductivity is speculated to be due to oxygen vacancies [5, 13]. It also has been reported that the conductivity of Cu_2O thin film can be changed by varying the pH solution in electrodepostion process [4, 14]. The electrical properties of Cu_2O can be controlled by the intrinsic defects such as copper and oxygen vacancies [15].

The purpose of the present work was to study the synthesis condition to electrochemically prepare high-performance *n*-type Cu_2O. The focus of this study was to investigate new strategy of enhancing the photocurrent of *n*-type Cu_2O via controlling the dissolved concentration of oxygen in deposition solution called deaeration.

6.2 Experimental methods

6.2.1 Preparation of Cu_2O film

6.2.1.1 Preparation of working electrode

Indium tin oxide (ITO) substrates on glass substrate with a sheet resistance of 18Ω/cm were used as the working electrodes for the electrodeposition of Cu_2O. Prior to the film deposition, ITO/glass was degreased in ultrasonicated acetone for 15 minutes, rinsed in de-ionized water. After cleaning process, chemical etching was performed on samples to remove inorganic contamination and native oxides on sample surface. ITO/glass was etched chemically, in diluted hydrochloric acid (HCl) for 2 minutes, and finally rinsed in de-ionized water.

6.2.1.2 Preparation of solution

Electrodepostion of Cu_2O on ITO substrates was studied in an aqueous solution of sodium acetate and cupric acetate. Cupric acetate was used as Cu^{+2} source for Cu_2O electrochemical deposition. Sodium acetate was added to solution making complexes releasing copper ions slowly into the medium allowing a uniform growth of Cu_2O thin film [16]. All chemicals were from commercial sources. They were used without further purification. All solutions were prepared from de-ionized water.

6.2.1.3 Deposition parameters and procedure

A single-compartment, three-electrode electrochemical cell, was used for film deposition. Electrodeposition was carried out with a Princeton Applied Research potentiostat 273A. The

commercial Ag/AgCl (4M KCl) and graphite/carbon counter electrode were used as the reference and counter electrode, respectively. The electrolyte was kept in a water-jacked cell and temperature was controlled by a Polystat circulation water bath. Electrodeposition was carried out in the potentiostatic mode at different applied potential values with respect to the reference electrode. The applied potential window was chosen from voltammetry curves obtained in the solution. All working electrode used for voltammetric curves had a contact area of 0.2 cm^2 with electrolyte. After deposition, the films were rinsed in de-ionized water and dried at room temperature.

A set of thin films with area of 0.385 cm^2 were deposited on ITO substrates in the electrochemical cell containing 0.02 M copper acetate ($Cu(CH_3CO_2)_2$) and 0.1 M sodium acetate at various deposition potentials (-50 to -250 mV with respect to the Ag/AgCl), in order to study the film properties. Deposition time period was controlled in order to obtain films of thickness ~750 nm. Film thickness was calculated by monitoring the total charge passed during the film deposition. Deaeration of solution was carried either by nitrogen or Argon stripping or ultrasonic degassing. Stripping will utilize Henry's law by reducing the partial pressure of oxygen whereby the equilibrium is shifted from dissolved oxygen towards oxygen in the gas phase. Prior to deposition the solution was purge at room pressure with flow rate of 100 ml/min.

6.2.2 Characterization

The surface morphology of the films was studied using FEI JEOL JSM-7600TFE scanning electron microscope (SEM). The crystal phases of the samples were determined using x-ray diffractometer (Philips X'pert) with CuKα radiation source. The optical properties of the films

were determined by photocurrent characterization carried out in a custom built three-electrode electrochemical cell. A Pt mesh, Ag/AgCl reference electrode, and the Cu_2O film were used as the counter, reference, and working electrode, respectively. A 100-W soft white light lamp was used as the light source and it was positioned 20 cm away from working electrode. The illumination switch was controlled manually to chop the light in certain time intervals. For photocurrent measurements, using Princeton Applied Research potentiostat, the electrolyte was an aqueous solution of 0.1 M sodium acetate. To avoid false signals raising from oxygen reduction the electrolyte was continuously purged with N_2 to remove oxygen.

6.3 Results and discussion

The linear sweep voltammogram of Cu_2O films deposited from cupric acetate solution at pH 6.2 is shown in Figure 6.1. The sweep is scanned cathodically at 10 mV/s in solution containing 0.02M copper acetate and 0.1M sodium acetate while temperature maintained at 60^oC. Two cathodic peaks are obtained. First cathodic peak attributes to the formation of Cu_2O on the substrate during the cathodic reduction of cupric acetate solution according to the following reaction.

$$\boldsymbol{2Cu^{2+} + H_2O + 2e^- \Rightarrow Cu_2O + 2H^+}$$

Under potentiostatic conditions of lower potential at second cathodic peak, metallic Cu will be formed on substrates according to the following reaction.

$$\boldsymbol{Cu^{2+} + 2e^- \Rightarrow Cu}$$

Therefore at higher negative potential the formation of Cu and at moderate negative potential the formation of Cu_2O will take place. The more negative potential correspond to higher current density, higher current density means higher reaction rate which is proportional to growth rate.

Figure 6.2 shows Photoelectrochemical behaviors of Cu_2O films deposited at -100 mV vs Ag/AgCl and pH 6.2. The zero bias photocurrent obtained without applying an external bias between the Cu_2O electrode and counter electrode. It is clear that the photocurrent produced by Cu_2O film strongly depends on the nitrogen purging time. The photocurrent increases with increase in purging time. Other set of samples is prepared in pH bath 5.8 and 5.5. The zero-bias photocurrent of these electrodes once again shows the same trend: photocurrent increases as the purging time increases.

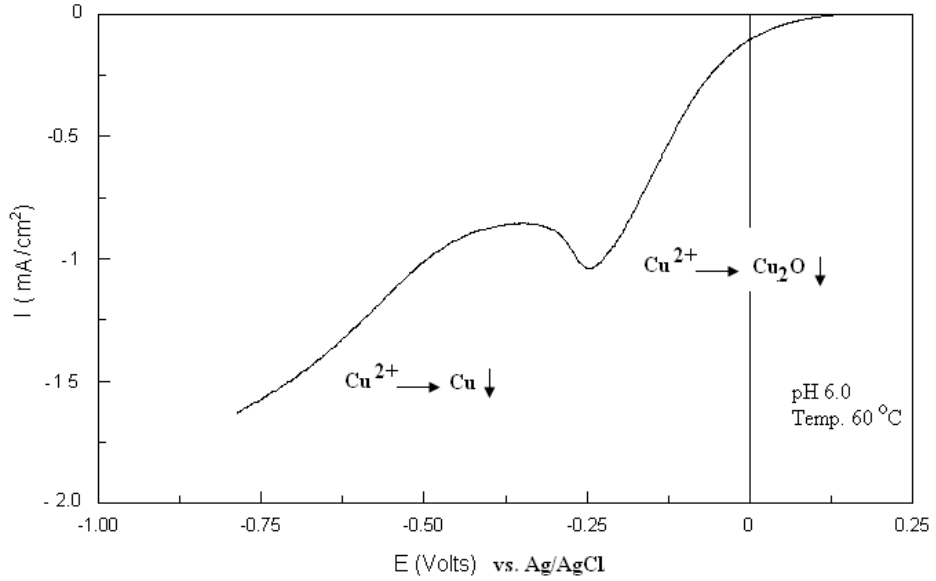

Figure 6-1 Linear sweep voltammogram of Cu_2O films deposited on ITO.

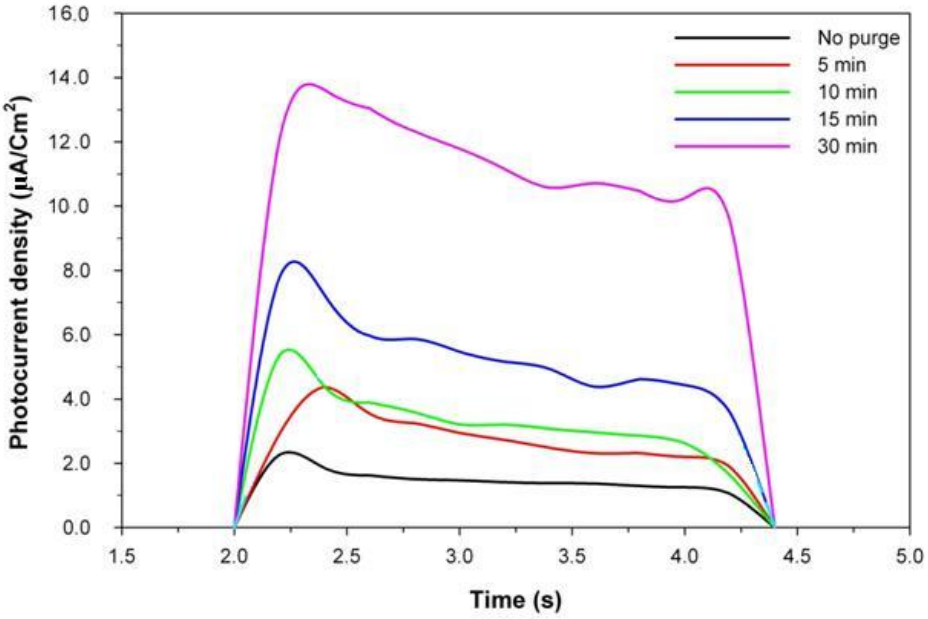

Figure 6-2 Photocurrent generated of the Cu_2O films deposited in N_2 purged solution.

Figure 6.3 shows the effect of Argon bubbling during the film electrode position on its response in photocurrent. A set of similar samples is prepared. Argon gas is used as a purging agent. Similar results is obtained and confirmed that the increase in photocurrent is due to bubbling during electrodepostion which may change the morphology of the films for better photocurrent response. XRD results indicate that the chemical composition of the films did not change with and without nitrogen or argon bubbling in the electrodeposition bath. Furthermore to confirm this hypothesis a set of samples is prepared with the same deposition parameters and ultrasonic degassing procedure is performed as a method of deaeration. Figure 6.4 shows that similar behaviors are obtained regardless of the method of deaeration. Therefore it could be confirm that the photoconductivity of the thin film Cu_2O can be controlled by the dissolved concentration of oxygen in deposition solution. The similar increments in the photocurrent are obtained in samples prepared with same deposition parameters and pH bath of 5.5.

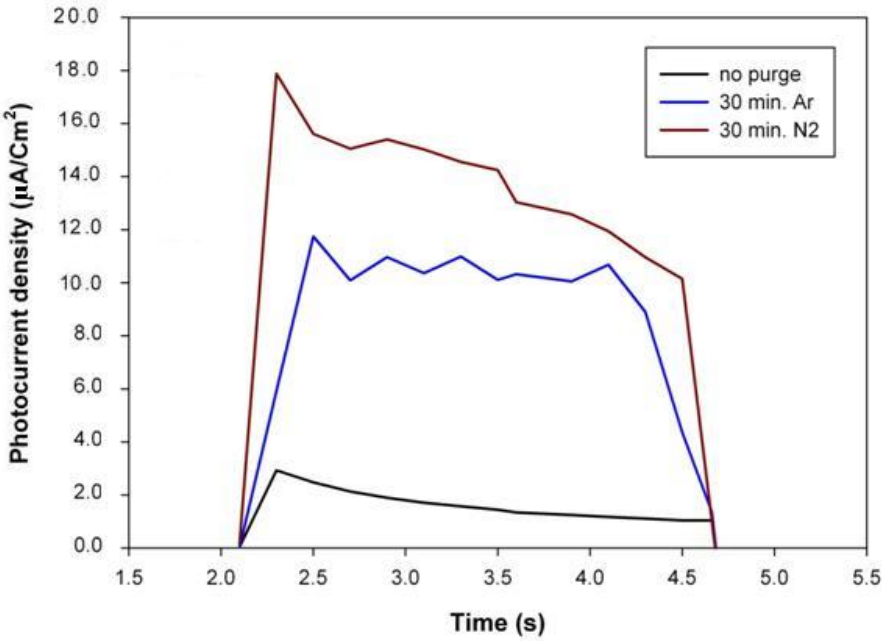

Figure 6-3 Photocurrent generated of the Cu_2O films deposited in Ar and N_2 purged solution.

The corresponding photocurrents are less than values obtained for pH 6.2 but all samples followed the same trend and showed substantial increments in photoelectrochemical current.

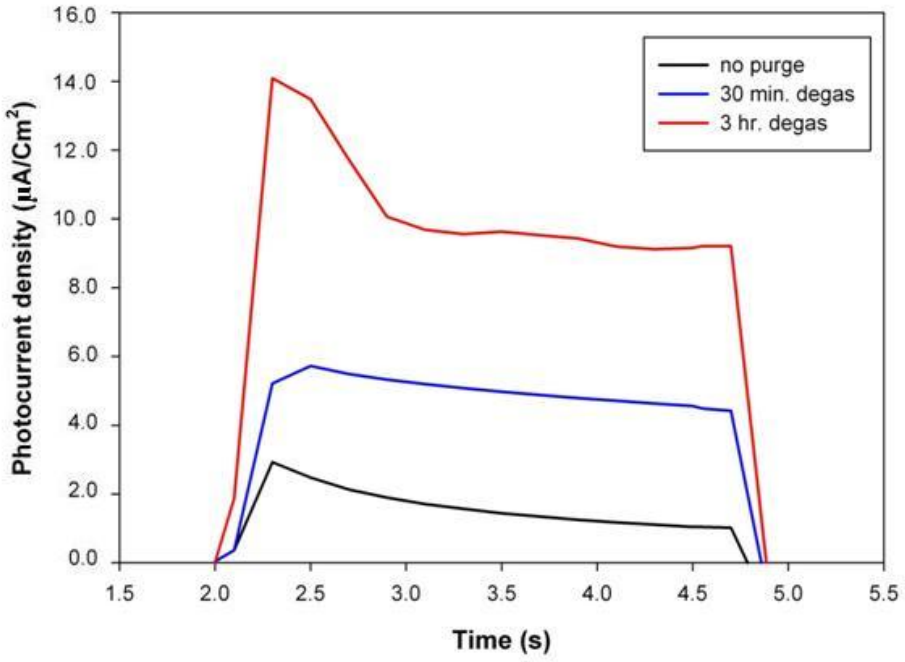

Figure 6-4 Photoelectrochemical behaviors of Cu_2O films deposited in ultrasonicated solution.

Heat treatment effects on optical and electrical properties of electrodeposited Cu_2O have been studied by several authors [16-19]. All reports confirmed that the annealing will improve the optical and electrical properties of electrodeposited Cu_2O, although the optimal annealing temperature depends on deposition history. For example Mahalingam et al. found that annealing Cu_2O thin film at 350 °C for 30 min reduced the electrical resistivity from 10^6 ohm-cm to 10^3 ohm-cm [18]. In order to investigate the effect of annealing on our samples, several samples are chosen randomly to be annealed. The annealing temperature is kept below 300 °C; heat treatment above this temperature will change the conductivity type from *n*-type to *p*-type as the film become cupric oxide [5, 17]. In our studies we found that for *n*-type electrodeposited Cu_2O film the annealing temperature should be kept below 200°C. Therefore the annealing of samples are performed in vacuum for 20 min at 175 °C, the samples showed enhancement in current-voltage characteristics, which can be seen in figure 6.5. Local impurities might be the reason for low performance of un-annealed samples. Obviously, the photocurrent of annealed samples displays substantial increments in the photocurrent at the zero-bias potential. In comparison with as-grown Cu_2O film, the annealed sample deposited under 30 min nitrogen purge exhibits approximately 35 times enhancement. In figure 6.5 the enhancement in photocurrent annealed *n*-Cu_2O thin film is presented. All samples prepared showed enhancement in generated photocurrent regardless of deaeration methods. For the comparison propose one *n*-Cu_2O thin film sample is prepared without nitrogen or argon bubbling as a reference sample.

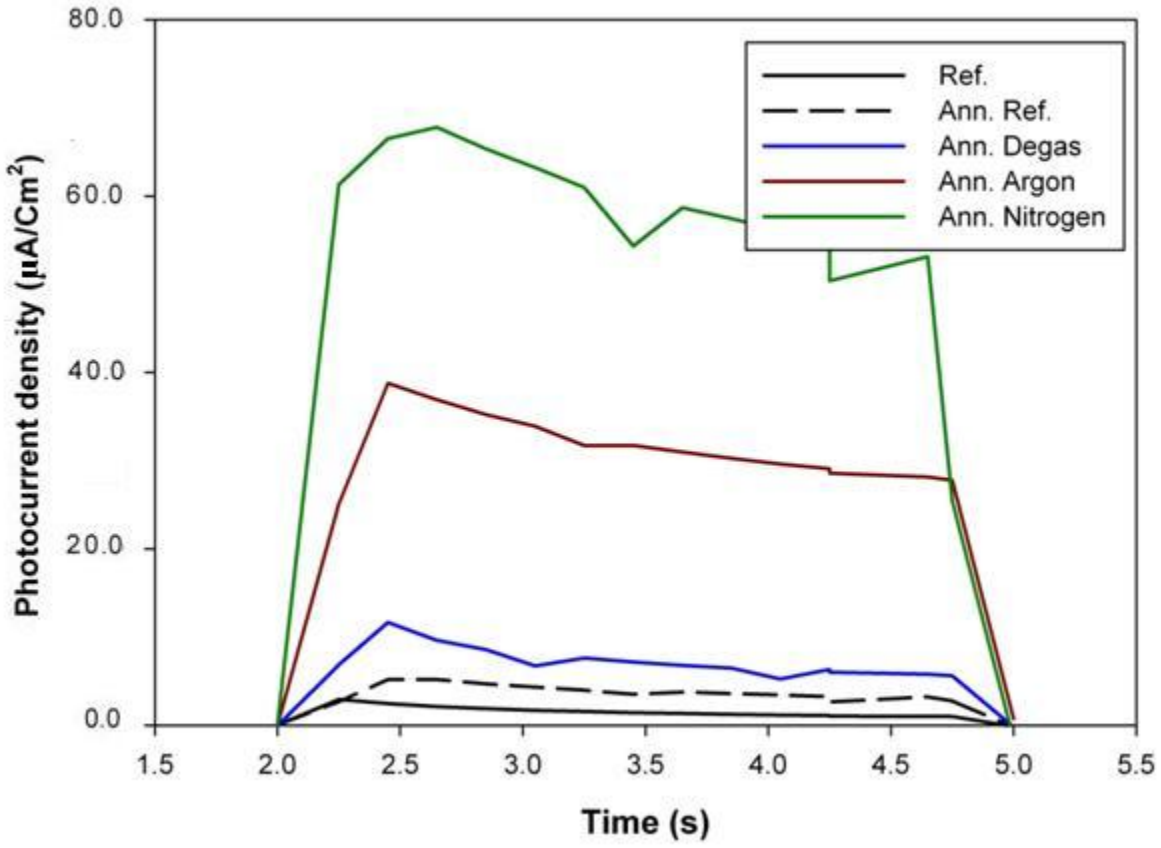

Figure 6-5 Photoelectrochemical behaviors of Cu_2O after heat treatment.

In order to investigate the purity of electrodeposited Cu_2O thin film, one sample from each deaeration techniques were chosen for XRD spectrum characterization. Figure 6.6 provides the XRD patterns for the electrodeposited Cu_2O films under nitrogen purge environment. The diffraction peaks were consistent with what were expected in Cu_2O (JCPDS: 5-667) without the impurity of Cu or CuO or any other phase. Similar XRD pattern was obtained for the sample purged under Argon and the sample prepared under ultrasonic degassing. The conclusion was that the deaeration methods used in this study had no noticeable effect on purity of prepared Cu_2O thin films.

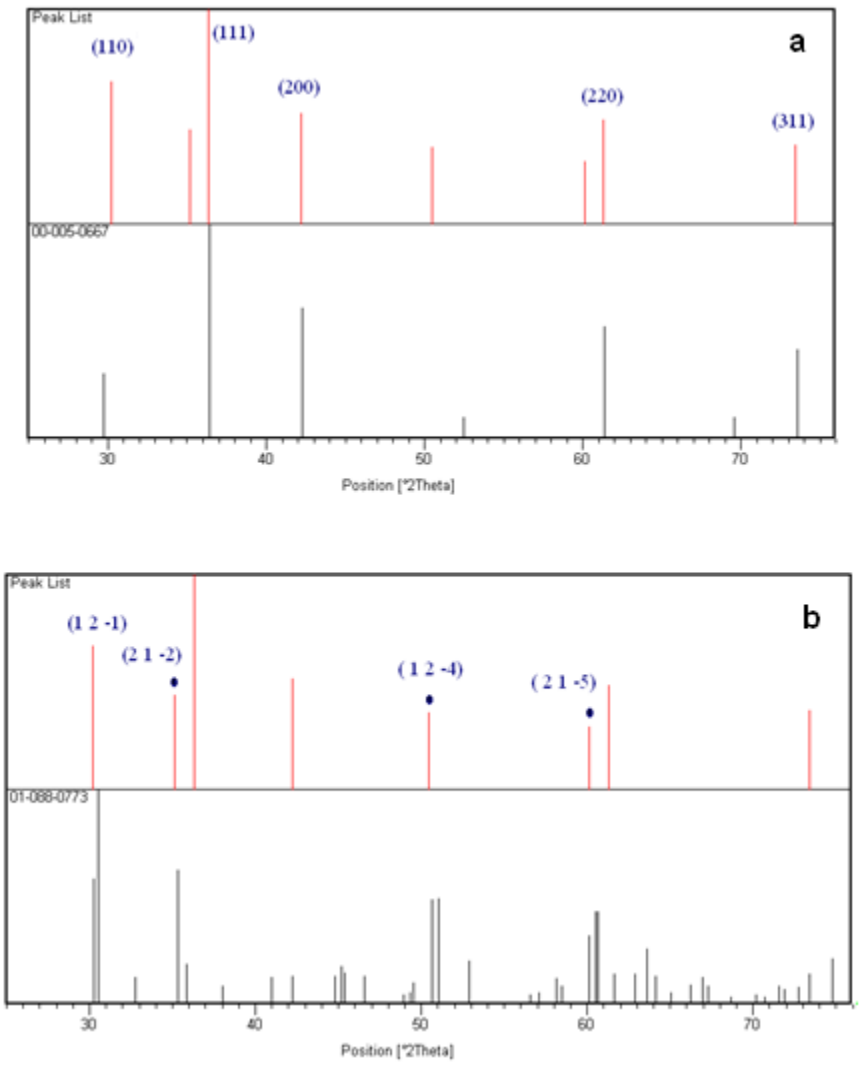

Figure 6-6 XRD patterns for the electrodeposited Cu_2O film in nitrogen purged solution, a) XRD obtained compared with reference Cu_2O, b) XRD obtained compared with reference ITO.

Figure 6.7 shows the SEM images of the microstructure of the Cu_2O films that been deposited under no purge, 5 minutes, 10 minutes, 15 minutes and 15 minutes bubbling time.

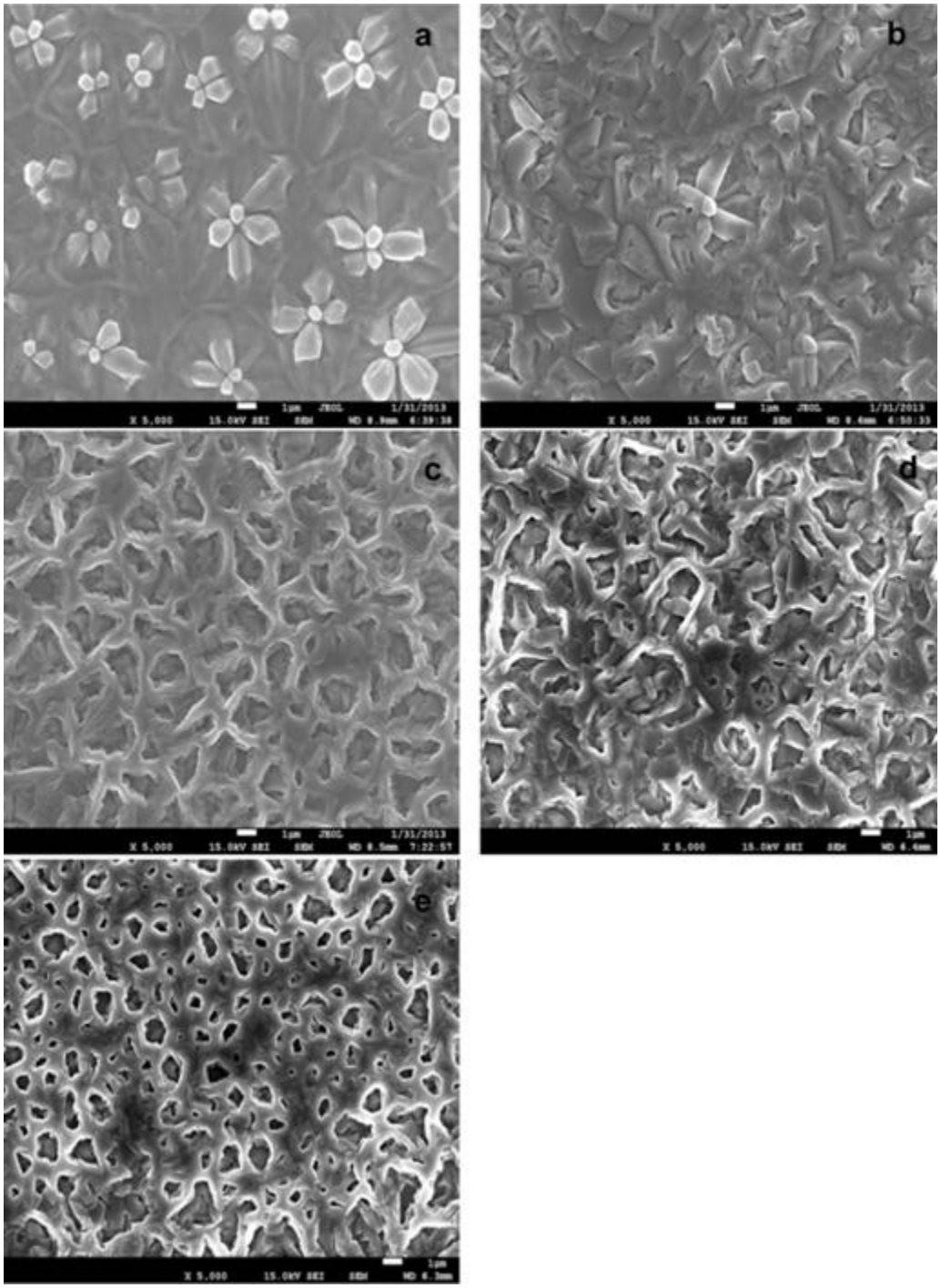

Figure 6-7 SEM images of the Cu_2O films deposited in different purging time. (a) without purge (b) 5 minutes bubbling with N_2, (c) 10 minutes bubbling with N_2; (d) 15 minutes bubbling with N_2 and; (e) 30 minutes bubbling with N_2.

When the concentration of dissolved oxygen in electrolyte is high (no nitrogen purge), the flower-like shapes Cu_2O films are formed. The morphology of the Cu_2O thin film gradually

changes to ring shape as the purging time increases. At low purging time big pores are observed. As the purging time increases the pores size are reduced as shown in figure 6.7 (b-e). The surface morphology changed to the densely packed network shape structure. In this structure (Cu_2O film deposited without nitrogen purge) we obtained the lowest photocurrent density. This might be due to voids between flowers like shape (large) grains, which caused leakage current. The Cu_2O film deposited under N_2 become more compact than the film deposited under no N_2 purge.

Effect of applied deposition potential on produced photocurrent was investigated. Figure 6.8 shows the SEM images of the microstructure of the Cu_2O films that been deposited at various applied potentials. All other parameters kept unchanged. The deposition solution was purge under nitrogen for 5 min. prior to the deposition. The zero-bias photocurrent of these electrodes was 4.5, 7.5, 12 and 22 $\mu A/cm^2$ for applied deposition potential of -100, -150, -200 and -250 mV, respectively. All potentials are versus Ag/AgCl reference electrode.

Better understanding of Cu_2O stoichiometry is desirable to determine the origin and mechanism of *p*- and *n*-type Cu_2Oformation. The relation between the oxygen and the copper ion content in the electrodeposition bath should be determined. It is speculated that due to the oxygen vacancies or the excess of copper ion in the composition of the deposited film, the *n*-type Cu_2O is achieved. This will help to identify the origin of the *n*-type conductivity.

A standalone system for measurement and control of the oxygen partial pressure is needed to achieve the above goal. We are proposing a set up that contains a three-electrode electrochemical cell in closed chamber connected to a mass flow meter and a potentiometric sensor. Through the mass flow meter we could precisely measure the amount of gas entering into the system and by the potentiometric sensor we could precisely control and measure oxygen partial pressure (pO_2)

during the entire deposition time. After deposition samples could be characterized by inductively coupled plasma atomic emission spectroscopy (ICP-AES) and X-ray photoelectron spectroscopy (XPS). By these techniques we could trace copper ions and oxygen composition in the film and determine the relation between the oxygen and the copper ion content in the electrodeposition films.

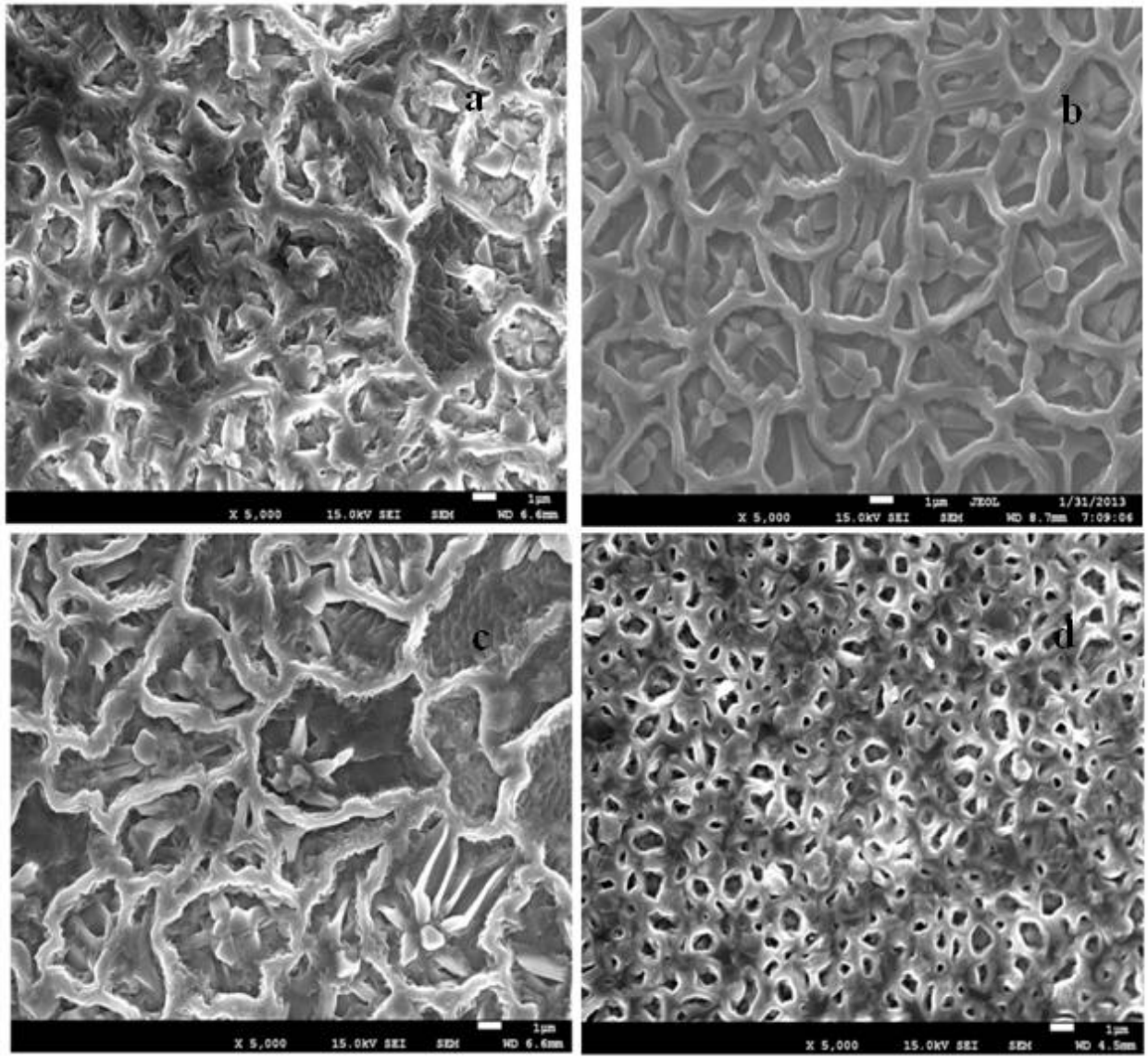

Figure 6-8 SEM images of the Cu_2O films deposited under 5 minutes fixed N_2 purge time applied potential of (a) -100, (b) -150, (c) -200 and (d) -250 mV vs. Ag/AgCl.

6.4 Conclusion

The *n*-type Cu_2O films were fabricated on ITO substrate. Oxygen deficiency in the Cu_2O lattice may be the origin of the *n*-type behavior. Nitrogen purging prior the electrodepostion has effect in the morphological changes of Cu_2O particles in the reaction process. The photocurrent density of *n*-type Cu_2O were enhanced by longer purging time. The efficiencies we obtained were improved. Oxygen deficiency in the Cu_2O lattice may be the origin of the *n*-type behavior. Whether the presents of nitrogen has a direct or indirect effect on the photocurrent enhancement remains to be investigated.

References

[1] B. P. Rai, "Cu2O solar cells: A review," *Solar Cells,* vol. 25, pp. 265-272, 1988.

[2] L. C. Olsen*, et al.*, "Experimental and theoretical studies of Cu2O solar cells," *Solar Cells,* vol. 7, pp. 247-279, 1982.

[3] A. Mittiga*, et al.*, "Heterojunction solar cell with 2% efficiency based on a Cu2O substrate," *Applied Physics Letters,* vol. 88, pp. 163502-2, 2006.

[4] K. Han and M. Tao, "Electrochemically deposited p–n homojunction cuprous oxide solar cells," *Solar Energy Materials and Solar Cells,* vol. 93, pp. 153-157, 2009.

[5] W. Siripala and J. R. P. Jayakody, "Observation of n-type photoconductivity in electrodeposited copper oxide film electrodes in a photoelectrochemical cell," *Solar Energy Materials,* vol. 14, pp. 23-27, 1986.

[6] C. Jayewardena*, et al.*, "Fabrication of n-Cu2O electrodes with higher energy conversion efficiency in a photoelectrochemical cell," *Solar Energy Materials and Solar Cells,* vol. 56, pp. 29-33, 1998.

[7] C. A. N. Fernando and S. K. Wetthasinghe, "Investigation of photoelectrochemical characteristics of n-type Cu2O films," *Solar Energy Materials and Solar Cells,* vol. 63, pp. 299-308, 2000.

[8] J. Liang*, et al.*, "Thin cuprous oxide films prepared by thermal oxidation of copper foils with water vapor," *Thin Solid Films,* vol. 520, pp. 2679-2682, 2012.

[9] M. Seo*, et al.*, "Composition and Structure of Anodic Oxide Films on Copper in Neutral and Weakly Alkaline Borate Solutions," *Bulletin of the Faculty of Engineering, Hokkaido University,* vol. 102, 1981.

[10] V. F. Drobny and D. L. Pulfrey, "Properties of reactively-sputtered copper oxide thin films," *Thin Solid Films,* vol. 61, pp. 89 - 98, 1979.

[11] M. T. S. Nair*, et al.*, "Chemically deposited copper oxide thin films: structural, optical and electrical characteristics," *Applied Surface Science,* vol. 150, pp. 143-151, 1999.

[12] W. M. Sears and E. Fortin, "Preparation and properties of Cu2O/Cu photovoltaic cells," *Solar Energy Materials,* vol. 10, pp. 93-103, 1984.

[13] R. Garuthara and W. Siripala, "Photoluminescence characterization of polycrystalline n-type Cu2O films," *Journal of Luminescence,* vol. 121, pp. 173-178, 2006.

[14] L. C. Wang*, et al.*, "Electrodeposited copper oxide films: Effect of bath pH on grain orientation and orientation-dependent interfacial behavior," *Thin Solid Films,* vol. 515, pp. 3090-3095, 2007.

[15] G. P. Pollack and D. Trivich, "Photoelectric properties of cuprous oxide," *Journal of Applied Physics,* vol. 46, pp. 163-172, 1975.

[16] L.-C. Chen*, et al.*, "Annealing Effects of Sputtered Cu2O Nanocolumns on ZnO-Coated Glass Substrate for Solar Cell Applications," *Journal of Nanomaterials,* vol. 2013, p. 6, 2013.

[17] Y. Tang*, et al.*, "Electrodeposition and characterization of nanocrystalline cuprous oxide thin films on TiO2 films," *Materials Letters,* vol. 59, pp. 434-438, 2005.

[18] T. Mahalingam*, et al.*, "Photoelectrochemical solar cell studies on electroplated cuprous oxide thin films," *Journal of Materials Science: Materials in Electronics,* vol. 17, pp. 519-523, 2006/07/01 2006.

[19] R.-M. Liang*, et al.*, "Effect of annealing on the electrodeposited Cu2O films for photoelectrochemical hydrogen generation," *Thin Solid Films,* vol. 518, pp. 7191-7195, 2010.

Chapter 7 : GENERAL DISCUSSION

Photovoltaic limited efficiency and high cost of silicon solar cells are key issues for solar cell to become an alternative to the use of readily available fossil fuel. Therefore the development of new cost effective and non-toxic photovoltaic materials and energy efficient processes is essential. Transition metal oxides have a great potential to fulfill these requirements. Among them cuprous oxide (Cu_2O) has potential alternative to silicon due to its, non-toxicity and simple low-cost fabrication process from abundantly available materials. Cu_2O has direct band-gap energy of 2.0 eV and a relatively high absorption coefficient in the visible region. Its calculated theoretical electrical power conversion efficiency is approximately 20 %. However limited understanding of conductivity type of Cu_2O semiconductor as well difficulty in doping and lack of *n*-type Cu_2O has hindered the efficient production of Cu_2O based photovoltaic cells.

The objective of the present study was to carefully prepare *p*-type and *n*-type Cu_2O thin films by adjusting electrodepostion parameters and obtain optimum preparation parameters for future fabrication of high efficiency homojunction *p*-*n* Cu_2O solar Cell.

Two different substrates were used as the working electrodes for the electrodeposition of Cu_2O. One was transparent conducting oxide - ITO (indium tin oxide) on glass substrate with a sheet resistance of 18Ω/cm. The other one was Copper foil with a thickness of 18 μm.

Two different electrolyte solutions were used for Cu_2O electrochemical deposition. For deposition of *p*-type Cu_2O, the electrolyte solutions was the aqueous solution contained 0.4 M copper sulfate and 3 M sodium lactate ($NaC_3H_5O_3$, 60% w/w aqueous solution). For *n*-type Cu_2O, the electrolyte solutions was the aqueous solution contained 0.01 M copper acetate and 0.1 M sodium acetate.

A single-compartment, three-electrode electrochemical cell, was used for film deposition. Electrodeposition was carried out with a Princeton Applied Research potentiostat 273A. The commercial Ag/AgCl (4M KCl) and Pt mesh were used as the reference and counter electrode, respectively. The electrolyte was kept in water-jacked cell and temperature was controlled between 30°C and 70 °C by Polystat circulation water bath. Electrodeposition was carried out in the potentiostatic mode at different applied potential values with respect to the reference electrode. The applied potential window was chosen from cyclic voltammetry (CV). After deposition, the films were rinsed in de-ionized water and dried at room temperature.

The surface morphology of the films was studied using scanning electron microscope (SEM). The purity and crystal phases of each Cu_2O layers were examined by X-ray diffraction (XRD). The optical properties of the films were determined by photocurrent characterization carried out in a custom built three-electrode electrochemical cell. The conversion of photon of light into electrical energy was characterized by solid -liquid junction called Photo-electrochemical cell (PEC). The PEC was characterized by measuring current voltage characteristics (I-V) in dark as well as in light in the same cell used for photocurrent characterization.

I-V measurements were performed to determine the resistivity of *p*-type Cu_2O films. A circular Cu electrode was placed on top of Cu_2O films. A voltage was sweep between the substrate and the top electrode and the current was measured at room temperature with the Princeton Applied Research potentiostat 273A. From the slope of I-V curve, the area of top electrode, and the thickness of deposited film, the resistivity was determined.

Our study reveled that the increases in temperature will widen the Cu_2O deposition window toward more negative cathodic potentials and increases the deposition current and 60–70^{o}C is an

optimum temperature for deposition of Cu_2O. The deposition potential also is one of important parameter in deposition of Cu_2O and should be kept between -0.2 to -0.6 V vs. Ag/AgCl. At more negative the current started to oscillate and Cu was co-deposited. In order to avoid co-deposition of Copper, the potential window used in this study was kept below -0.5 V vs. Ag/AgCl.

Other important parameters found to be bath pH. Samples deposited at pH bath 8 and above all showed cathodic behavior which represents the typical behavior of the *p*-type semiconductor. All samples deposited at this potential and bath pH range composed of pure Cu_2O without the trace of Cu or CuO deposition. However thin film crystal preferred ordination for pH<10 bath is (100) plane and for pH> 11 is (111) plane.

The resistivity of deposited film depends on deposition conditions and decreases slightly as solution pH increases. The smallest value was obtained at pH 13.0, which is lower by two orders of magnitude than of film prepared at pH 9.0. The photocurrent increases with increase in solution pH, the film deposited at pH 13 produce more photocurrent than film deposited at pH 8.5. Therefore as the bath pH increases the photocurrent response was increased as well.

The effect of bath pH on the morphology and grain size of Cu_2O film is investiagted. There is a noticeable differences in cyristal shape and grain size. The grain size increases as the bath pH increases. The mechanism for the dependence of grain size on bath pH is currently unknown.

The surface morphology is found to be 4-sided pyramids with a relatively uniform size distribution. For (100) orientation plane and size 3-faced pyramid shape with large cyrstal grain for (111) plane. Temperture and applied poetential also have effect of the morphology of deposited Cu_2O. The film prepared at higher temperature has better crystallinity with less cracks

and defects in crystals. The degree of texture changes with the applied potential. A decrease in grain size i observed when the applied potential changes from -0.3 to -0.7 V versus Ag/AgCl.

The *n*-type Cu_2O films are deposited in an acetate bath containing 0.01 M copper acetate and 0.1 M sodium acetate by electrodepostion. Voltammetric curve revealed that the deposition potential should be more positive than -0.25 V for given temperature and the corresponding current in this range are lower than that of *p*-type Cu_2O deposition. We reveled that that deposition current increased and cathodic peaks are slightly shifted to the negative potential side with increase in bath pH. All samples prepared in the pH range of 4.8-6.0, produced anodic current under illumination, confirming their *n*-type conductivity.

It was noted that photoresponse increases for the samples prepared under more negative applied potential. The best photoresponse for pH 5.5 were obtained for Cu_2O deposited at -0.25 V vs. Ag/AgCl. It is observed that the photocurrent is a function of deposition potential for electrodepostion preformed in acidic medium.

Heat treatment effects on optical and electrical properties of electrodeposited Cu_2O have been investigated. After annealing in vacuum for 80 min at 150 °C, the samples showed enhancement in current-voltage characteristics.

A two-step electro-deposition process is implemented to fabricate *p*-*n* homo junction cuprous oxide on Indium tin oxide (ITO) substrate. The electro-deposition of *p*-Cu_2O and *n*-Cu_2O was performed potentiostatically without stirring in a single-compartment, three-electrode electrochemical cell. The current-voltage (I-V) curves under dark and illumination of a fabricated cell: ITO/ *p*-Cu_2O/*n*-Cu_2O/Cu illuminated through the ITO substrate are shown in Figure 5.22. This curve of the *p*-Cu_2O/*n*-Cu_2O homojunction shows clearly a behavior which is

similar to those of the I-V polarization curves of the *p*-*n* solar cell junction. The short circuit current and open circuit voltage are respectively determined as 235 microA/cm^2 and 0.35 Volt. The fill factor (*FF*) and the cell conversion efficiency of light to electricity are determined to be respectively 0.305 and 0.082%. However obtained efficiency is not in desirable range. This could be due to weak contact between top electrode and *n*-Cu_2O film and also weak junction between *p*-$Cu_2O$and *n*-Cu_2O films.

Furthermore the *n*-type Cu_2O is prepared under different atmosphere. Nitrogen purging prior the electrodepostion has affected the morphology of Cu_2O particles in the reaction process. We observed that the photocurrent density of *n*-type Cu_2O is enhanced by bubbling Nitrogen/Argon. The longer bubbling time showed better photocurrent density.

Chapter 8 : CONCLUSION AND RECOMMENDATIONS

8.1 Conclusion

In this Dissertation, we carried out potentiostatic electrodepostion of single phase cuprous oxide (Cu_2O) thin films in an aqueous solution. Cu_2O is a photovoltaic absorber. The electrical, structural and optical characteristics as deposited cuprous oxide are investigated.

The deposition parameters such as temperature, solution pH and applied potential are studied. It was noted that the deposition pH has a significant effect in controlling the structural, electrical properties of Cu_2O films. Cuprous oxide deposited in alkaline media (pH >8) in solution containing copper sulfate and lactic acid is *p*-type semiconductor. Films deposited at pH range of 8-9 have preferred orientation of (100) and have higher electrical resistance than films deposited in pH ~ 11 and higher, as this range have preferred orientation of (111). The crystallite shapes changes from 4-sided pyramids with relatively uniform size distribution in (100) oriented film to 3-faced pyramid shape with less uniform size distribution in (111) oriented film. The grain sizes of deposited films are increased as bath pH increased. The resistivities of films are decreased with increase pH values. The potential ranges of -200mV to -600mV Vs Ag/AgCl in copper sulfate and sodium lactate solution are suitable potential to obtain *p*-Cu_2O. The film deposited at pH 8-9 exhibit lower photoactivity than those deposited at pH 12-13. The bath temperature has strong effect on the composition and microstructure of the Cu_2O thin films. Annealing above 300^oC causes the oxidation of *p*-Cu_2O. Annealing above 200 ^oC causes the conductivity conversion for *n*-type to *p*-type. Annealing decreases the electrical resistivity of Cu_2O thin film and enhances its photo-response.

Cu_2O films were prepared on an Indium tin oxide glass substrate. The effect of different atmospheric treatments on the photoresponse of ITO/*n*-Cu_2O thin films was studied. We developed a method for enhancing the photocurrent of *n*-Cu_2O films. We showed that prepared film under nitrogen atmosphere has significant enhancement in the photocurrent produced in *n*-type Cu_2O. It is reasonable to believe that the origin of *n*-type Cu_2O is related to the oxygen incorporation in the crystal lattice, which is controlled by amount of dissolved oxygen in the solution. Hence lower concentration of oxygen is producing better *n*-type Cu_2O either with oxygen vacancy or additional copper.

With the optimum parameters obtained in this work a two-step electro-deposition process is implemented to fabricate *p*-*n* homo junction cuprous oxide on Indium tin oxide (ITO) substrate which was used as a transparent conductive oxide for the homo junction Cu_2O solar cell. The photovoltaic characterization was performed. The short circuit current and open circuit voltage are respectively determined as 235 microA/cm^2 and 0.35 Volt. The fill factor (*FF*) and the cell conversion efficiency of light to electricity are determined to be respectively 0.305 and 0.082%. However obtained efficiency is not in desirable range. This could be due to weak contact between top electrode and *n*-Cu_2O film and also weak junction between *p*-$Cu_2O$and *n*-Cu_2O films. Optimization of electrodepostion condition would improve the efficiencies of the solar cells.

8.2 Recommendations

Based on this work we can improve the low value of electrical power conversion efficiency of Cu_2O based solar cells by future work.

1) Both *p*- and *n*-type Cu_2O films prepared in this work have high resistivity. Future work need to be done to lower the resistivity of electrodeposited Cu_2O by doping. Doping will enhance the carrier concentration and carrier mobility which are critical factors for performance of solar cells. Key issue for doping are the selection of dopant which should be stable in deposition solution and simultaneously deposited with cuprous oxide. Iodide can be a potential donor doping material in Cu_2O and copper iodide (CuI) can be introduced in the electrodepostion bath. Therefore co-deposition of Iodide in Cu_2O could be investigated.
2) The systematic correlation between the resistivity and the Cu_2O *p-n* homojunction cell performance should be evaluated because it will help to identify the best films for optimized cells.
3) Better understanding of Cu_2O stoichiometry is desirable to understand the origin and mechanize of *p*- and *n*-type Cu_2O.
4) Cu_2O has a band gap of 2.0–2.2 eV, which is not an ideal value for solar cells. By controlling the stoichiometric of Cu_2O or by incorporating other atoms in the lattice, the energy band gap can be engineered. It should be interesting to correlate the Cu_2O particle size to its band gap value.
5) Better understanding of Cu_2O stoichiometry is desirable to understand the origin and mechanism of *p*- and *n*-type Cu_2Oformation. Determination of the relation between the oxygen and the copper ion content in the electrodeposition bath in necessary. Because it is speculated that due to the oxygen vacancies or the excess of copper ion in the composition of the deposited film, the *n*-type Cu_2O will be achieved. This will help to identify the origin of the *n*-type conductivity.

Annex A.

The thickness calculation of the deposited films by weighting method.

m_1	m_2	m_2-m_1=M	V=M/ρ	L= V/A	L*10000=µm	~ L
***p*-Cu_2O**						
0.1823	0.1832	0.0009	0.00015	0.000114	1.14	1.1
0.1004	0.1019	0.0015	0.00025	0.000189	1.89	1.9
0.1052	0.1074	0.0022	0.000367	0.000278	2.78	2.8
0.0991	0.1016	0.0025	0.000417	0.000316	3.16	3.2
0.1907	0.1935	0.0028	0.000467	0.000354	3.54	3.5
0.1075	0.1104	0.0029	0.000483	0.000366	3.66	3.7
***n*-Cu_2O**						
0.1606	0.1614	0.0008	0.000133	0.000101	1.01	1
0.1675	0.169	0.0015	0.00025	0.000189	1.89	1.9
0.1734	0.1754	0.002	0.000333	0.000253	2.52	2.5
0.179	0.1814	0.0024	0.0004	0.000303	3.03	3
0.1127	0.1153	0.0026	0.000433	0.000328	3.28	3.3
0.1279	0.1307	0.0028	0.000467	0.000354	3.53	3.5

Where m_1, m_2, ρ, L and A are the initial substrate mass, the substrate mass after deposition, the density of Cu_2O, the thickness and the deposited area respectively.